Role of the β subunit of L-type calcium channels in cardiac hypertrophy

Dissertation zur Erlangung des

naturwissenschaftlichen Doktorgrades

der Julius-Maximilians-Universität Würzburg

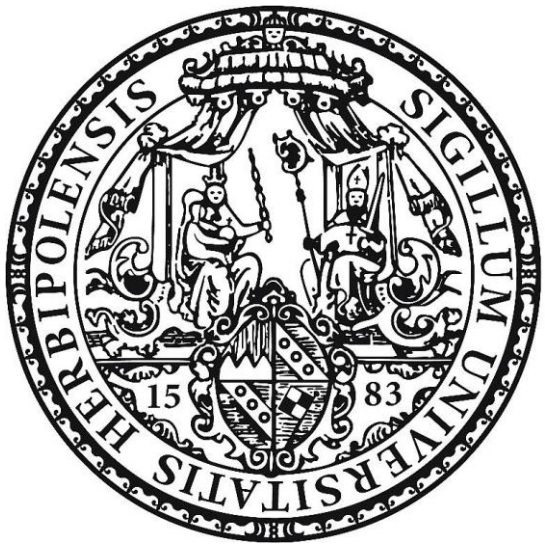

vorgelegt von

Simone Pickel

aus Schweinfurt

Würzburg, 2019

Eingereicht am: ……..……..

<u>Mitglieder der Promotionskommission:</u>

Vorsitzender: ……..

Gutachter: Prof. Dr. Michaela Kuhn

Gutachter: PD Dr. Sören Doose

Tag des Promotionskolloquiums: ……..…

Doktorurkunde ausgehändigt am: ……..

Table of contents

List of abbreviations

AID	α-interaction domain
AMC	Adult mouse cardiomyocytes
AMPA	α-amino-3-hydroxy-5-methyl-4-isoxazolepropionic acid receptor
Ang II	Angiotensin II
BCA	BC Assay Reagent A
BID	β-interacting domain
bp	Base pairs
Calpep.	Calpeptin
CaMKII	Calmodulin-dependent kinase II
cAMP	3',5'-adenosine monophosphate
$Ca_v\alpha_1$	Voltage-gated calcium channels α1 subunit
$Ca_v\beta$	Voltage-gated calcium channels β subunit
$Ca_v\alpha_2\delta$	Voltage-gated calcium channels $\alpha_2\delta$ subunit
$Ca_v\gamma$	Voltage-gated calcium channels γ subuni
CBFHH	Calcium and bicarbonate-free Hanks with HEPES
CT	C-terminus
Cyt.	Cytosolic fraction
DAG	Diacylglycerol
DAPI	4',6-Diamidino-2-Phenylindole
DHP	Dihydropyridines
dH_2O	Destilled water
DNA	Deoxyribonucleic acid
ECL	Enhanced chemiluminescence
ER	Endoplasmic reticulum
FBS	Fetal bovine serum
Fig.	Figure
g	Gravitational acceleration, 9,81 m/s^2
GAPDH	Glycerinaldehyd-3-phosphat-Dehydrogenase
GK	Guanylate Kinase
$G_{\alpha q}$	G-protein-coupled α_1-adrenergic receptors
HPLC	High perfomance liquid chromatography
HRP	Horseradish peroxidase
HVA	High voltage activated calcium channels
IP3	Inositol 1,4,5-triphosphate
kb	Kilobase pairs
kDa	Kilodalton
LTCC	L-type voltage gated calcium channel
LV	Left ventricle
LVA	Low voltage activated calcium channels
M	Molar
MAGUK	Membrane associated guanylate kinase
MEF2	Myocyte enhancer factor 2
Mem.	Membrane fraction
MEM	Minimum essential medium

Moi	Multiplicity of infection
mRNA	Messenger RNA
MS	Mass spectrometry
MWCO	Molecular weight cut-off
Na^+/K^+-ATPase	Sodium potassium ATPase
NFAT	Nuclear factor of activated T cells
NFκB	Nuclearfactor-κB
NGS	Normal goat serum
NLS	Nuclear localization signal
NRC	Neonatal rat cardiomyocytes
nt	Nucleotides
NT	N-terminus
Nuc.	Nuclear fraction
OD	Optical densitiy
PCR	Polymerase chain reaction
PE	Phenylephrine
Pfu	Plaque forming unit
PKA	Protein kinase A
PKC	Protein kinase C
PLC	Phospholipase C
Pln	Phospholamban
PRD	Proline rich domain
P/S	Penicillin/streptomycin
qRT-PCR	Quantitative real time PCR
RNA	Ribonucleic acid
RV	Right ventricle
RyR	Ryanodine receptor
SERCA	Sarcoplasmic reticulum Ca^{2+}-ATPase
shRNA	Short hairpin RNA
shRNAsc	Scrambled shRNA
SH3	Src Homology-3
TAC	Transverse aortic constriction
T&D	Trypsin and DNase
VDI	Voltage-dependent inactivation
Vera.	Verapamil
VGCCs	Voltage-gated calcium channels
WT	Wildtype
YFP	Yellow Fluorescent protein

Abstract

L-type calcium channels (LTCCs) control crucial physiological processes in cardiomyocytes such as the duration and amplitude of action potentials, excitation-contraction coupling and gene expression, by regulating the entry of Ca^{2+} into the cells. Cardiac LTCCs consist of one pore-forming α_1 subunit and the accessory subunits $Ca_v\beta$, $Ca_v\alpha_2\delta$ and $Ca_v\gamma$. Of these auxiliary subunits, $Ca_v\beta$ is the most important regulator of the channel activity; however, it can also have LTCC-independent cellular regulatory functions. Therefore, changes in the expression of $Ca_v\beta$ can lead not only to a dysregulation of LTCC activity, but also to changes in other cellular functions. Cardiac hypertrophy is one of the most relevant risk factors for congestive heart failure and depends on the activation of calcium-dependent prohypertrophic signaling pathways. However, the role of LTCCs and especially $Ca_v\beta$ in this pathology is controversial and needs to be further elucidated.

Of the four $Ca_v\beta$ isoforms, $Ca_v\beta_2$ is the predominant one in cardiomyocytes. Moreover, there are five different splice variants of $Ca_v\beta_2$ ($Ca_v\beta_{2a\text{-}e}$), differing only in the N-terminal region. We reported that $Ca_v\beta_{2b}$ is the predominant variant expressed in the heart. We also revealed that a pool of $Ca_v\beta_2$ is targeted to the nucleus in cardiomyocytes. The expression of the nuclear $Ca_v\beta_2$ decreases during *in vitro* and *in vivo* induction of cardiomyocyte hypertrophy and overexpression of a nucleus-targeted $Ca_v\beta_2$ completely abolishes the *in vitro* induced hypertrophy. Additionally, we demonstrated by shRNA-mediated protein knockdown that downregulation of $Ca_v\beta_2$ enhances the hypertrophy induced by the α_1-adrenergic agonist phenylephrine (PE) without involvement of LTCC activity. These results suggest that $Ca_v\beta_2$ can regulate cardiac hypertrophy through LTCC-independent pathways. To further validate the role of the nuclear $Ca_v\beta_2$, we performed quantitative proteome analyses of $Ca_v\beta_2$-deficient neonatal rat cardiomyocytes (NRCs). The results show that downregulation of $Ca_v\beta_2$ influences the expression of various proteins, including a decrease of calpastatin, an inhibitor of the calcium-dependent cysteine protease calpain. Moreover, downregulation of $Ca_v\beta_2$ during cardiomyocyte hypertrophy drastically increases calpain activity as compared to controls after treatment with PE. Finally, the inhibition of calpain by calpeptin abolishes the increase in PE-induced hypertrophy in $Ca_v\beta_2$-deficient cells. These results suggest that nuclear $Ca_v\beta_2$ has Ca^{2+}- and LTCC-independent functions during the development of

hypertrophy. Overall, our results indicate a new role for $Ca_v\beta_2$ in antihypertrophic signaling in cardiac hypertrophy.

Zusammenfassung

Durch die Regulation des Calciumeintritts in die Zellen kontrollieren L-Typ-Calciumkanäle (LTCCs) wichtige physiologische Prozesse wie die Dauer und Amplitude von Aktionspotentialen, die elektromechanische Kopplung und die Genexpression in Kardiomyozyten. Kardiale LTCCs bestehen aus einer porenformenden α_1 Untereinheit und Hilfsuntereinheiten wie $Ca_v\beta$, $Ca_v\alpha_2\delta$ und $Ca_v\gamma$. Von diesen Hilfsuntereinheiten ist $Ca_v\beta$ der wichtigste Regulator der Kanalfunktion, wobei $Ca_v\beta$ auch LTCC-unabhängige zelluläre und regulatorische Funktionen haben kann. Veränderungen in der Expression dieses Proteins können daher zu einer Fehlregulation der LTCC-Aktivität führen, jedoch auch zu Veränderungen von anderen zellulären Funktionen. Einer der häufigsten Risikofaktoren für kongestive Herzinsuffizienz ist die kardiale Hypertrophie, welche abhängig ist von der Aktivierung von Calcium-abhängigen prohypertrophen Signalwegen. Die Rolle von LTCCs und insbesondere von $Ca_v\beta$ in dieser Erkrankung ist jedoch kontrovers und muss noch weiter erforscht werden.

Von den vier $Ca_v\beta$ Splicevarianten ist $Ca_v\beta_2$ die dominierende Form in Kardiomyozyten. Darüber hinaus existieren fünf verschiedene Splicevarianten von $Ca_v\beta_2$ ($Ca_v\beta_{2a\text{-}e}$), die sich jeweils nur in der N-terminalen Region unterscheiden. Wir konnten demonstrieren, dass von diesen Splicevarianten überwiegend $Ca_v\beta_{2b}$ im Herzen exprimiert wird. Außerdem konnten wir zeigen, dass ein Teil von $Ca_v\beta_2$ im Nukleus von Kardiomyozyten zu finden ist. Die Expression von nuklearem $Ca_v\beta_2$ verringert sich während der *in vitro* und *in vivo* induzierten kardialen Hypertrophie und außerdem verhindert die Überexpression von im Kern lokalisiertem $Ca_v\beta_2$ die *in vitro* induzierte Hypertrophie komplett. Zusätzlich konnten wir demonstrieren, dass die Reduktion von $Ca_v\beta_2$ mittels shRNA zu einer Steigerung der Hypertrophie induziert durch die Stimulation mit dem α_1-adrenergen Agonisten Phenylephrin (PE) führt, ohne dass die LTCC-Aktivität beteiligt ist. Diese Ergebnisse legen nahe, dass $Ca_v\beta_2$ die Entstehung von Hypertrophie durch LTCC-unabhängige Signalwege beeinflussen kann. Um die Rolle von nuklearem $Ca_v\beta_2$ zu bekräftigen, haben wir quantitative Proteomanalysen von $Ca_v\beta_2$ defizienten neonatalen Rattenkardiomyozyten (NRCs) durchgeführt. Die Ergebnisse zeigen, dass die Reduktion von $Ca_v\beta_2$ die Expression verschiedener Proteine beeinflusst, zum Beispiel wird Calpastatin, ein Inhibitor der calciumabhängigen Cysteinproteasen Calpain, herunterreguliert. Außerdem wird durch die

$Ca_v\beta_2$ Reduktion während der Hypertrophie von Kardiomyozyten die Calpainaktivität verglichen mit den Kontrollen signifikant erhöht. Letztendlich konnten wir zeigen, dass die Inhibierung von Calpain durch Calpeptin die gesteigerte PE-induzierte Hypertrophie in $Ca_v\beta_2$-defizienten Zellen verhindert. Diese Ergebnisse lassen eine Calcium- und LTCC-unabhängige Funktion von nuklearem $Ca_v\beta_2$ während der Entwicklung von Hypertrophie, annehmen. Insgesamt deuten unsere Ergebnisse auf eine neue Rolle von $Ca_v\beta_2$ in den antihypertrophen Signalwegen in der kardialen Hypertrophie hin.

1. Introduction

1.1. Voltage-gated calcium channels

Ca^{2+} is one of the most important second messengers in the cells and is involved in different biological processes such as muscular contraction, neurotransmission, hormone release and gene expression. The influx of calcium into the cells through Ca^{2+} channels can be induced by various stimuli like voltage, ligand, temperature, and mechanical stretch. Voltage-gated calcium channels (VGCCs) were discovered in 1953 in crustacean muscle fibers [1]. They are integral cell membrane protein complexes, which open after membrane depolarization and convert the electrical signal of an action potential to an intracellular Ca^{2+} signal.

VGCC complexes consisting of five different subunits, referred to as $Ca_v\alpha_1$, $Ca_v\beta$, $Ca_v\alpha_2$, $Ca_v\delta$ and $Ca_v\gamma$, were first identified in skeletal muscle cells (Fig.1) [2]–[4]. $Ca_v\alpha_2$ and $Ca_v\delta$ are connected by disulfide bonds and form the $Ca_v\alpha_2\delta$ subunit [2]. The α_1 subunit is the pore-forming subunit that internalizes Ca^{2+}, but the other subunits are required for the regulation of the channel activity.

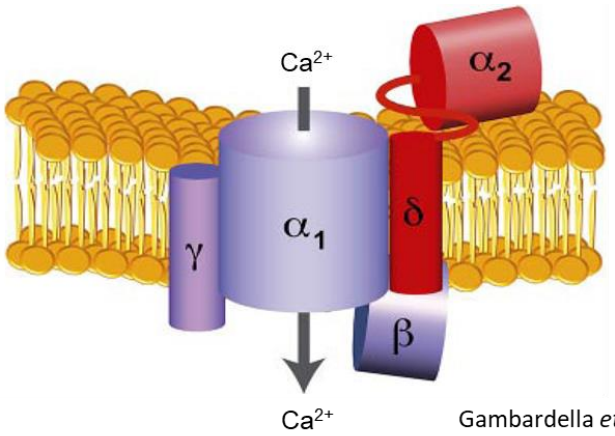

Figure 1. Subunit composition of VGCCs [5]
VGCCs consist of an α_1 subunit, a β subunit, a γ subunit and an $\alpha_2\delta$ subunit. The α_1 subunit is the pore-forming subunit by which calcium can enter the cells after channel opening. The β, γ and $\alpha_2\delta$ subunits are auxiliary subunits that modulate the properties of the VGCCs.

VGCCs are classified into two different subtypes, high-voltage-activated (HVA) and low-voltage-activated (LVA) channels, according to the membrane voltage needed for activation [6]. In mammals, 10 genes encode 10 different $Ca_v\alpha_1$ subunits. These genes are called *Cacna1a-1I* and *1s* and they encode 3 different classes of $Ca_v\alpha_1$ (Ca_v1.1-1.4, Ca_v2.1-2.3, Ca_v3.1-3.3, Table 1), which are grouped based on sequence similarity [7]. Subsequent

research showed that these three VGCC classes can be further divided in L-, N-, P/Q-, R- and T-type channels according to their biophysical and pharmacological properties [7]–[11]. L-type calcium channels (LTCCs), consisting of the $Ca_v1.1$, $Ca_v1.2$, $Ca_v1.3$, and $Ca_v1.4$ isoforms, together with P/Q-type channels ($Ca_v2.1$), N-type channels ($Ca_v2.2$) and the R-type channels ($Ca_v2.3$), belong to the HVA channels, while the T-type channels, $Ca_v3.1$-3.3, belong to LVA channels (Table 1) [7]. While HVA channels like the L-, N-, P/Q- and R-type channels are formed by the $Ca_v\alpha_1$, $Ca_v\beta$, $Ca_v\alpha_2\delta$ subunits, and in some cases the $Ca_v\gamma$ subunit, T-type channels only consist of an α_1 subunit [12].

Table 1. Name, classification, sensitivity and tissue distribution of VGCCs [7], [13]

Ca^{2+} channel	Type of Ca^{2+} current	Blocker	Nomenclature $Ca_v\alpha_1$ subunit	Tissue distribution
$Ca_v1.1$	L-type	DHP	$Ca_v1.1/\alpha_{1S}$	Skeletal muscle
$Ca_v1.2$			$Ca_v1.2/\alpha_{1C}$	Cardiac muscle, endocrine cells, neurons
$Ca_v1.3$			$Ca_v1.3/\alpha_{1D}$	Endocrine cells, neurons, heart
$Ca_v1.4$			$Ca_v1.4/\alpha_{1F}$	Retina
$Ca_v2.1$	P/Q-type	ω-agatoxin IVA	$Ca_v2.1/\alpha_{1A}$	Neurons
$Ca_v2.2$	N-type	ω-conotoxinGVIA	$Ca_v2.2/\alpha_{1B}$	Neurons
$Ca_v2.3$	R-type	SNX-482 (cell type-dependent)	$Ca_v2.3/\alpha_{1E}$	Neurons
$Ca_v3.1$	T-type	TTA-A2	$Ca_v3.1/\alpha_{1G}$	Cardiac muscle, skeletal muscle
$Ca_v3.2$			$Ca_v3.2/\alpha_{1H}$	Cardiac muscle, neurons
$Ca_v3.3$			$Ca_v3.3/\alpha_{1I}$	Neurons

LTCCs are known to have, in contrast to the other VGCC groups, a long-lasting activity. They also need a strong depolarization for activation and can be blocked by small amounts of L-type channel antagonists such as dihydropyridines (DHP), phenylalkylamines, and benzothiazepines [14]. L-type currents are the main Ca^{2+} currents in muscle and endocrine cells. Although the P/Q-, N- and R-type channels also require a strong depolarization, they are insensitive to blockage by L-type channel inhibitors. Compared to LTCCs, N-type calcium

channel currents are inhibited by ω-conotoxin GVIA treatment [15]. P/Q-type channels are sensitive to ω-agatoxin IVA, whereas R-type channels are not blocked by any of these inhibitors, with the exception of SNX-482 in some cell types [10], [16], [17]. Moreover, there are several blockers for T-type channels like TTA-A2 [18], [19].

VGCCs have a diverse distribution among cell types, with Ca_v2 channels being primarily found in neurons (Table 1). Ca_v2 channels are important for the synaptic transmission and for hormone release from secretory cells [20]. Ca_v3 channels are also expressed in neurons and, during early development, in cardiac muscle [20], [21]. They contribute to pacemaker activity in the sinoatrial node, regulate neuronal excitability, and are important for neurotransmitter release. In contrast to Ca_v2 and Ca_v3 channels, Ca_v1 channels have a wider distribution. They are expressed in neurons, skeletal muscle, endocrine cells, retinas and also in the heart.

1.1.1. L-type calcium channel $Ca_v1.2$ in cardiomyocytes

Although the four different LTCC (Ca_v1) isoforms have similar electrophysiological and pharmacological properties, they differ in their tissue distribution. Since $Ca_v1.1$ is responsible for skeletal muscle contraction, it is the main isoform expressed in this tissue [20]. In contrast, $Ca_v1.4$ expression is limited to the retina. $Ca_v1.2$ and $Ca_v1.3$ have a wider distribution and can be found in most electrically excitable cells, including neurons and cardiomyocytes [20].

$Ca_v1.2$ and $Ca_v1.3$ are expressed in the heart [22]. $Ca_v1.3$ is the main isoform in the sinoatrial node and the atrioventricular node [22]–[25]. In cardiomyocytes, the main LTCCs are the $Ca_v1.2$ channels. They are essential for the excitation-contraction coupling mechanism [20]. In cardiomyocytes, plasma membrane depolarization leads to the opening of $Ca_v1.2$ channels and to an influx of Ca^{2+} ions into the cytoplasm. This calcium influx triggers the activation of the ryanodine receptor 2 (RyR2) in the membrane of the sarcoplasmic reticulum and leads to a massive release of calcium from this compartment [26]. This increase in intracellular calcium concentration activates cardiomyocyte contraction [21]. In addition, cardiac LTCCs are also responsible for the duration of the action potential and for gene transcription.

1.1.2. $Ca_v\alpha_1$ subunits

$Ca_v\alpha_1$ is the pore-forming subunit of LTCCs. Its different isoforms have a molecular weight of 190 to 250 kDa. They consist of four homologous repeats (I-IV), comprised of six transmembrane domains (S1-S6), and linked by cytoplasmic loops (Fig. 2). Additionally, a sequence known as the pore loop connects the transmembrane domains S5 and S6. This structure, present in each homologous repeat and containing negatively charged amino acids (mostly glutamate), forms the selectivity filter for Ca^{2+} of the LTCCs [27]. In addition, the positively charged arginine and lysine residues of the S4 segment constitute the voltage sensor, which is necessary for channel opening and closing. The S6 domains assemble the inner pore, which is also the binding site for some pore-blocking antagonists of LTCCs [28]. The N- and C-terminus of $Ca_v\alpha_1$ are located intracellularly in the cytoplasm. Moreover, the loop linking the homologous repeats I and II contains an α-interaction domain (AID) where the auxiliary $Ca_v\beta$ subunit can bind [29]. This binding site is very important, since the $Ca_v\beta$ subunit is the main regulator of LTCCs. Other proteins besides $Ca_v\beta$ can bind to $Ca_v\alpha_1$, including $Ca_v\alpha_2\delta$, $Ca_v\gamma$, calmodulin, scaffolding proteins and downstream proteins.

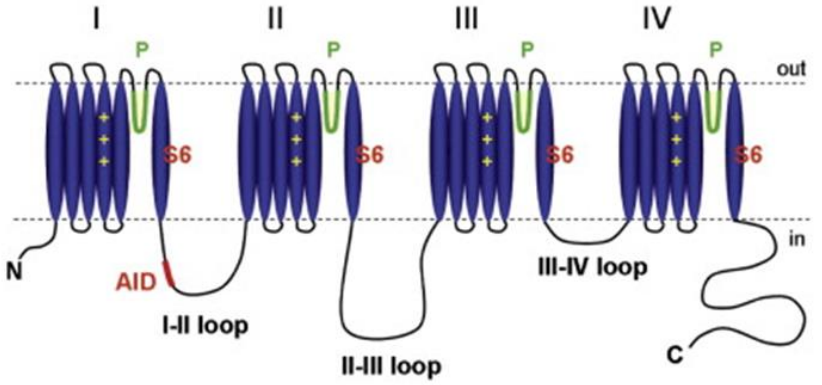

Figure 2. Predicted structure of the $Ca_v\alpha_1$ subunit membrane topology [30]
The six transmembrane domains from each homologous repeat (I-IV) of the $Ca_v\alpha_1$ subunit are represented in blue. All repeats are connected by cytosolic loops. The α-interaction domain (AID), necessary for the binding of the $Ca_v\beta$ subunit is located between the loops I and II. The N- and C-terminal domains are intracellularly located.

The *Cacna1* genes of LTCCs can undergo extensive alternative splicing, which can produce a huge number of different Ca_v channels with distinct physiological properties [31]–[34]. The composition of these splice variants varies between tissues and cells. Mutations in the *Cacna1* gene can lead to diseases in humans, including episodic ataxia type 2, stationary congenital night blindness, malignant hyperthermia, Timothy syndrome and cardiac arrhythmias [20], [35].

1.1.3. $Ca_v\alpha_2\delta$ subunits

The auxiliary subunit $Ca_v\alpha_2\delta$ is a protein with a molecular weight of 140-180 kDa. The functional $Ca_v\alpha_2\delta$ complex is formed by the extracellular α_2 and δ subunits, which are proteolytically cleaved from one polypeptide and later linked by disulfide bonds [2], [36], [37]. Furthermore, the small $Ca_v\delta$ subunit is attached to the membrane via a glycophosphatidylinositol anchor, whereas the posttranslationally glycosylated $Ca_v\alpha_2$ subunit interacts with the pore-forming $Ca_v\alpha_1$ subunit [2], [38], [39]. Several studies revealed that $Ca_v\alpha_2\delta$ can change the biophysical properties of the channel and modulates its Ca^{2+} currents [40]–[42]. $Ca_v\alpha_2\delta$ not only facilitates the trafficking of the $Ca_v\alpha_1$ subunit to the plasma membrane, but also promotes its permanence there [43], [44].

Until now, four distinct $Ca_v\alpha_2\delta$ subunits ($Ca_v\alpha_2\delta_1$-$Ca_v\alpha_2\delta_4$) have been identified, each encoded by a distinct gene [37], [45], [46]. Moreover, each $Ca_v\alpha_2\delta$ isoform has multiple alternative splice variants, which can differentially affect the electrophysiological and pharmacological properties of the channel [45], [47], [48]. $Ca_v\alpha_2\delta$ is expressed with Ca_v1 and Ca_v2 in different tissues, including heart, brain and skeletal muscle [2], [49]–[51]. Mutations in the $Ca_v\alpha_2\delta$ gene can lead to a number of diseases and phenotypes. For example, knockout mice lacking $Ca_v\alpha_2\delta_2$ show a wide range of alterations in the cardiovascular, immune, respiratory and nervous systems [52]. Furthermore, downregulation of $Ca_v\alpha_2\delta_1$ leads to abnormalities of the L-type calcium currents in cardiomyocytes [53]. In contrast, overexpression of $Ca_v\alpha_2\delta_1$ is known to play a role in neuropathic pain [54], [55].

1.1.4. $Ca_v\gamma$ subunits

The $Ca_v\gamma_1$ subunit was cloned in 1990 and first purified together with the skeletal muscle LTCC $Ca_v1.1$ [3], [56]. It is a protein of approximately 30-35 kDa. Until now, eight genes that encode eight γ-like proteins (γ_1-γ_8) were identified by sequence homology [57]–[59]. These proteins consist of four transmembrane segments with intracellular N- and C-termini [56]. In homologous expression systems, the $Ca_v\gamma$ subunits can shift the voltage-dependent inactivation or activation of LTCCs, which leads to small reductions of the current [60]–[63]. However, the specific effect of the $Ca_v\gamma$ subunit on LTCC activity depends on the composition of the $Ca_v\alpha_1$, $Ca_v\beta$ and $Ca_v\alpha_2\delta$ isoforms. $Ca_v\gamma_1$ knockout mice show no phenotypical changes compared to wild-type (WT) mice, but have slower LTCC inactivation and bigger Ca^{2+}

currents [61], [64]. However, the $Ca_v\gamma$ subunit is not needed for the assembly and trafficking of the calcium channel to the plasma membrane. Of the eight $Ca_v\gamma$ subunits, $Ca_v\gamma_1$ and $Ca_v\gamma_6$ seem to have a primary role as LTCC regulators in native tissues, in contrast to γ_2, γ_5, γ_7 and γ_8, who regulate proteins like the transmembrane α-amino-3-hydroxy-5-methyl-4-isoxazolepropionic acid (AMPA) receptor [65], [66]. Therefore, the primary task of these γ subunits seems to be the regulation of AMPA receptors instead of VGCCs in neurons.

1.1.5. $Ca_v\beta$ subunits

The $Ca_v\beta$ subunit is the most important regulator of LTCCs. The $Ca_v\beta$ subunit was first purified with $Ca_v\alpha_1$ and $Ca_v\gamma$ as a part of the skeletal muscle calcium channel [3]. This protein was later cloned and sequenced and is now referred to as $Ca_v\beta_{1a}$ subunit [67], [68]. Three other genes (*Cacnb2*, *Cacnb3*, *Cacnb4*), encoding $Ca_v\beta_2$, $Ca_v\beta_3$ and $Ca_v\beta_4$, were identified by homology cloning [68]–[70]. The four $Ca_v\beta$ genes have multiple splice variants that are expressed in different tissues and can confer diverse biophysiological properties to the channel. These proteins are cytosolic and have approximate molecular weight of 50-80 kDa.

1.1.5.1. Structure of $Ca_v\beta$

All $Ca_v\beta$ isoforms share a similar primary structure consisting of five different regions. The first, third and fifth regions are variable (yellow, blue, green, Fig. 3), whereas the second (red, Fig. 3) and the fourth (green, Fig. 1) regions are highly conserved among the $Ca_v\beta$ isoforms [71]–[73]. The NT domain of $Ca_v\beta$ is highly variable between the different isoforms. In $Ca_v\beta_4$, the structure of the NT domain, obtained by NMR, consists of a fold containing two α-helices and two antiparallel β sheets [74]. The CT domain of the $Ca_v\beta$ subunits is also highly variable and its alternative splicing gives rise to several splice variants.

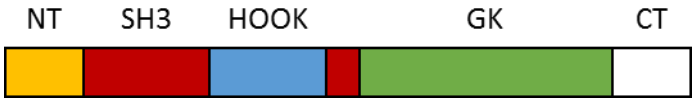

Figure 3. Linear structure of $Ca_v\beta$
$Ca_v\beta$ consists of five different regions. The NT (yellow), HOOK (blue) and CT (white) regions are variable and give rise to multiple splice variants. In contrast, the SH3 (red) and GK (green) domains are highly conserverd between the $Ca_v\beta$ isoforms.

The core region consists of the Src homology 3 (SH3), the HOOK and the guanylate kinase (GK)-like domains [73]. Based on this core region, $Ca_v\beta$ can be classified among the membrane-associated guanylate kinases (MAGUKs), which work as scaffolds of multiprotein

complexes. MAGUKs normally contain a PDZ motif at the NT domain that is however not present in $Ca_v\beta$. Of the three core domains, the SH3 and GK domains are conserved between the different $Ca_v\beta$ isoforms, whereas the HOOK region is subject to alternative splicing. Overall, the core region performs many of the key functions of the $Ca_v\beta$ subunit [71], [73], [75], [76]. Both the SH3 and GK domains, are known to participate in the interaction of $Ca_v\beta$ with other proteins.

The SH3 domains of $Ca_v\beta$ have five sequential β strands in two orthogonally packed sheets. However, the last two β strands are disturbed by the HOOK region, producing a non-continuous SH3 domain [73], [77]–[79]. In proteins like amphyphisin [80], syndapin [81] or sorting nexin 9 [82], the SH3 region binds to a proline-rich domain (PRD) in their interaction partners. Specifically, the SH3 domain of $Ca_v\beta$ is known to interact with the PRD of dynamin-1 and regulate channel endocytosis [83].

In yeast, GK domains catalyse the conversion of GMP to GDP. Although the $Ca_v\beta$-GK shares a common structure with yeast guanylate kinases, the catalytic sites of the GK region in the $Ca_v\beta$ subunit are mutated and consequently inactive [73], [78], [79], as reported also for other MAGUK proteins [84]. The $Ca_v\beta$-GK region contains the α_1-binding pocket where the 18 amino-acid-long AID of the $Ca_v\alpha_1$ subunit binds with strong affinity. The AID, located in the I-II linker of LTCCs, is known to be the main $Ca_v\beta$ interaction site. While the GK region is binding to the AID, the SH3 domain does not contribute to it [73], [78], [79].

The SH3 and GK domains interact strongly with each other intramolecularly [73], [78], [79]. The last β sheet of $Ca_v\beta$-SH3 interacts with the GK region and the rest of the SH3 domain. The interaction between SH3 and GK is important for the function of $Ca_v\beta$ [76], [85]. Mutations in one of these domains or changes in this interaction can lead to modified gating effects of $Ca_v\beta$ [86].

1.1.5.2. Splice variants of $Ca_v\beta$

As mentioned before, $Ca_v\beta$ is encoded by four different genes (*Cacnb1, Cacnb2*, *Cacnb3*, *Cacnb4*), all of which contain 14 exons, with the exception of *Cacnb3* with only 13 exons. All these genes can produce multiple splice variants or truncated forms that differ in their tissue distribution [52], [87]. The variable NT, HOOK and CT regions are therefore subject to alternative splicing. $Ca_v\beta$ isoforms are expressed in nearly all excitable cells, like

cardiomyocytes, neurons and skeletal muscle cells. $Ca_v\beta_1$ is widely expressed in brain and skeletal muscle [67], [88], [89]. Furthermore, $Ca_v\beta_2$ can be found mainly in the heart, but also to a lesser extent in the nervous system [68], [90]. $Ca_v\beta_3$ is expressed in brain, kidney, lung, skeletal muscle and other tissues. In contrast, $Ca_v\beta_4$ exists predominantly in the nervous system, but can also be found in skeletal muscle and kidney [52], [69], [91]. The expression levels of different $Ca_v\beta$ splice variants can vary during development. Examples of expression level changes during pre- and postnatal development are the increase of $Ca_v\beta_4$ in brain or the decrease of $Ca_v\beta_{2c}$, -β_{2d}, and -β_{2e} in the heart [92], [93]. The different variants of the $Ca_v\alpha_1$ subunit can assemble with the $Ca_v\beta$ and $Ca_v\alpha_2\delta$ subunits in diverse combinations, which increases the functionality and diversity of Ca^{2+} channels. Moreover, calcium channels consisting of various subunit combinations can even coexist in the same tissue.

The auxiliary subunit $Ca_v\beta_2$ is predominant among the four $Ca_v\beta$ isoforms in the heart [68], [94], [95]. Until now, five different $Ca_v\beta_2$ splice variants ($Ca_v\beta_{2a\text{-}e}$) have been identified, differing only in their NT region (Fig. 2, yellow) [68], [87], [92], [96], [97]. Of these splice variants, $Ca_v\beta_{2b}$ is the most abundant cardiac isoform [87] and the one that predominantly binds to $Ca_v1.2$ in the heart.

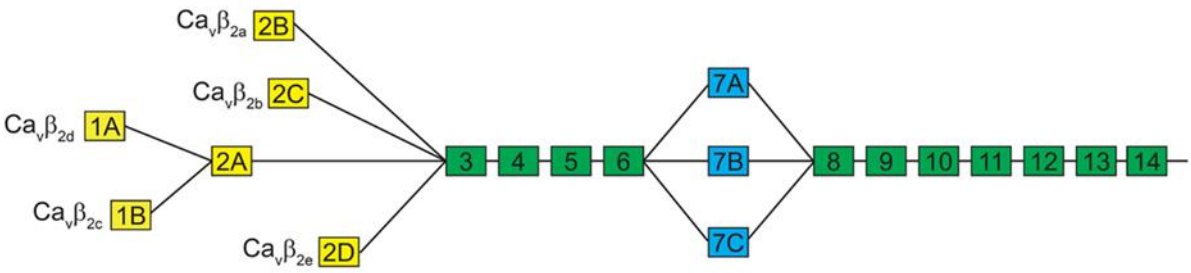

Figure 4. Splice variants of $Ca_v\beta_2$
The gene encoding $Ca_v\beta_2$ consists of 14 different exons. The five splice variants $Ca_v\beta_{2a\text{-}e}$ differ only in the amino acid sequence of their N-terminal region (yellow). Additional splice variants of $Ca_v\beta_2$ result from the splicing at exon 7 (7A, 7B or 7C).

1.1.5.3. Role of $Ca_v\beta$ in channel gating

As mentioned before, the $Ca_v\beta$ subunit is a cytosolic protein. However, due to its interaction with $Ca_v\alpha_1$ it translocates to the plasma membrane where it binds to the channel in a 1:1 ratio through the AID [98]. The interaction between the two subunits can modulate the gating properties of LTCCs.

$Ca_v\beta$ is required at least in heterologous expression systems for the targeting of $Ca_v\alpha_1$ to the plasma membrane and therefore for the normal surface expression of $Ca_v\alpha_1$. The plasma membrane expression of $Ca_v\alpha_1$ is extremely low and Ca^{2+} currents are almost undetectable in HEK293 cells and Xenopus oocytes overexpressing $Ca_v\alpha_1$ in the absence of $Ca_v\beta$ subunits. In these systems, co-expression of $Ca_v\beta$ and $Ca_v\alpha_1$ leads to a drastic increase of Ca^{2+} currents, which is attributed to the enhanced surface expression and open probability of the channel [99], [100]. The mechanism whereby $Ca_v\beta$ targets the $Ca_v\alpha_1$ subunit to the plasma membrane is not completely understood. One hypothesis is that $Ca_v\beta$ can mask an endoplasmic reticulum (ER) retention signal in the I-II linker of $Ca_v\alpha_1$ [101]. Other possibilities are the prevention of ubiquitination and proteosomal degradation of $Ca_v\alpha_1$ mediated by $Ca_v\beta$ or the rearrangement of $Ca_v\alpha_1$ after the binding of $Ca_v\beta$, which would reduce the strength of ER retention signals [102]–[104].

$Ca_v\beta$ promotes and enhances channel function by shifting the voltage-dependent activation of the LTCCs to more hyperpolarized voltages [42], [105]. This means that less membrane depolarization is required for channel opening in the presence of the $Ca_v\beta$ subunit, which leads to a higher open probability. All the $Ca_v\beta$ isoforms confer the same properties, with $Ca_v\beta_{2a}$ promoting the highest increase in channel opening probability [106].

$Ca_v\beta$ subunits also regulate the voltage-dependent inactivation (VDI) of the channel. Except for $Ca_v\beta_{2a}$ and $Ca_v\beta_{2e}$, all $Ca_v\beta$ isoforms shift the VDI to more hyperpolarized voltages and therefore facilitate the inactivation of the channel [107]. On the contrary, $Ca_v\beta_{2a}$ and $Ca_v\beta_{2e}$ shift the VDI to more depolarized stages [42], [105], [108]. This suppression of the channel´s VDI induced by $Ca_v\beta_{2a}$ is caused by a palmitoylation signal located at the N-terminus of $Ca_v\beta_{2a}$ [109]–[111], while the effect of $Ca_v\beta_{2e}$ is mediated by the presence of several positively charged amino acids at its N-terminus [112].

The role of $Ca_v\beta$ in cardiomyocytes is nevertheless still controversial. Whereas global knockout of $Ca_v\beta_2$ leads to death at early embryonic stages due to impaired cardiac development and contractions [113], a cardiomyocyte-specific deletion of $Ca_v\beta_2$ in adult mice causes only a slight decrease of L-type calcium currents [114]. To address the contradictory role of the $Ca_v\beta$ subunit in channel trafficking and regulation in the heart, Yang *et al* used transgenic mice with a mutated AID sequence preventing the $Ca_v\alpha_1$ subunit to interact with $Ca_v\beta$ [115]. These authors showed that the $Ca_v\beta$ subunit is not required for the

trafficking of the pore-forming $Ca_v\alpha_1$ subunit to the plasma membrane in adult cardiomyocytes, and that the function of $Ca_v\alpha_1$ was only slightly altered. These results suggest that $Ca_v\beta$ does not regulate LTCC activity in cardiomyocytes.

Apart from directly affecting the properties of LTCCs by binding to the $Ca_v\alpha_1$ subunit, $Ca_v\beta$ can also indirectly regulate the electrophysiological characteristics of the channel by interacting with other proteins. For example, the interaction of $Ca_v\beta$ with RIM1 suppresses the VDI of Ca_v1 and Ca_v2 channels and slows their inactivation kinetics [116]. $Ca_v\beta$ also interacts with proteins of the RGK family (Rad, Rem, Rem2, Gem). This interaction is important for the inhibition of LTCCs by the RGK proteins [52], [117], [118]. Moreover, several other reports describe that $Ca_v\beta$ is necessary for inhibition of channel activity promoted by $G_{\beta\gamma}$ proteins [119], [120].

1.1.5.4. LTCC-independent functions of $Ca_v\beta$

Different studies have shown that $Ca_v\beta$ not only regulates channel gating, but also has calcium channel-independent functions especially regulating the expression of diverse genes in different tissues. $Ca_v\beta$ can interact with various non-calcium channel-related proteins, including Ahnak and dynamin [83], [121]. In zebrafish, deletion of the *cacnb4* gene leads to death in early developmental stages. However, the injection of a *cacnb4* mutant that cannot interact with $Ca_v\alpha_1$ produces a non-lethal phenotype. This observation suggests that $Ca_v\beta_4$ can have important calcium channel-independent functions in this organism [122]. Another study revealed the interaction of $Ca_v\beta_3$ with a splice variant of Pax6, a transcription factor that is essential for the development of the eye and the nervous system. $Ca_v\beta_3$ was shown to suppress the transcriptional activity of Pax6 *in vitro* and was also detected in the nucleus in the presence of Pax6 [123]. Moreover, a splice variant of $Ca_v\beta_{4c}$ regulates the transcription and nuclear localization of heterochromatin protein 1 *in vitro* [124]. In skeletal muscle progenitor cells, $Ca_v\beta_{1a}$ functions as a suppressor of myogenin and changes gene expression in the nucleus [125]. Moreover, all $Ca_v\beta$ isoforms have been reported to translocate to the nucleus, either alone or by interacting with nucleus-targeted proteins, as are the cases of $Ca_v\beta_{1a}$ in muscle progenitor cells, $Ca_v\beta_2$ in the cardiac HL-1 cell line or $Ca_v\beta_4$ in rat cardiomyocytes [126]–[130].

1.2. Cardiac hypertrophy

The heart consists of different cell types such as cardiomyocytes, fibroblasts and endothelial cells. Cardiomyocytes are responsible for heart contraction. They are terminally differentiated, in contrast to the other cell types, and do not proliferate in adults [131]. Cardiac hypertrophy can be described as an increase in cardiomyocyte size and heart mass to decrease stress on the ventricular walls and maintain contractility. It can be triggered by various external or internal stimuli like mechanical force or neurohumoral signals [131], [132] and classified as physiological or pathological hypertrophy (Fig. 5).

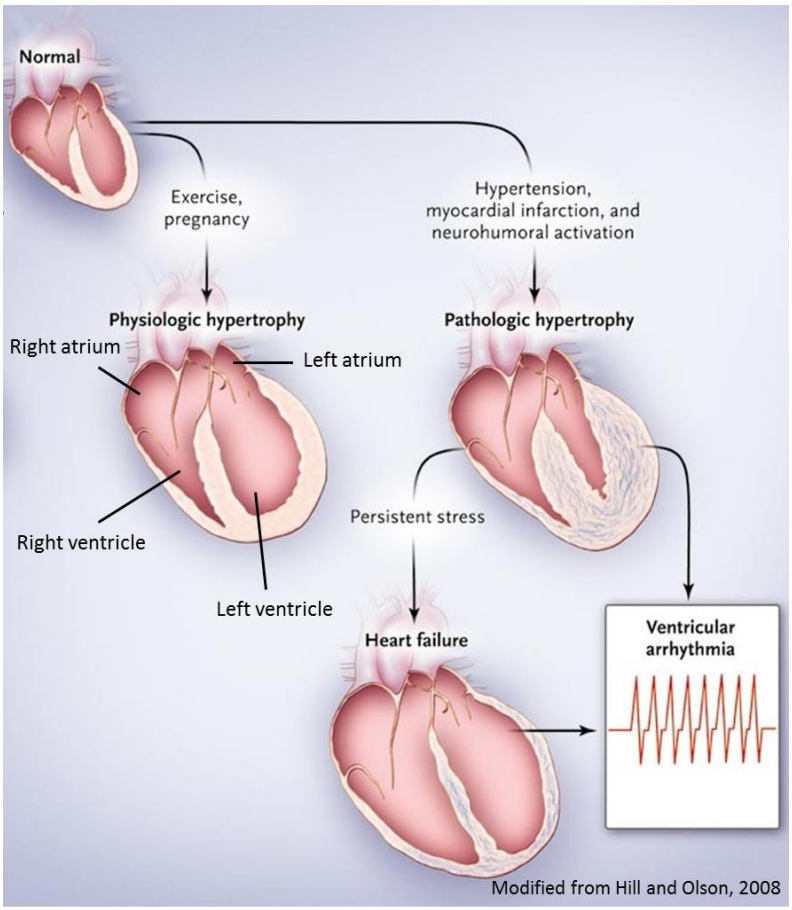

Figure 5. Development of physiological or pathological hypertrophy [133]
The enlargement of the heart can be classified as physiological or pathological hypertrophy. Physiological hypertrophy is the increase in ventricular wall thickness in response to exercise or pregnancy and is reversible. Moreover, physiological hypertrophy seems to be harmless and does not cause a change of the normal cardiac function. On the other hand, pathological hypertrophy develops through different stimuli or diseases like hypertension, myocardial infarction and neurohumoral activation. In pathological hypertrophy, the ventricular walls increase drastically and the heart cannot preserve its normal function. Under persistent stress, pathological hypertrophy can lead to heart failure.

Physiological hypertrophy describes the normal heart growth during development, pregnancy or under exercise and can be reversible (Fig. 5) [132], [134]–[136]. In this context, the heart keeps its normal function and the increase in cardiac mass is mild, with a linear

increase of the heart weight-to-body weight ratio. Physiological hypertrophy is triggered by signals from growth hormones and mechanical forces, which can activate different signaling pathways including phosphoinositide 3-kinase, Akt, AMP-activated protein kinase and mammalian target of rapamycin [132], [137], [138]. Physiological hypertrophy is supposed to be harmless or even beneficial in healthy persons.

Pathological hypertrophy is defined as an increase in heart mass as a result of pressure overload, hypertensive stress, myocardial injury and excessive production of neurohumoral transmitters, and occurs in disorders like myocardial infarction, valvular diseases and hypertension (Fig. 5) [139]. Moreover, prolonged pathological cardiac hypertrophy can enhance the risk of heart failure and sudden death. Besides the increase and dilatation of the left ventricle, hypertrophy also induces an abnormal cardiac function, with lower ejection fraction and reduced systolic and diastolic functions [131]. Furthermore, pathological hypertrophy causes an increase of the heart weight-to-body weight ratio. At the cellular level, pathological hypertrophy leads to increased cardiomyocyte size, cell death, ventricular remodeling, enhanced protein synthesis, sarcomere disorganization, altered calcium handling and fibrosis [131]. In addition, the expression of the molecular fetal gene programe, including atrial natriuretic peptide, brain natriuretic peptide, skeletal α-actin and β-myosin heavy chain, is associated with pathological hypertrophy [140], [141].

Transverse aortic constriction (TAC) is used to induce cardiac hypertrophy in mice or rats by restraining the aorta to stimulate pressure overload in the heart (Fig.6) [142]. Hypertrophy can also be induced in animal hearts or cell cultures through treatment with α- or β-adrenergic-receptor agonists like phenylephrine and isoprenaline, or hormones like angiotensin II.

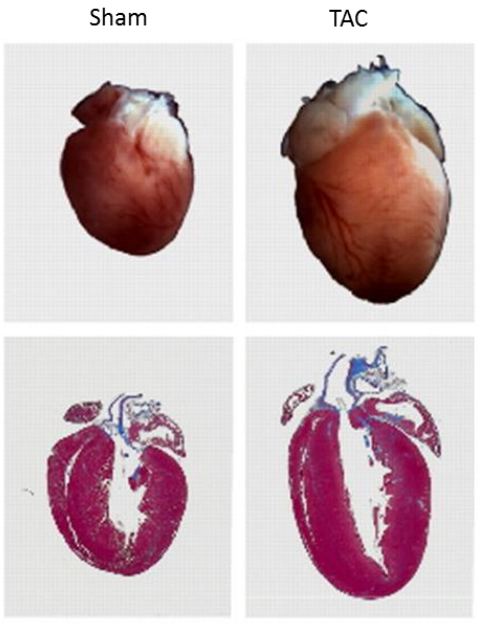

Modified from Cao *et al.*, 2011

Figure 6. Sham- and TAC-operated mouse hearts [143]
Pressure overload was induced by 10 weeks of TAC in WT mice (right), which led to an increase of heart size and thickening of ventricular walls compared to sham-operated mice (left). Accordingly, TAC-operated hearts developed hypertrophy after the surgery.

1.2.1. Role of calcium in the development of cardiac hypertrophy

Calcium has an important role in the development of cardiac hypertrophy. Elevation of intracellular Ca^{2+} levels in cardiomyocytes leads, through different Ca^{2+}-dependent signaling pathways, to an increase in protein synthesis and enlargement of the cells. One signaling pathway that is associated with Ca^{2+} in pathological hypertrophy is the calcineurin/nuclear factor of activated T cells (NFAT) signaling cascade [144]. Stimulation of the G-protein-coupled α_1-adrenergic receptors ($G_{\alpha q}$) by hormones or synthetic drugs activates phospholipase C (PLC), which triggers the production of inositol 1,4,5-triphosphate (IP3) and diacylglycerol (DAG) [131], [145]. The increase in IP3 levels induces the opening of IP3 receptors on the membrane of the sarcoplasmic reticulum and the release of Ca^{2+} ions from this compartment. The elevation of cytosolic Ca^{2+} levels activates the calcineurin/NFAT signaling pathway (Fig. 7). Calcineurin is a Ca^{2+}-activated serine-threonine protein phosphatase that dephosphorylates NFAT. Upon dephosphorylation, NFAT translocates to the nucleus and acts as a transcription factor, regulating the expression of hypertrophic genes [144]. In addition, elevated Ca^{2+} levels also activate calmodulin-dependent kinase II (CaMKII) and the nuclear factor-κB (NFκB) (Fig. 7). CaMKII, a serine/threonine kinase activated by Ca^{2+}/calmodulin, stimulates myocyte enhancer factor 2 (MEF2) signaling, which

alters gene expression and generates hypertrophy [146]. NFκB can translocate to the nucleus, after the degradation of its inhibitor, where it activates the expression of hypertrophy-related genes [147], [148].

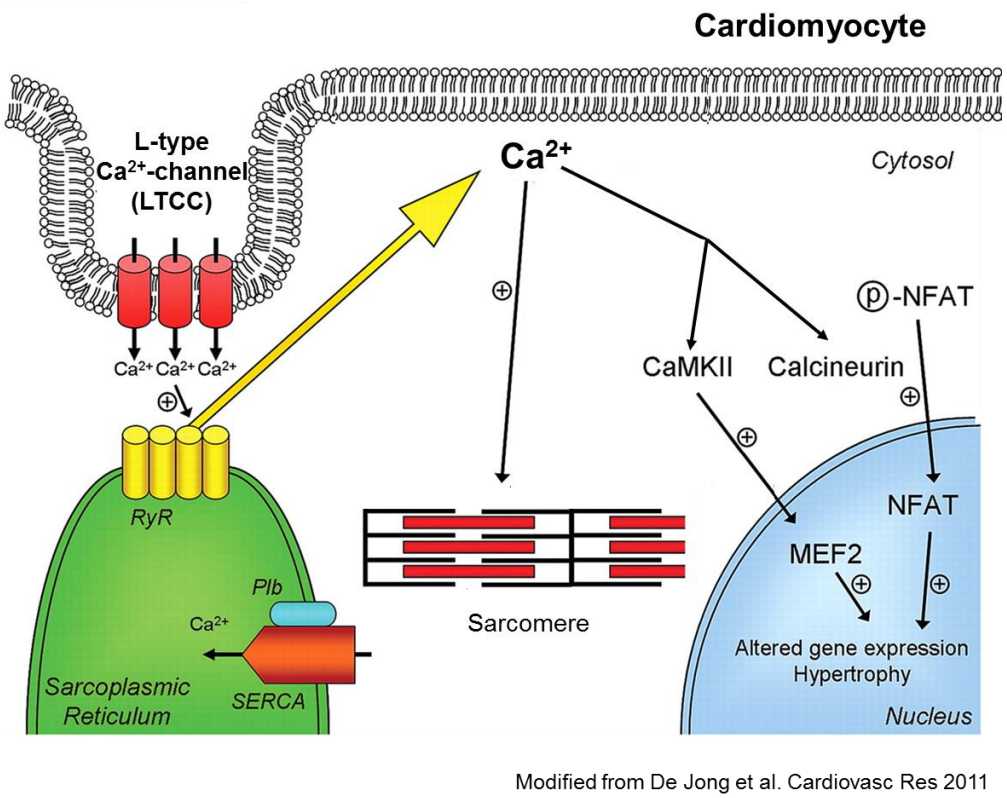

Modified from De Jong et al. Cardiovasc Res 2011

Figure 7. Ca^{2+} signaling mechanism in cardiomyocytes [149]
The plasma membrane depolarization in cardiomyocytes leads to the opening of L-type Ca^{2+} channels. Ca^{2+} can then flow to the cytosol, where it activates a calcium-induced calcium release from the sarcoplasmic reticulum via the ryanodine receptor (RyR). The increase of calcium in the cytosol activates contractile elements like the sarcomeres, which enables the cardiomyocyte to contract. After contraction, Ca^{2+} can enter the sarcoplasmic reticulum again through the sarcoplasmic reticulum Ca^{2+}-ATPase (SERCA), which is regulated by phospholamban (Pln). A calcium overload in the cytosol due to adrenergic stimulation or mechanical stress can activate hypertrophy signaling pathways. Ca^{2+} stimulates for example CaMKII and Calcineurin, which then activate the transcription factor MEF2 and NFAT. These transcription factors start the expression of hypertrophy-related genes.

In vitro, the stimulation of β-adrenergic receptors by agonists like isoprenaline also leads to pathological hypertrophy. The β-adrenergic receptors are G-protein-coupled receptors ($G_{\alpha s}$). The binding of catecholamines to these proteins can stimulate the adenylyl cyclase, which promotes the conversion of ATP into 3',5'-cyclic adenosinemonophosphate (cAMP). Subsequently, cAMP can stimulate the cAMP-dependent protein kinase (PKA), which can phosphorylate and activate many proteins involved in Ca^{2+} signaling pathways, including LTCCs and proteins of the sarcoplasmic reticulum membrane [150], [151]. This can lead to an increase in the cytosolic Ca^{2+} concentration of the cardiomyocyte that could activate

calcineurin/NFAT, CaMKII and NFκB signaling. However, the relevance of this mechanism *in vivo* remains still controversial.

1.2.2. LTCCs in cardiac hypertrophy

The calcium influx through LTCCs is the main initiator of excitation-contraction coupling in cardiomyocytes [150]. The entry of calcium by LTCCs triggers the calcium-induced calcium release from the sarcoplasmic reticulum, which leads to cardiomyocyte contraction (Fig. 7). The activation of α- and β-adrenergic signaling cascades leads to an increases in LTCC open probability and therefore to more calcium influx. This produces a calcium overload, which can activate the expression of hypertrophy-related genes. However, the role of LTCC activity in the development of cardiac hypertrophy remains contradictory [151]–[154].

Different studies have suggested that an increase in Ca^{2+} influx through LTCCs is associated with hypertrophy and remodeling of the ventricles. However, the mechanism behind that is not well understood [155]–[157]. Human patients with hypertrophic obstructive cardiomyopathy have upregulated $Ca_v\alpha_1$ and $Ca_v\beta_2$ subunit expression [158]. Moreover, it has been described that mice with overexpressed $Ca_v1.2$ subunits experience ventricle hypertrophy and remodeling [152], [159]. However, decreasing the LTCC currents can even have a negative impact on cardiac hypertrophy. Different reports described a decrease in LTCC activity during hypertrophy [154]. Moreover, a heterozygous cardiac-specific deletion of $Ca_v1.2$ in mice leads to a less than 50 % reduction of LTCC calcium currents [153]. Additionally, these heterozygous mice had increased cardiac hypertrophy and mortality after TAC, presumably due to a basal leakage of calcium from the ER that compensates the reduced calcium currents in these animals compared to the controls [153]. In accordance with these results, LTCC blockers like verapamil do not improve the health of patients with heart failure or even worsen cardiac hypertrophy [160]–[162]. Therefore, Ca^{2+} currents through LTCCs propably do not contribute to hypertrophy or heart failure. This would suggest that hypertrophy in cardiomyocytes is not dependent on LTCC activity.

The role of $Ca_v\beta_2$ in cardiac hypertrophy remains controversial. In 2011, Chen *et al* showed that the cardiac-specific overexpression of $Ca_v\beta_{2a}$ in transgenic mice elevates LTCC calcium currents and leads to the development of hypertrophy. However, it is important to remark that in this study they used $Ca_v\beta_{2a}$, a splice variant that is not predominantly expressed in

cardiomyocytes [163]. $Ca_v\beta_{2a}$ could have confered different electrophysiological properties to LTCCs as compared to $Ca_v\beta_{2b}$, and therefore has differentially influenced LTCC currents and a changed the outcome of this experiment.

In summary, the role of LTCC in cardiac hypertrophy is still controversial, with some authors reporting an increase in LTCC currents and others describing the opposite. It is important to note that the inhibition of LTCCs during hypertrophy in clinical trials does not have beneficial effects. Therefore, LTCC channel activity is presumably not important in hypertrophy and instead some LTCC-independent pathways could influence the progression and development of this pathology. Therefore, the role of LTCCs, and especially of its $Ca_v\beta_2$ subunit, in cardiac hypertrophy needs to be further elucidated.

1.2.3. Role of calpain in the development of cardiac hypertrophy

Calpains are cytosolic calcium-dependent cysteine proteases [164] that can be activated by the binding of Ca^{2+} [165]. The calpain activity is also controlled by the specific endogenous inhibitor calpastatin. The main calpain proteases in mammals are calpain 1 (μ) and calpain 2 (m), which are activated by different amounts of Ca^{2+} [165]. In muscle fibers, calpains 1 and 2 are localized in the Z disks, where they degrade sarcolemmal proteins [166]–[168]. The activity of calpain is highly specific to target proteins. Moreover, calpains are able to contribute to hypertrophy through hypertrophy-inducing signaling pathways [169].

A change in calpain activity or a dysregulation of the endogenous inhibitor calpastatin can influence the development of cardiac hypertrophy [148], [170], [171]. It has been shown that the stimulation of cardiomyocytes with angiotensin II (Ang II) increases calpain activity, which leads to the activation of the NFκB and calcineurin/NFAT pathways [148], [172].

In 2005, Burkard *et al* described that the increase in calpain activity induced by Ang II stimulation enhances the proteolysis of the autoinhibitory subunit of calcineurin by calpain [172]. Consequently, calcineurin activity rises and this leads to the dephosphorylation of NFAT. NFAT and the cleaved calcineurin then translocate to the nucleus, where NFAT activates the expression of hypertrophy-related gene [172].

Contrastingly, another group reported in 2008 the development of hypertrophy induced by Ang II through a NFAT-independent, but NFκB-dependent mechanism [148]. Additionaly,

they reported that Ang II stimulation increases the nuclear localization of the NFκB p65 subunit in cardiomyocytes, indicating its enhanced activity [148]. The binding of Ang II to $G_{\alpha q}$ protein-coupled receptors activates PLC and the production of IP3. IP3 triggers calcium release from the sarcoplasmic reticulum. This release of calcium promotes the activation of chromogranin B by calpain, which triggers NFκB activation and the expression of BNP [173], [174]. NFκB activation may also be linked to chromogranin B activation. Moreover, calpains contribute to the degradation of NFκB inhibitory proteins. This leads to the translocation of NFκB to the nucleus and to the expression of hypertrophy-related genes. From these two mechanisms, it can be concluded that increased calpain activity leads to enhanced NFκB activity and translocation to the nucleus, where the expression of hypertrophy-related genes is regulated [169], [175]. Together, these reports show that calpain stimulates the development of cardiac hypertrophy. Changes in calpain expression or activity can therefore influence hypertrophy-associated signaling pathways.

1.3. Aim of the project

Since the role of LTCCS in cardiac hypertrophy remains controversial, the aim of this project was to investigate the role of the $Ca_v\beta_2$ subunit during the development of this pathology. It is known that the $Ca_v\beta$ subunit can promote the trafficking of the $Ca_v\alpha_1$ subunit to the plasma membrane and changes its electrophysiological properties. Therefore, the $Ca_v\beta$ subunit can contribute to LTCC activation and to an increase in intracellular calcium levels, thereby inducing the activation of calcium-dependent signaling pathways that can trigger pathological hypertrophy. On the other hand, the $Ca_v\beta_2$ subunit might also regulate the expression of hypertrophy-related genes through non-LTCC related functions. To address the questions of whether and how $Ca_v\beta$ can modify cardiac hypertrophy, we used neonatal rat cardiomyocytes (NRCs) and adult mice as *in vitro* and *in vivo* models to induce hypertrophy. For this purpose, we worked with a combination of molecular and cell biological techniques.

2. Materials

2.1. Chemicals

Acetic acid (glacial) (100 %)	Merck, Darmstadt, GER
Acetonitrile (100 %)	Merck, Darmstadt, GER
Acrylamide solution	Carl Roth, Karlsruhe, GER
Ampicillin sodium salt	Carl Roth, Karlsruhe, GER
Ammonium persulfate (APS)	Sigma-Aldrich, Steinheim, GER
Aqua ad iniectabilia	B. Braun Melsungen, Melsungen, GER
Avicel® PH-101	Sigma-Aldrich, Steinheim, GER
BC Assay Reagent A	Interchim, Montluçon Cedex, FRA
Bovine Serum Albumin Fraction V (BSA)	Carl Roth, Karlsruhe, GER
5-Bromo-2'-deoxyuridine (BrdU)	Sigma-Aldrich, Steinheim, GER
2,3-Butanedione monoxime (BDM)	Sigma-Aldrich, Steinheim, GER
Caffeine	Sigma-Aldrich, Steinheim, GER
Calcium chloride dihydrate ($CaCl_2$ x $2H_2O$)	Sigma-Aldrich, Steinheim, GER
Calpeptin	Sigma-Aldrich, Steinheim, GER
Chloramphenicol	Merck, Darmstadt, GER
Crystal violet	Sigma-Aldrich, Steinheim, GER
ß-Mercaptoethanol	Sigma-Aldrich, Steinheim, GER
Dimetyl sulfoxide (DMSO)	Sigma-Aldrich, Steinheim, GER
DL-Dithiothreitol (DTT)	AppliChem, Darmstadt, GER
DL-Dithiothreitol (DTT)	Sigma-Aldrich, Steinheim, GER
Dulbecco's MEM	Biochrom, Berlin, GER
D-(+)-Glucose	Merck, Darmstadt, GER
D-(+)-Glucose	Sigma-Aldrich, Steinheim, GER
D-(+)-Glucose monohydrate	Merck, Darmstadt, GER
Ethanol Rotipuran® ≥ 99.8 % p.a.	Carl Roth, Karlsruhe, GER
Ethanol 96 % (denatured)	Brüggemann Alcohol Heilbronn, Heilbronn, GER
Ethanol 98 % (denatured)	Carl Roth, Karlsruhe, GER
Fetal bovine serum (heat inactivated) (FBS)	Gibco by Life Technologies, Grand Island, USA
Fetal Bovine Serum	Sigma-Aldrich, Steinheim, GER
Fura-2, AM	Life technologies, Eugene, USA
Glycerol	Merck, Darmstadt, GER
Glycine	Sigma-Aldrich, Steinheim, GER
Halt™ Protease Inhibitor Cocktail	Thermo Scientific, Rockford, USA
Hanks' balanced salt solution (HBSS)	Sigma-Aldrich, Steinheim, GER
Hydrochloric acid (5 M) (HCl)	Merck, Darmstadt, GER
4-(2-Hydroxyethyl) piperazine-1-ethanesulfonic acid (HEPES) buffer solution	Sigma-Aldrich, Steinheim, GER
HEPES sodium salt	AppliChem, Darmstadt, GER
HEPES sodium salt	Sigma-Aldrich, Steinheim, GER

ImmunoSelect®Antifading Mounting Medium DAPI	Dianova, Hamburg, GER
Iodoacetamide	Merck, Darmstadt, GER
Isoflurane	CP-Pharma, Burgdorf, GER
Isoprenaline hydrochloride	Sigma-Aldrich, Steinheim, GER
Kanamycin sulfate	Carl Roth, Karlsruhe, GER
Laminin, Mouse, Natural	BD Biosciences, Heidelberg, GER
Laminin	Roche, Mannheim, GER
LB-Agar-Powder according to Miller	AppliChem, Darmstadt, GER
LB-Medium-Powder according to Miller	AppliChem, Darmstadt, GER
Leica Microsystems™ Immersion Type G	Leica Microsystems, Wetzlar, GER
L-Glutamine Solution 200 mM	Sigma-Aldrich, Munich, GER
L-Glutamine 200 mM	Merck, Darmstadt, GER
L-Phenylephrine hydrochloride	Sigma-Aldrich, Steinheim, GER
Magnesium chloride hexahydrate ($MgCl_2$ x 6 H_2O)	Carl Roth, Karlsruhe, GER
Magnesium sulfate heptahydrate ($MgSO_4$ x 7 H_2O)	Merck, Darmstadt, GER
Magnesium sulfate heptahydrate ($MgSO_4$ x 7 H_2O)	Sigma-Aldrich, Steinheim, GER
Minimum Essential Medium Eagle with Hanks (MEM)	Sigma-Aldrich, Munich, GER
MEM/HANKS	Merck, Darmstadt, GER
Methanol Rotisolv® HPLC Gradient	Carl Roth, Karlsruhe, GER
N,N,N',N'-Tetramethylethylenediamine (TEMED)	Sigma-Aldrich, Steinheim, GER
Normal goat serum (NGS)	Sigma-Aldrich, Steinheim, GER
Opti-MEM I Reduced Serum Medium	Thermo Scientific, Rockford, USA
Paraformaldehyde solution 4 % in PBS	Santa Cruz Biotechnology, Dallas, USA
Paraformaldehyde 32 %	Science Services, Munich, GER
Penicillin-Streptomycin (P/S)	PAN-Biotech, Aidenbach, GER
Penicillin-Streptomycin (P/S)	Sigma-Aldrich, Steinheim, GER
Phenol:Chloroform:Isoamyl Alcohol 25:24:1	Sigma-Aldrich, Steinheim, GER
Pierce® ECL Western Blotting Substrate	Thermo Scientific, Rockford, USA
Pierce® RIPA Buffer	Thermo Scientific, Rockford, USA
Ponceau S solution	Sigma-Aldrich, Steinheim, GER
Potassium bicarbonate ($KHCO_3$)	Merck, Darmstadt, GER
Potassium chloride (KCl)	Merck, Darmstadt, GER
Potassium chloride (KCl)	Sigma-Aldrich, Steinheim, GER
Potassium dihydrogen phosphate (KH_2PO_4)	Carl Roth, Karlsruhe, GER
Potassium dihydrogen phosphate (KH_2PO_4)	Merck, Darmstadt, GER
Probenecid	Life technologies, Eugene, USA
Protease Inhibitor Cocktail tablets (cOmplete Mini)	Roche, Mannheim, GER
Sodium acetate buffer solution 3M	Sigma-Aldrich, Steinheim, GER
Sodium bicarbonate ($NaHCO_3$)	Merck, Darmstadt, Germany
Sodium bicarbonate ($NaHCO_3$)	Sigma-Aldrich, Steinheim, GER
Sodium chloride (NaCl)	Carl Roth, Karlsruhe, Germany
Sodium chloride (NaCl)	Merck, Darmstadt, Germany
Sodium dodecyl sulfate (SDS)	Sigma-Aldrich, Steinheim, GER
Sodium hydroxide pellets	Sigma-Aldrich, Steinheim, GER
Sodium hydroxide solution (2M) (NaOH)	AppliChem, Darmstadt, GER
Sodium phosphate dibasic (Na_2HPO_4)	Merck, Darmstadt, GER
Sodium phosphate dibasic (Na_2HPO_4)	Sigma-Aldrich, Steinheim, GER

Taurine	AppliChem, Darmstadt, GER
TE buffer (1 x) pH=8.0	AppliChem, Darmstadt, GER
Terralin® Liquid	Schülke & Mayer, Norderstedt, GER
Trifluoroacetic acid (TFA)	Merck, Darmstadt, GER
Titriplex III	Merck KGaA, Darmstadt, GER
Triton™ X100	Sigma-Aldrich, Steinheim, GER
Trizma® base	Sigma-Aldrich, Steinheim, GER
TRIzol® Reagent	Life technologies, Carlsbad, USA
Tween® 20	Sigma-Aldrich, Steinheim,GER
Universal Agarose	Bio & Sell, Nürnberg, GER
Urethane	Sigma-Aldrich, Steinheim, GER
UVAsol® Chloroform	Merck KGaA, Darmstadt, GER
UVAsol® Ethanol for spectroscopy	Merck KGaA, Darmstadt, GER
Vitamin B12	Sigma-Aldrich, Munich, GER
(±)-Verapamil hydrochloride	Sigma-Aldrich, Steinheim, GER
Water	Sigma-Aldrich, Steinheim, GER

2.2. Equipment

Analytical balance ALJ	KERN & SOHN, Balingen-Frommern, GER
Automated Cell Counter TC20™	Bio-Rad Laboratories, Munich, GER
Balance 1204 MP	Sartorius, Göttingen, GER
Biological Safety Cabinets Safe2020	Thermo Scientific, Rockford, USA
Centrifuge MIKRO 220R	Andreas Hettich, Tuttlingen, GER
Centrifuge Rotina 380R	Andreas Hettich, Tuttlingen, GER
Confocal Microscope TCS SP5	Leica Microsystems, Wetzlar, GER
CO_2 Incubator HERA Cell150i &240i	Thermo Scientific, Rockford, USA
CO2 Incubator HERA Cell 150	Thermo Scientific, Rockford, USA
FluorChem® HD2 System	Biozym Scientific, Hessisch Oldendorf, GER
Gel Logic 100 Imaging System	Eastman Kodak Company, Rochester, USA
Incubator B5042E	Heraeus, Hanau, GER
LightCycler® 480 Instument	Roche, Mannheim, GER
LTQ Orbitrap Elite mass spectrometer	Thermo Scientific, Rockford, USA
Magnetic stirrer IKA Combimag Ret	IKA®-Werke, Staufen, GER
Magnetic stirrer with heater	SunLab Germany, Mannheim, GER
Microscope Motic AE31	IonOptix Limited, Dublin, IRL
Microscope DMi1	Leica Microsystems, Wetzlar, GER
Microscope DMi8	Leica Microsystems, Wetzlar, GER
Microcentrifuge Heraeus™ Fresco™	Thermo Scientific, Rockford, USA
Mikro Dismembrator U	Sartorius, Göttingen, GER
Mini centrifuge	A. Hartenstein, Würzburg, GER
Minishaker MS1	IKA®-Werke, Staufen, GER
Multifuge 1 S-R	Thermo Scientific, Waltham, USA

Myocyte and Contractility System	IonOptix Limited, Dublin, IRL
pH meter p525	WTW, Weilheim, GER
pH meter p537	WTW, Weilheim, GER
Power Supply	CONSORT nv, Turnhout, BEL
Power Supply	VWR International, Radnor, USA
Precision balance	Sartorius, Göttingen, Germany
Precision balance PLJ	KERN & SOHN, Balingen-Frommern, GER
Saftey Cabinet Heraeus® HERAsafe® KS	Heraeus, Hanau, GER
Shaker Unimax 1010 Incubator 1000	Heidolph Instruments, Schwabach, GER
Thermocycler T1	Biometra, Göttingen, GER
Thermomixer® C	Eppendorf, Hamburg, GER
Thermomixer® compact	Eppendorf, Hamburg, GER
UltiMate 3000 RSLCnano system	Thermo Scientific, Rockford, USA
Vacuum concentrator (RVC2-25CD plus)	Martin Christ Gefriertrocknungs-anlagen, Osterode am Harz, GER
Wallac Victor^2 1420 Multilabel Counter	Perkin Elmer, Turku, FIN
Water bath	GFL Gesellschaft für Labortechnik, Burgwedel, GER
Water bath alpha	LAUDA,Lauda-Königshofen, GER
Water bath TW 12	JULABO, Seelbach, GER
Water bath WNB 45	Memmert, Büchenbach, GER

2.3. Enzymes

All enzymes for cloning or restriction control experiments were purchased from NewEngland Biolabs, Frankfurt, Germany. All enzymes bought from other companies are listed in the following:

Deoxyribonuclease I from bovine pancreas (DNase)	Sigma-Aldrich, Steinheim, GER
Liberase DH	Roche, Mannheim, GER
LR Clonase® II enzyme mix	Life Technologies, Darmstadt, GER
Proteinase K	Thermo Scientific, Rockford, USA
Trypsin	Serva, Heidelberg, GER
Trypsin	Sigma-Aldrich, Steinheim, GER
Trypsin 250	BD Biosciences, Heidelberg, GER

2.4. Protein and DNA standards

All protein or DNA ladders were purchased from Thermo Scientific, Rockford, USA.

2.5. Kits

BLOCK-iT™ Adenoviral RNAi Expression System	Life Technologies, Darmstadt, GER
Calpain-Glo™ protease assay	Promega, Madison, USA
High Fidelity PCR Master	Roche, Mannheim, GER

LightCycler®480 Probes Master	Roche, Mannheim, GER
Nucleo Spin® Plasmid Miniprep kit	Marchery-Nagel, Düren, GER
pAd/CMV/V5-DEST™ Gateway® Vectors	Life Technologies, Darmstadt, GER
pAd/PL-DEST™Gateway® Vectors	Life Technologies, Darmstadt, GER
Qiaquick gel purification	Qiagen, Hilden, GER
QuantiTect® Reverse Transcription Kit	Qiagen, Hilden, GER
Quick Ligation Kit	New England Biolabs, Frankfurt, GER
Subcellular Protein Fractionation Kit for Tissue	Thermo Scientific, Rockford, USA
Subcellular Protein Fractionation Kit for Cultured Cells	Thermo Scientific, Rockford, USA
X-tremeGENE HP DNA Transfection Reagent	Roche, Mannheim, GER

2.6. Buffers and solutions

Ampicillin (100 mg/ml)	0.1 g Ampicillin in 1 ml dH_2O
APS (10 %)	0.1 g APS in 1 ml dH_2O
Avicel (1.2 %)	1.2 g Avicel in 100 ml dH_2O
BDM (500 mM)	5.05 g in 100 ml dH_2O
BrdU (20 mM)	1 g BrdU in 162 ml dH_2O
BSA (5 %)	5 g BSA in 100 ml TBS-T (1x)
Buffer A	10 mM ammonium bicarbonate in dH_2O, pH 8.3
Buffer B	Buffer A + 100% acetonitrile in a ratio of 50:50 (v/v)
Calcium and bicarbonate-free Hanks with HEPES (CBFHH)	8 g NaCl 0.4 g KCl 0.2 g $MgSO_4$ x 7 H_2O 1 g D (+) Glucose monohydrate 0.06 g KH_2PO_4 0.048 Na_2HPO_4 4.77 g HEPES, pH 7.4 pH 7.4 Fill up to 1 L with dH_2O
Calpeptin (1 mM)	13 ml DMSO for solving the powder
Caffeine	34.4 mg of Caffeine in 2 ml of Ca^{2+} Tyrode
$CaCl_2$ (1 M)	7.35 g $CaCl_2$ x 2 H_2O in 50 ml dH_2O
$CaCl_2$ (100 mM)	147 mg $CaCl_2$ x 2 H_2O in 10 ml dH_2O
Calcium Tyrode	1 L of Normal Tyrode 1 ml of $CaCl_2$ (1 M)
CBFHH solution	100 ml CBFHH 1 ml Pen/Strep
Chloramphenicol (5 mg/ml)	0.05 g Chloramphenicol in 1 ml Ethanol (99.8 %)
Crystal violet (1 %)	1 g Crystal Violet 100 ml 20 % Ethanol

$CuSO_4$	4g $CuSO_4$ in 100 ml dH_2O
Digestion buffer	150 µl Liberase stock solution 450 µl Trypsin stock solution 3.75 µl $CaCl_2$ (100 mM) Fill up 30 ml of perfusion buffer
DMEM (2 % FBS)	DMEM, 2 % FBS, 1 % L-Glutamine, 1 % P/S
DMEM (10 % FBS)	DMEM, 10 % FBS, 1 % L-Glutamine, 1 % P/S
DNase (2 mg/ml)	40 mg DNase + 20 ml NaCl Store at -20 °C
DTT (1 M)	1.54 g of DDT Fill up to 10 ml with dH_2O Store at -20 °C
EDTA (0.5 M) (ethylenedinitrilotetraacetic acid)	186.12 g Titriplex III pH 8.0 Fill up to 1 L with dH_2O
Fura 2-AM (1 mM)	lyophilized Fura 50 µl DMSO Store at -20 °C in the dark
Fura-2-AM (working solution)	4 µl Fura (1 mM) + 4 µl of Probenecid (250 mM) in 2 ml normal tyrode
Kanamycin (100 mg/ml)	0.1 g Kanamycin in 1 ml dH_2O
Laminin (BD)	6 µl in 1 ml PBS
LB-Agar (40 g/L)	40 g LB-Agar in 1 L dH_2O
LB-Medium (25 g/L)	25 g LB-Medium in 1 L dH_2O
Liberase stock solution	90 mg Liberase In 50 ml of dH_2O Store at -20 °C
MEM0	10.8 g MEM Powder 10 ml Pen/Strep 1 ml Vitamine B12 350 mg $NaHCO_3$ 10 ml L-Glutamine Fill up to 1 L with Aqua ad iniectabilia
MEM5 without BrdU	MEM 0, 5 % FBS
MEM5	MEM 0, 5 % FBS, 0.5 % BrdU
Normal Tyrode	8.18 g NaCl 0.3 g KCl 0.2 g $MgCl_2$ 1.8 g Glucose 1.19 g HEPES pH 7.4 Fill up to 1 L with dH_2O
PFA (8 %)	10 ml PFA 32% 30 ml PBS

PBS (10 x)	80 g NaCl 2 g KCl 14.4 g Na_2HPO_4 2.4 g KH_2PO_4 Fill up to 1 L with dH_2O
PBS (1 x)	900 ml dH_2O 100 ml 10x PBS
Perfusion buffer (10 x)	65.99 g NaCl 3.51 g KCl 816.6 mg KH_2PO_4 1067.9 mg Na_2HPO_4 x 2 H_2O 2958.0 mg $MgSO_4$ x 7 H_2O 10.08 g $NaHCO_3$ 10.1 g $KHCO_3$ 23.83 g HEPES 37.53 g Taurine Fill up to 1 L with dH_2O
Perfusion buffer	980 ml Perfusion buffer (1x) 20 ml BDM 0.991 g Glucose
Plaque medium (2 x)	DMEM, 5 % FBS, 2 % L-Glutamin, 2 % P/S
Plating medium	1.078 g MEM/Hanks 0.088 g $NaHCO_3$ 5 ml FBS 2 ml BDM (500 mM) 1 ml P/S Fill up to 10 ml with dH_2O
Phenylephrine (10 mM)	0.02 g phenylephrine Fill up to 10 ml with dH_2O Store at -20 °C
Probenecid (250 mM)	Probenecid 1 ml HBSS Store at -20 °C
SDS (10 %)	5 g SDS Fill up to 50 ml with dH_2O
SDS Loading Buffer (5 x)	0.23 ml dH_2O 2.25 ml Tris 1 M, pH 6.8 0.5 g SDS 5.0 ml Glycerol 100 % 2.5 ml DTT 1 M 5.0 mg Bromophenol blue
SDS Running Buffer (10 x)	30.3 g Trizma 144.0 g Glycine 10.0 g SDS fill up to 1 L with dH_2O
SDS Running Buffer (1 x)	900 ml dH_2O 100 ml 10 x SDS Running Buffer

Sodium hydroxide solution (1 M)	20 g NaOH Fill up to 0.5 L with dH_2O
Stripping buffer	7,6 g Tris Base 20 g SDS pH 6,7 fill up to 1 L with dH_2O
Stop buffer I	9 ml perfusion buffer 1 ml FBS (10 %) 1.25 µl $CaCl_2$ 100 mM
Stop buffer II	28.5 ml perfusion buffer 1.5 ml FBS (5 %) 3.75 µl $CaCl_2$ 100 mM
TAE (50 x)	242 g Tris Base 57.1 ml Acetic acid 100 ml 0.5 M EDTA pH 8.0 fill up to 1 L with dH_2O
TAE (1 x)	20 ml 50x TAE Fill up to 1 L with dH_2O
TBS (10 x)	12.1 g Trizma 87.7 g NaCl pH 7.4 fill up to 1 L with dH_2O
TBS-T (1 x)	900 ml dH_2O 100 ml 10x TBS 1 ml Tween
Tris 1 M	12.11 g Trizma pH 6.8 fill up to 100 ml with dH_2O
Tris 1.5 M	18.15 g Trizma pH 8.8 fill up to 100 ml with dH_2O
Triton (1 %)	100 µl Triton fill up to 10 ml with dH_2O
Trypsin + DNase solution (T & D)	12.5 mg Trypsin per rat pup 2 ml DNase 250 ml CBFHH
Trypsin for mass spectrometry	0.015 µg/µl in buffer A
Trypsin stock solution	500 mg Trypsin in 50 ml dH_2O Store at -20 °C
Urethane	1 g Urethane in 1.5 ml dH_2O
Verapamil (10 mM)	0.0049 g Verapamil 1 ml dH_2O
Vitamine B12 (2 mg/ml)	50 mg Vitamine B12 in 25 ml dH_2O Store at -20 °C
Western blot stripping buffer	7.6 g Trizma (62.5 mM) 20 g SDS (2%) pH 6,7

	fill up to 1 L with dH_2O
Western blot transfer buffer (10 x)	30.3 g Trizma 144 g Glycine
Western blot transfer buffer (1 x)	700 ml dH_2O 100 ml 10x transfer buffer 200 ml Methanol

2.7. Other materials

Amersham Protran 0.2 µm NC nitrocellulose	GE Healthcare, Freiburg, GER
Amicon Ultra-15-100K	Merck KGaA, Darmstadt, GER
Blotting Paper	A. Hartenstein, Würzburg, GER
Bottle Top Filter	Thermo Scientific, Rockford, USA
Cell Culture Dishes, 60/15 mm	Greiner Bio-One, Frickenhausen, GER
Cell Culture Flasks 75 cm^2	Greiner Bio-One, Frickenhausen, GER
Cell Culture Multiwell Plate, 6 well, Collagen Type I	Greiner Bio-One, Frickenhausen, GER
Cell Scraper 16 cm	Sarstedt, Nümbrecht, GER
Cell Strainer 70 µm Nylon	Corning, Kaiserslautern, GER
Cover Glass Square #1 (25x25)	Corning, Kaiserslautern, GER
CryoTube™ Vials	Thermo Scientific, Rockford, USA
ImmEdge-Pen	LINARIS Biologische Produkte, Dossenheim, GER
Microplates (96-well)	Thermo Scientific, Rockford, USA
Microscope Cover Glass (24x24)	Paul Marienfeld, Lauda-Königshofen, GER
Mini-Protean Tetra Cell System	Bio-Rad, Hercules, USA
NEB 5-alpha Competent *E. coli* (High Efficiency)	New England Biolabs, Frankfurt, GER
Objektträger Superfrost® Plus	Gerhard Menzel, Braunschweig, GER
Pasteur Pipettes (one time use)	A. Hartenstein, Würzburg, GER
Pasteur Pipettes	Kimble Chase, Meiningen, GER
Pasteur Pipettes 150 mm	A. Hartenstein, Würzburg, GER
PerfectBlue™ Vertical Double Gel Systems TwinExWS	VWR International, Radnor, USA
Quick Screen Electrophoresis System	IBI Scientific, Dubuque, USA
Serological Pipettes (5 ml, 10 ml, 25 ml, 50 ml)	Greiner Bio-One, Frickenhausen, GER
Tissue Culture dishes Nunclon™ Delta Surface (60 x 15 mm, 100 x 17 mm, 150 x 18 mm)	Thermo Scientific, Roskilde, DNK
Tissue Culture Plate (6-well) Nunclon™ Delta Surface	Thermo Scientific, Roskilde, DNK
Tubes (15 ml, 50 ml)	Greiner Bio-One, Frickenhausen, GER
Tubes (15 ml, 50 ml)	Sarstedt, Nümbrecht, GER
Wide tip serological pipettes (10 ml)	A. Hartenstein, Würzburg, GER

2.8. Primers and Universal ProbeLibrary probes

All primers were purchased from Sigma Life Science (Munich, GER). A stock solution of 100 µM was prepared in TE buffer according to the datasheet from Sigma.

Table 2. Primers for PCR or qRT-PCR reaction

Name	5´→3´-Sequence	Method used
Sense SH3	AAAAAAGCTAGCATGGGTTCGGCAGACTCCTACACCAGC	NLS construct
Antisense GK	TGCTCACCATGCGGCCGCAGTTGGGGAGGTTACTGCTGGGAG	NLS construct
Sense NT	CCCAAGCTGGCTAGCATGCTG	NLS construct
Antisense LK	TGCTCACCATGCGGCCGCATGGTACCACATCGTAAGGAGGAGTGTG	NLS construct
Sense GK	GGCTACAGCATGAACAGAGAGCCAAGTCCATGAGACCAGTGGTGTTGGTG	NLS construct
Antisense CT	TCCTCGCCCTTGCTCACCATG	NLS construct
Antisense SH3	CTTGGCTCTCTGTTCATGCTGTAGCC	NLS construct
Sense YFP pENTRc	AAAAAAGGATCCATGGTGAGCAAGGGCGAGGAG	Adenovirus
Antisense YFP pENTR3c	AGATATCTCGAGTTACTTGTACAGCTCGTCCATGCCG	Adenovirus
Sense b2b NLS WT	AAAAAAGGATCCATGCCGCCGAAAAAAAAACGCAAAGTGCTGGATCGCCAGCTGGTGAGC	Adenovirus
Sense shRNA18	CACCGGTGTCTTCTCAGACTCAATCCGAAGATTGAGTCTGAGAAGACACC	Adenovirus
Antisense shRNA18	AAAAGGTGTCTTCTCAGACTCAATCTTCGGATTGAGTCTGAGAAGACACC	Adenovirus
Sense shRNA338	CACCGCTGTGAAATCGGATTTATTCCGAAGAATAAATCCGATTTCACAGC	Adenovirus
Antisense shRNA3388	AAAAGCTGTGAAATCGGATTTATTCTTCGGAATAAATCCGATTTCACAGC	Adenovirus
Sense shRNA508	CACCGCTATAGACATAGATGCTACTCGAAAGTAGCATCTATGTCTATAGC	Adenovirus
Antisense shRNA508	AAAAGCTATAGACATAGATGCTACTTTCGAGTAGCATCTATGTCTATAGC	Adenovirus
Sense shRNA892	CACCGCGGAAGTTCAGAGTGAAATTCGAAAATTTCACTCTGAACTTCCGC	Adenovirus
Antisense shRNA882	AAAAGCGGAAGTTCAGAGTGAAATTTTCGAATTTCACTCTGAACTTCCGC	Adenovirus
Sense shRNAsc	CACCGGTCTTCGACTTCATGCAATCCGAAGATTGAGTCTGAGAAGACACC	Adenovirus
Antisense shRNAsc	AAAAGGTGTCTTCTCAGACTCAATCTTCGGATTGCATGAAGTCGAAGACC	Adenovirus
Sense mb2a UPL16	GCGAGTACGGGTGTCCTATGGTTC	qRT-PCR
Sense mb2b UPL16	CTCAATCCAGTATTCCTGGGGGTTC	qRT-PCR
Sense mb2c-d UPL16	AACAGTTTTGTCCGCCAGGGTTC	qRT-PCR
Sense mb2e UPL16	CTGAAGAGTTCGGACATCTGTGGTTC	qRT-PCR
Antisense b2 NT UPL16	CTGCCGCTCAGCTTCTCTAC	qRT-PCR
Sense Rpl13 UPL16	CTCGGCCGTTCTCCTGTA	qRT-PCR
Antisense Rpl13 UPL16	TTGTGGAAGTGGGGCTTC	qRT-PCR

For qRT-PCR the Universal ProbeLibrary probe 16 (UPL 16) (GGAGGCAG) from Roche, Mannheim, GER was used. UPLs are short FAM-labeled hydrolysis probes.

2.9. Plasmids and Adenoviruses

The following table (Table 3) is showing the plasmids that were produced and used during this work. The gene sequences necessary for planning the cloning strategy were obtained from NCBI or Ensembl. The design and strategic planning for the production of these plasmids was done with the help of Vector NTI (Thermo Scientific, Rockford, USA). The vector pcDNA3.1 (-) and the Gateway™ pENTR™ 3C Dual Selection Vector were purchased from Thermo Scientific, Rockford, USA. The plasmid pEYFP-C1 was obtained from Clonetech, Mountain View, USA.

Table 3. Produced Plasmids

Name of construct	Plasmid backbone	Inserted gene or sequence	Antibiotic resistence
shRNA18	pENTR3c	For inserted sequence see Table 2 primer for PCR for respective shRNA	Kanamycin
shRNA338	pENTR3c	For inserted sequence see Table 2 primer for PCR respective shRNA	Kanamycin
shRNA508	pENTR3c	For inserted sequence see Tab. 2 primer for PCR respective shRNA	Kanamycin
shRNA892	pENTR3c	For inserted sequence see Table 2 primer for PCR respective shRNA	Kanamycin
shRNAsc	pENTR3c	For inserted sequence see Table 2 primer for PCR respective shRNA	Kanamycin
YFP	pENTR3c	YFP from pEYFP-C1 vector (Clontech, Mountain View, USA)	Kanamycin
$Ca_v\beta_{2b}$-YFP	pENTR3c	$Ca_v\beta_{2b}$ (Accession number:XM_006254303; *Rattus norvegicus*) + YFP	Kanamycin
NLS-$Ca_v\beta_{2b}$-YFP	pENTR3c	SV40 large T antigen (PPKKKRKV) + $Ca_v\beta_{2b}$(Accession number: XM_006254303) + YFP	Kanamycin
YFP	pcDNA3.1.	YFP from pEYFP-C1 vector	Ampicillin
$Ca_v\beta_{2b}$ YFP	pcDNA3.1.	$Ca_v\beta_{2b}$-YFP	Ampicillin
$Ca_v\beta_{2b}\Delta$ NT/CT YFP	pcDNA3.1.	$Ca_v\beta_{2b}$ without NT and CT (AS 1-17 and 421-605))	Ampicillin
$Ca_v\beta_{2b}\Delta$ GK/CT YFP	pcDNA3.1.	$Ca_v\beta_{2b}$ without GK and CT (AS 226-605)	Ampicillin
$Ca_v\beta_{2b}\Delta$ CT YFP	pcDNA3.1.	$Ca_v\beta_{2b}$ without CT (AS 421-605)	Ampicillin
$Ca_v\beta_{2b}\Delta$ NT YFP	pcDNA3.1.	$Ca_v\beta_{2b}$ without NT (AS 1-17)	Ampicillin
$Ca_v\beta_{2b}\Delta$NT/Hook/CT YFP	pcDNA3.1.	$Ca_v\beta_{2b}$ without NT, Hook, and CT (AS 1-17, 138-225 and 421-605)	Ampicillin
$Ca_v\beta_{2b}\Delta$ NT/SH3 YFP	pcDNA3.1	$Ca_v\beta_{2b}$ without NT and SH3 (AS 1-17 and 18-137)	Ampicillin

2.10. Composition of SDS gels

All SDS gels were used at 8, 10 or 12 % according to the molecular weight of the proteins to detect. The composition of the resolving and stacking gels is shown in Table 4 and 5, respectively.

Table 4. Composition of resolving gels with different percentages of acrylamide

	8 %	**10 %**	**12 %**
dH_2O	4.62 ml	3.96 ml	3.3 ml
Tris 1.5 M, pH 8.8	2.5 ml	2.5 ml	2.5 ml
SDS (10 %)	100 µl	100 µl	100 µl
Acrylamide	2.67 ml	3.33	4.0
APS (10 %)	100 µl	100 µl	100 µl
TEMED	10 µl	10 µl	10 µl

Table 5. Composition of stacking gel

	Volume
dH_2O	3.05 ml
Tris 1.0 M, pH 8.8	1.2 ml
SDS (10 %)	50 µl
Acrylamide	650 µl
APS (10 %)	25 µl
TEMED	5 µl

2.11. Cell lines and Animals

HEK293A cells were purchased from Thermo Scientific, Rockford, USA. Pregnant Wistar rats were ordered from Charles River Laboratories, Sulzfeld, Germany. Adult mice for TAC surgery were also ordered from Charles River Laboratories at an age of 5 weeks. The mice used for RNA isolation, whole heart lysates or cell fractionation experiments were 3-month old. The animals were bred in the own mouse facility of the Institute of Physiology, Würzburg, GER.

2.12. Antibodies

The following primary and secondary antibodies were purchased from different companies and used either for western blot or for immunofluorescence (Table 6 and 7).

Table 6. Primary antibodies

Antibody	Host	Protein molecular weight	Company	Method
α-actinin	mouse	100kDa	Sigma-Aldrich, St. Louis, USA	Immunofluorescence
Calpastatin	mouse	126 kDa	Santa Cruz Biotechnology, Heidelberg, GER	Western blot
$Ca_v\beta_2$	rabbit	72 kDa	Atlas Antibodies AB, Stockholm, Sweden	Western blot/Immunofluorescence
$Ca_v\beta_2$	rabbit	72 kDa	Novus Biologicals, Abingdon, UK	Western blot/Immunofluorescence
$Ca_v\beta_{2b}$	rabbit	72 kDa	Own production	Western blot/Immunofluorescence
$Ca_v1.2$	rabbit	250 kDa	Alomone labs, Jerusalem, Israel	Western blot/Immunofluorescence
GAPDH	rabbit	37 kDa	Cell Signaling Technology, Frankfurt, GER	Western blot
GFP (YFP)	rabbit	27 kDa	Abcam, Cambridge, UK	Western blot
Histone H3	rabbit	15 kDa	Abcam, Cambridge, UK	Western blot
Na^+ K^+ ATPase	rabbit	100 kDa	Abcam, Cambridge, UK	Western blot
RYR2	mouse	565 kDa	Thermo Scientific, Rockford, USA Germany	Immunofluorescence

Table 7. Secondary antibodies

Antibody	Host	Tag	Company	Method
mouse	goat	Cy3	Thermo Scientific, Rockford, USA	Immunofluorescence
rabbit	goat	HRP	Jackson Immuno Research laboratories, West Grave, USA	Western blot
rabbit	goat	Alexa Fluor™ 488	Thermo Scientific, Rockford, USA	Immunofluorescence
mouse	goat	HRP	Jackson Immuno Research laboratories, West Grave, USA	Western blot
mouse	goat	Alexa Fluor™ 488	Thermo Scientific, Rockford, USA	Immunofluorescence
mouse	goat	Alexa Fluor™ 633	Thermo Scientific, Rockford, USA	Immunofluorescence

The secondary antibodies used for western blot were tagged with horseradish peroxidase (HRP) for the development of the membranes with ECL reagent. For immunofluorescence,

antibodies were tagged with different Alexa Fluor tags or Cy3 to evaluate the cells by fluorescence or confocal microscopy.

2.13. Programs and databases

Table 8. Programs and databases

Programs/Databases	Company	Task
Alpha View® Software	AlphaInnotech, Kasendorf, GER	Pictures of western blots
Ensembl	http://www.ensembl.org/index.html	Genom database, sequencing
IonWizard 6.3	IonOptixLimited, Dublin, IRE	Analysis of Ca^{2+} measurements
LAS X	Leica Microsystems, Wetzlar, GER	Software for taking fluorescence images
LightCycler® 96	Roche, Mannheim, GER	qRT-PCR
LS AF Lite	Leica Microsystems, Wetzlar, GER	Software for taking confocal pictures
Microsoft Excel	Microsoft Corporation, Redmond, USA	Calculation and graphing tool
Mascot search algorithm (version 2.5)	Matrix Science Ltd., London UK	Analysis of raw files from mass spectrometry
Molecular Imaging Software	Eastman Kodak Company, Rochester, USA	Pictures of agarose gels
National Center for Biotechnology (NCBI)	http://www.ncbi.nlm.nih.gov/pubmed?otool=ideubwlib	Gene informations, sequencing
Progenesis QI software	Nonlinear Dynamics, Newcastle, UK	Label-free quantification of peptides
Proteom Discoverer software (ver. 1.4.1.14)	Thermo Scientific, Rockford, USA	Protein identification
UniProtKB/Swiss-Prot	https://www.uniprot.org/	Analysis of raw files from mass spectrometry
Universal ProbeLibrary Assay Design Center	https://lifescience.roche.com/en_de/brands/universal-probe-library.html#assay-design-center	Design of probes for qRT-PCR
Image J	Wayne Rasband, National Institute of Health, USA	Western blot quantification, cell area measurement, fluorescence intensity measurement
Vector NTI	Thermo Scientific, Rockford, USA	Strategies for cloning and restriction analysis, sequence analysis

3. Methods

3.1. Molecular biology

For knockdown of $Ca_v\beta_{2b}$ (Accession Number XM_006254303) by short hairpin RNA (shRNA) in NRCs, appropriate complementary single-stranded DNA oligonucleotides were designed using the Block-iT™ RNAi designer platform (Thermo Fisher Scientific). Complementary oligonucleotides for each construct were annealed at 55°C and cloned, according to the manufacturer´s instructions, into the pENTR™/U6 entry vector using the Block-iT™ U6 RNAi entry vector kit (Thermo Fisher Scientific). The sequences of the complementary single-stranded DNA primers used are displayed in section 2.8 (shRNAsc, shRNA18, shRNA338, shRNA508 and shRNA892) and the generated plasmids in section 2.9.

For protein overexpression, the YFP sequence of the vector pEYFP-C1 was amplified by PCR and cloned into the pENTR™3c vector to produce the pENTR3c-YFP plasmid. To produce the plasmid pENTR3c-$Ca_v\beta_{2b}$-YFP, the rat $Ca_v\beta_{2b}$ gene (Accession Number XM_006254303) from the pcDNA3.1 (-) $Ca_v\beta_{2b}$-CFP vector [176] was amplified by PCR and this fragment was inserted in-frame upstream of the YFP sequence into the pENTR3c-YFP plasmid using standard overlapping PCR methods. The pENTR3c-NLS-$Ca_v\beta_{2b}$-YFP plasmid was generated by inserting the nuclear localization signal (NLS) of the SV40 large T antigen (PPKKKRKV) at the N-terminus of $Ca_v\beta_{2b}$ in the pENTR3c-$Ca_v\beta_{2b}$-YFP vector using standard overlapping PCR methods.

For protein overexpression of $Ca_v\beta_{2b}$-YFP constructs missing different structural regions, $Ca_v\beta_{2b}$-YFP was amplified by PCR from the plasmid pENTR3c-$Ca_v\beta_{2b}$-YFP. This fragment was cloned into the pcDNA3.1 (-) vector. To generate constructs missing different structural regions, specific primers for the amplification of the distinct regions were used (section 2.9) and inserted in frame upstream of the YFP sequence of the pcDNA3.1 (-) vector. The constructs were produced by standard overlapping PCR methods. The 6 different constructs are displayed in section 2.9.

3.1.1. PCR reaction

For PCR reaction, the following reagents from Roche High Fidelity PCR Master were mixed (Table 9).

Table 9. PCR reagent mix

Reagent	Volume
Mastermix	12.5 µl
Primer sense (10 µM)	1 µl
Primer antisense (10 µM)	1 µl
DNA	100 ng
dH_2O	Up to 25 µl

The PCR reaction mix was placed in a thermocycler with the following PCR program (Table 10).

Table 10. PCR program for Roche High Fidelity PCR Master

Time	Temperature in °C	
2 min	94	
10 s	94	10 x
1 min10 s	Depending on primer	
1 min	72	
15 s	94	35 x
30 s	Depending on primer	
1 min	72	
5 min	72	
∞	4	

After the PCR program was finished the product size of the PCR reaction mix was examined on a 1-2 % TAE agarose gel containing SYBRSafe. If necessary for futher working steps, the product was extracted from the gel and purified with the QIAquick gel purification kit according to the manufacturer's instructions. The purified DNA was stored at 4 °C until further use.

3.1.2. Restriction and ligation reactions

To ligate the PCR inserts with a vector backbone both of them were cut with the same restriction enzymes. The corresponding restriction enzymes had to be choosen according to the sequence of the vector and the insert. The restriction reaction was set up like in Table 11 shown.

The restriction mix was placed for 2-3 h at 37 °C. The restriction fragments were separated in a 1-2 % TAE agarose gel. The right sized fragments were cut out of the gel and purified with the QIAquick gel purification kit according to the manufacturer's instructions.

Table 11. Restriction reaction of Vector/Insert

Component	Volume
DNA	Vector: 2-3 µg / Insert: PCR product
Restriction enzyme I	1-2 µl
Restriction enzyme II	1-2 µl
10x Enzyme buffer	1/10 of final volume
dH_2O	Fill up to same volume for Vector and Insert

Subsequently, the ligation of vector and insert was performed with the Quick Ligation Kit. Therefore, the components in Table 12 were mixed and incubated for 10 min at 22 °C. The ligation mix was immediately processed afterwards.

Table 12. Ligation mix

Component	New contruct	Negative control
Vector	2 µL	2 µL
Insert	8 µl	--
Quick Ligation Buffer (2x)	10 µl	10 µl
Quick Ligase	1 µl	1 µl
dH_2O	--	8 µl

3.1.3. NEB 5-alpha competent *E.coli* transformation and overnight culture

Transformation of NEB 5-alpha competent *E.coli* cells was performed according to the providers's instruction. For transformation, 7 µl of ligation product or 100 ng of plasmid DNA were mixed with the cells and kept on ice for 20 min. Cells were then heat-shocked for 1 min at 42 °C and incubated at 37 °C with 300 µl of LB medium. They were then plated on a selection plate and incubated at 37 °C overnight. On the next day, the growth of the colonies was checked and the plate was stored at 4 °C.

To prepare overnight cultures for plasmid mini preparations, LB medium was mixed with 100 µg/ml of the corresponding antibiotic. For each overnight culture, one colony from the transformation plate was picked. The cultures were incubated overnight at 37 °C while shaking. On the next day, a mini preparation was performed with the Nucleo Spin® Plasmid

Miniprep Kit according to the manufacturer's instructions. The concentration of the plasmid DNA was measured using a NanoDrop spectrophotometer and stored at 4 °C until use.

To reassure the cloning was successful and the correct plamid DNA was generated, restriction controls of the plasmids were done. We prepared a restriction mixture containing 1 µg of plasmid DNA and 0.5 µl of fitting restriction enzyme. The reaction mix was incubated for 2 h at 37 °C before the different fragments were checked by TAE agarose gel. If the fragments had the right size, a sequencing reaction was prepared according to the manufacturer's instructions and sent for sequencing to GATC Biotech, Cologne, GER. The sequencing results were analyzed via Vector NTI.

3.2. Production of adenovirus

3.2.1. LR recombination

Before starting with the LR recombination, it was necessary to produce a plasmid DNA with the pENTR™/U6 vector including the gene of interest. The LR recombination was done according to the manufacturer´s instructions of BLOCK-iT™ Adenoviral RNAi Expression System or pAd/CMV/V5-DEST™ Gateway® Vectors and pAd/PL-DEST™Gateway® Vectors with small changes. The incubation of the LR reaction mix was extended to 18 h at 25 °C. Afterwards, NEB 5-alpha competent *E.coli* cells were transformed with 3 µl of the LR recombination reaction and plated onto ampicillin agar plates to select for true adenoviral expression clones.

From each plate, 2-4 colonies were picked to grow an overnight culture in LB medium with 100 µg/ml ampicillin. On the next day, 100 µl of the overnight culture were plated onto a chloramphenicol agar plate and placed in an incubator at 37 °C overnight. If no bacterial colony grew on the chloramphenicol plates, the picked colony was a true adenoviral expression clone. Only true expression clones were used for producing working adenoviruses. The rest of the overnight culture was used to purify plasmid DNA with the Nucleo Spin® Plasmid kit according to the manufacturer's instructions. After elution in dH_2O, the DNA concentration was measured using a NanoDrop spectrophotometer and the samples were stored at 4 °C until use.

3.2.2. Production of adenovirus in HEK293A cells

Before transfecting the expression clone into HEK293A cells, it was necessary to digest the vector with the enzyme PacI to expose the viral ITRs and to remove the bacterial sequences. The following table (Table 13) shows the components of the digestion mixture.

Table 13. PAC digestion

	Volume
DNA	20 µg
PacI	2 µl
CutSmart	10 µl
dH_2O	up to 100 µl

The digestion mixture was incubated overnight at 37 °C. On the next day, the enzyme was heat-inactivated for 20 min at 65 °C. After digestion, the plasmid DNA was purified using phenol/chloroform extraction and ethanol precipitation. For phenol/chloroform extraction, the plasmid DNA was mixed with the same volume of phenol/chloroform mixture and centrifuged at 15 000 xg for 5 min at room temperature. The upper phase containing the DNA was transferred to a new reaction tube. After that, 1/10 (v/v) 3 M sodium acetate, pH 5.2, was added to the plasmid DNA. Additionally, 100 % ethanol was added at a 2/1 (v/v) ratio with respect to the original DNA volume. The mixture was homogenized and placed on ice for 15 min. Then, it was centrifuged for 15 min at high speed and the supernatant was discarded. The pellet was washed with 70 % ethanol at room temperature, inverted and centrifuged at high speed for 10 min. Afterwards, the supernatant was removed. The pellet was dried for 15 min and finally resuspended in 30-50 µl of TE buffer. The concentration of the plasmid DNA was measured using a NanoDrop spectrophotometer.

HEK293A cells were seeded onto a 60-mm petri dish in DMEM containing 10 % FBS. When the cells reached 85-95 % of confluency, the medium was changed to DMEM medium with only 2 % FBS, and the cells were transfected with purified adenoviral plasmid DNA. An additional well with non-transfected cells was used as negative control. For the adenovirus plasmid DNA transfections, 5 µg of DNA were used and the transfections were performed as described in section 3.4.3. Transfected cells were kept in a CO_2 incubator at 37 °C and checked every day for lysis and viral plaques during 10-15 days. When 80-90 % of the cells were lysed, the adenovirus-containing cells were harvested by collecting the supernatant.

To release the viral particles, the solutions containing the virus-infected cells were frozen and thawed 3 times, each of at least 30 min at -80 °C and 15 min at 37 °C. After the freeze and thaw cycles the adenoviral stock was centrifuged at 3000 xg for 15 min at room temperature. The supernatant containing the adenovirus was stored at -80 °C. This adenovirus solution produced after the transfection with plasmid DNA was labeled stock solution.

3.2.3. Amplification and concentration of adenoviral stock

After preparation of the adenoviral stock solution, it was necessary to amplify the virus amount. Therefore, three 15-mm plates per adenoviral stock solution and one 15-mm plate for the negative control were seeded with HEK293A cells in DMEM with 10 % FBS. As soon as the cells reached a confluency of 90 %, the medium was changed to DMEM with 2 % FBS and cells were transduced with 50-100 µl of the adenoviral stock solution. The cells were controlled for the next 2-6 days for signs of lysis. When 80-90 % of the cells were lysed, they were harvested by collecting the supernatant. To release the new viral particles three freeze and thaw cycles, as previous described were done. Finally, the amplified virus stock was stored at -80 °C.

Generally, the titer of the adenoviral stock solution ranged between 1 x 10^7 to 1 x 10^8 plaque-forming units per ml (pfu/ml). To reach a higher titer, we concentrated the amplified virus stocks using an Amicon® Ultra 15 mL centrifugal filter device with a pore size of 100 kDa MWCO (molecular weight cut-off). The virus stock was filled into the filter unit and centrifuged for 10 min at 3000 xg. The flow-through was discarded, more virus stock was filled into the filter unit and resuspended to prevent blockage of the filter by the particles. This process was repeated until only 200-300 µl of the virus solution remained. This concentrated virus was finally aliquoted and stored at -80 °C until use.

3.2.4. Titering of adenoviral stock

The method described by Bear and Kehn-Hall *et al* [177] was used, with minor changes, to calculate the concentration of the viral stock in pfu/ml. On the day before transduction, two 6-well plates per viral stock solution were seeded with HEK293A cells. When the cells reached a confluency of 85-95 %, 10-fold serial dilutions of each adenoviral stock in a range of 10^{-5} to 10^{-9} were prepared in DMEM without serum. On each plate, 5 serial virus dilutions

and one negative control solution without virus where added. For each virus stock, replicas with the same dilutions were perfomed.

The culture medium was removed from the HEK293A cells and 100 µl of diluted virus solution were added onto each well, followed by complete growth medium (DMEM + 10 % FBS) up to a final volume of 700 µl. The plates were incubated for 2 h in an incubator at 37 °C, with gentle swirling every 20 min to ensure even coverage. For the last 45 min of incubation, another 200 µl of complete culture medium were added. After the incubation time, the medium was removed and the cells were overlayed with 3 ml of 2.4 % immobilizing medium (Avicel) mixed 1/3 (v/v) with plaque medium. The plates were incubated for 6 days in the incubator (37 °C, 5 % CO_2) without movement.

Thereafter, the Avicel overlay was removed and the cells where fixed for 30 min at room temperature using 4 % PFA solution. Subsequently, the wells were rinsed with dH_2O to remove residuals of the overlay before starting with the staining. For staining, the cells were covered with crystal violet solution during 15 min with gentle rocking and after this time the crystal violet was washed off the plates with water. Finally, the viral plaques were counted in the wells corresponding to virus dilutions where between 1 and 150 plaques were observed. For calculation of the virus concentration, the numbers of countable plaques at each dilution were averaged. After that, the titer was calculated with the following formula:

$$\frac{Average\ of\ plaques}{Dilution\ x\ volume\ of\ virus} = Pfu/ml$$

After determining the concentration of each dilution of the adenoviral stock, the mean was calculated. This value was used to calculate the multiplicity of infection (Moi), considering the volume of virus solution used for infection.

$$\frac{Moi\ x\ number\ of\ cells}{Pfu/ml} = Volume\ of\ virus$$

3.3. Isolation of primary cardiomyocytes

3.3.1. Isolation of neonatal rat cardiomyocytes

One- to three-day-old pups from 2-3 Wistar rats were used for the isolation of NRCs. First, the pups were euthanized by decapitation and the hearts were removed and transferred to

a 50-ml tube with a Calcium and bicarbonate-free Hanks with HEPES (CBFHH) solution containing penicillin/streptomycin (P/S) and placed on ice. After all hearts were collected, the tube was gently swirled to remove the remaining blood from the hearts. The hearts were then transferred to petri dishes with CBFHH solution containing P/S in order to cut the coronary vessels. When all the vessels were removed, the hearts were minced and cut into small pieces in a clean petri dish. The heart pieces were incubated for 15 min at 37 °C with 20 ml of Trypsin DNase enzyme solution (T&D) in a 50 ml beaker while on a magnetic stirrer. After incubation, 15 ml of the enzyme solution were discarded and 10 ml of fresh enzyme solution, preheated to 37 °C, were added to the heart pieces. Again, the beaker was placed on a magnetic stirrer for 10 min at 37 °C. Subsequently, the hearts were resuspended 10 times and then the tissue was left to settle down before 10 ml of the supernatant were transferred to a 50 ml tube containing 7.5 ml of FCS. We then added 10 ml of preheated T & D enzyme solution to the remaining tissue and the beaker was again placed for 10 min on the magnetic stirrer. These steps were repeated until the 250 ml T & D solution was completely used or all tissue was digested. The tubes with the heart cells were placed during the rest of the digestion in an incubator (37 °C, 5 % CO_2).

After the digestion, the cells were pelleted by centrifugation during 5 min at 500 xg. The supernatant was discarded and the pellet was resuspended in MEM5 (minimum essential medium, 5 % FBS) without BrdU using a volume that depended on the number of pups. For every 10 pups, 10 ml of medium were used for resuspension. Onto each 10-cm plate 10 ml of the cells were then plated. After resuspension, the cell solution was filtered through a steril filter of 0.22 µm. The filtered cell suspension was then plated in 10-cm plates and kept for 45-60 min in the incubator (37 °C, 5 % CO_2) to allow the fibroblasts to settle down and stick to the plate, as oppose to the cardiomyocytes, which remain in the supernatant. After the incubation, the supernatant with the cardiomyocytes was collected and the cells were counted with an automated cell counter. Finally, the cardiomyocytes were seeded onto 6-well plates or laminin-coated slides for microscopy and Ca^{2+} measurements (Table 14).

Table 14. Number of neonatal rat cardiomyocytes plated for different experiments

	Cell number
6-well plate	2 x 10^6
Immunocytochemistry	2 x 10^5
Ca^{2+} measurements	1.6 x 10^5

3.3.2. Isolation of adult mouse cardiomyocytes

The isolation of adult mouse cardiomyocytes (AMCs) was performed by Katharina Völker (Institute of Physiology I, University of Würzburg). For the isolation of AMCs, mice were anesthetized with urethane (injected volume= 5 x the weight of mice in µl) by intraperitoneal injection. The heart was removed together with the intact aorta and it was washed with ice-cold perfusion buffer to remove the remaining blood. After washing, the heart was hung from the canula of a perfusion system. First, the heart was flushed with preheated perfusion buffer for 5 min at 37 °C, at a flow rate of 3 ml/min. Afterwards, the heart was perfused with 37 °C of warm digestion buffer for 8 min, and then it was cut below the atria and transferred into a beaker with 2.5 ml of digestion buffer. The heart was then minced into small pieces by cutting with scissors for 30 s and finally the pieces were dispersed with a syringe during 30 s. The heart pieces were again dispersed for 3 min in 2.5 ml of stop solution, after which the solution was filterd through a 0.2 mesh in a 50-ml reaction tube. The solution containing the cells was transferred into a 15-ml reaction tube, where the cells were left to settle down for 10 min. Subsequently, the supernatant was added to 10 ml of stop solution II in a petri dish, where the recalcification was performed. For recalcification, different amounts of 100 mM calcium chloride, to reach in the petri dish the final calcium concentrations of 62, 112, 212, 500 or 1000 µM, were added. After each addition of calcium, the cells were left to adapt to the new calcium concentration for 4 min before more calcium was added. The cell solution was finally transferred back to a 15-ml tube and left there to settle down for 15 min at room temperature.

The cardiomyocyte pellet was resuspended in 4 ml of preheated and equilibrated plating medium and the shape and density of the cells were checked under the microscope. Before plating, the 60-mm petri dish or the slides were coated with laminin during 1-2 h. The cardiomyocytes were plated at the desired density and incubated for 2-4 h at 37 °C in a 5 % atmosphere of CO_2 to allow them to settle down. After incubation, the cells were washed two times with PBS to remove dead cells and then they were fixed or lysed, depending on the ensuing experiment.

3.4. Cell culture

3.4.1. Cultivation of HEK293A cells

For cultivation of HEK293A cells, DMEM medium supplied with 10 % FBS was used. Cells intended for virus transduction or amplification had the medium changed to DMEM medium supplied with 2 % FBS shortly before transduction. The cells were splitted when they reached a confluency of around 90-95 %. For splitting, cells were flushed down the flask or plate with the medium, centrifuged for 5 min at 1000 xg and the resulting pellet was resuspended in an appropriate amount of fresh medium. The cells were used until passage 20.

3.4.2. Cultivation of neonatal rat cardiomyocytes

After isolation of NRCs, the cells were kept for 6 days in culture and then used for protein extraction, immunocytochemistry or calcium measurement experiments. Table 15 shows the workflow and the different media used on each day.

Table 15. Workflow for the cultivation of neonatal rat cardiomyocytes until harvesting

Day	Treatment	Medium
1	Plating of cells	MEM 5 (5 % FBS, 1 % L-glutamine, 1 % P/S, 0.5 % BrdU)
2	Washing with PBS	MEM 5 (5 % FBS, 1 % L-glutamine, 1 % P/S, 0.5 % BrdU)
3	Infection with virus for 4 h	OptiMEM
	Changing medium after 4 h	MEM 1 (1 % FBS, 1 % L-glutamine, 1 % P/S)
4	Starving of cells	MEM 0 (1 % L-glutamine, 1 % P/S)
5	Stimulation of cells	MEM 0 (1 % L-glutamine, 1 % P/S) + Phe/Verapamil/Calpeptin
6	Harvesting of cells	--

On the second day, the cells were washed three times with PBS to remove dead cells and then fresh MEM medium containing 5 % FCS was added. One day later the cells were infected during 4 h with virus in OptiMEM at a Moi of 50 (pAD/CMV/V5-NLS-$Ca_v\beta_{2b}$-YFP or YFP) or 20 (pAD/BLOCK iT-Dest shRNA338, shRNA892 or scshRNA), after which they were put back on MEM 1 until day 4. Next, the cells were incubated for 24 h with MEM medium without FCS. On day 5, the cells were incubated for 24 h with MEM without FCS and containing 50 µM phenylephrine, 2 µM verapamil and/or 25 µM calpeptin. Finally, on day 6

the cells were used for calcium measurements, protein extraction, calpain assay or immunocytochemistry.

3.4.3. Transfection of cells

For transfection, HEK293A cells were seeded in 6-well plates or 10-cm dishes. Transfection was performed when the cells reached a confluency of 80-90 %, using the X-tremeGENE HP DNA Transfection Reagent according to the manufacturer's instructions. The ratio of transfection reagent to DNA was 3/1. In 10-cm dishes, 5-10 µg of DNA were used for transfection, whereas in 6-well plates, 2 or 5 µg of DNA per well were used for plasmids and adenovirus transfections, respectively. The transfection reagent and the DNA were mixed in OptiMEM and dropped over the cells after having incubated them for 20 min. The culture medium was changed on the following day after transfection. Transfected cells were harvested for further experiments 24-72 hours after transfection, whereas the cells transduced with adenovirus were harvested only after complete lysis of the cells.

3.5. Transverse aortic constriction surgery

TAC was performed by Marco Abeßer (Institute of Physiology I, University of Würzburg) as previously described [178] in 6-week-old wild-type C57Bl6 mice, with a body weight of 18-25 g. Sham-operated animals underwent an identical surgical procedure, but without ligation of aorta. Isoflurane (2.5 %) was used to anesthesize the animals. Two weeks after TAC, mice were euthanized for isolation of cardiomyocytes or organ extraction for the preparation of tissue lysates. All animal studies complied with the Guide for the Care and Use of Laboratory Animals (NIH publication no. 85-23, revised 1996) and were approved by the local animal care committees. For the TAC experiments we could participate from TAC heart samples as part of a project which was carried out by Prof. Dr. Kuhn (Permission number 55.2 2532-2-135: Kardiale Bedeutung des endothelialen Hormons C-typ natriuretisches Peptid (CNP) und seines Guanylyl Cyklase B (GC-B) Rezeptors. Approval: 02.02.2016–28.2.2020).

3.6. RNA and DNA methods

3.6.1. RNA isolation

For RNA isolation from hearts, the tissue was placed in a reaction tube and homogenized with an Ultraturrax in 1 ml of Trizol reagent. After this step, the RNA isolation procedure was perfomed according to the manufacturer's instructions from the TRIzol Reagent®. The RNA pellet was resuspended in 20 µl of RNase free water and aliquoted in 4 to 5 reaction tubes. These aliquots were stored at -80 °C until use.

To test the concentration and purity of the RNA, the RNA concentration and the A260/280 ratio was measured with a NanoDrop spectrophotometer. The A260/280 value should be higher than 1.8 with an optimal of 2.0, which shows high purity. To check for RNA degradation RNA was loaded on 1 % TAE agarose gel. If the RNA was intact, there were two bands, one for 28 S RNA and one for 18 S RNA. The ratio of 28 S to 18 S RNA should be around 2:1. No visible or smeared bands or a lower ratio of 28/18 S RNA indicates RNA degradation.

3.6.2. Reverse transcription reaction

Reverse transcription reaction was done according to the instructions of the QuantiTect® Reverse Transcription Kit. For each reaction, 1 µg of RNA was transcribed to cDNA and the RT primer mix from the kit was used. To increase the cDNA yield the reverse transcription mix was incubated as recommended in the manufacturer's protocol for 30 min at 42 °C. The cDNAs were stored at -20 °C until use.

3.6.3. qRT-PCR

For qRT-PCR, cDNA was prepared as described in the previous section. The cDNA was diluted 1/10 or 1/5 (v/v) according to the expression level of the gene to be detected. To set up the qRT-PCR the following reagents of Table 16 were added into a 96-well plate as duplicates and mixed for each sample. For each run, a standard curve in a range of 10 – 10^{-6} pg of cDNA of the gene of interest was performed to know the efficiency of the qRT-PCR. Efficiencies of the PCR ranging between 80-100 % were considered as good. A negative control with water instead of cDNA was also included. The expression of the reference gene Rpl 13 was measured with the same cDNA as the gene of interest to normalize the data.

Table 16. Composition of qRT-PCR reaction

	Volume
cDNA (1/10, 1/5)	5 µl
Mastermix	10 µl
Primer sense	0.8 µl
Primer antisense	0.8 µl
UPL 16	0.4 µl
Water (PCR grade)	Fill up to 20 µl

The 96-well plate was then incubated in the LightCycler instrument with the following program (Table 17). The annealing temperature was for all the reactions 60 °C.

Table 17. qRT-PCR cycler programm

	Temperature	Time	
Pre-Incubation	95 °C	600 s	
Amplification	95 °C	10 s	} 45 x
	60 °C	30 s	
	72 °C	1 s	
Cooling	40 °C	30 s	

The results were analysed with the LightCycler® 96 and Excel software. For the evaluation the equation of the efficiency-corrected relative quantification was used:

$$\text{Normalized relative ratio} = \frac{E_T^{CT(target)\,calibrator - CT(target)\,sample}}{E_R^{CT(reference)\,calibrator - CT(reference)\,sample}}$$

After calculation of the fold change, the gene expression of different samples was compared.

3.7. Protein biochemistry

3.7.1. Preparation of protein lysates

3.7.1.1. Total protein extraction from cardiomyocytes

For protein extraction from cardiomyocytes, either RIPA or PBS supplied with 1 % Triton were used as lysis buffers. A protease inhibitor cocktail from Thermo Scientific was added to the lysis buffers, according to the manufacturer´s instructions. Cells seeded into 6-well plates were washed once with ice-cold PBS and lysed with 120 µl of cold lysis buffer per well for 10 min on ice. The cells were then scraped off the plate and transferred into a prechilled reaction tube on ice, where the cells were allowed to further lyse for 15 min. Cells were then

centrifuged at 16 000 xg during 15 min at 4°C. The supernatants were collected, transferred into new reaction tubes and stored at -80 °C until use.

3.7.1.2. Cell fractionation of tissues and cultured cells

For cell fractionations of mouse hearts, the tissues were rapidly frozen after removal using liquid nitrogen and stored at -80 °C until use. The hearts were homogenized with a micro-dismembrator and the cell fractionation was performed with the Subcellular Protein Fractionation Kit for Tissues according to the manufacturers' instructions.

For cell fractionation of cultured cells, we scraped off the cells from the plate in PBS and centrifuged at 500 xg. The pellet was collected and the cell fractionation was performed with the Subcellular Protein Fractionation Kit for Cultured Cells following the the manufacturers' instructions.

The cytosolic fraction, membrane fraction, soluble nuclear fraction mixed with chromatin-bound nuclear fraction were stored at -80 °C until use.

3.7.2. Western blots

3.7.2.1. Protein determination

For protein determination, a BCA assay was performed. To prepare a standard curve, eight BSA concentrations in a range from 10-1000 µg/ml were used. The samples and standards were transferred into a 96-well microtiter plate and the BCA working reagent was added (BCA/$CuSO_4$) (50/1 (v/v)). Thereafter, the plate was incubated at 37 °C for 30 min. Samples corresponding to the standard curve with BSA, water and lysis buffer control were evaluated in duplicates, whereas all test samples were assessed in triplicates. Finally, the optical densitiy (OD) was measured at 562 nm. With these values, a standard curve was plotted in Excel software and the protein concentration in the samples was interpolated from ODs.

3.7.2.2. SDS-PAGE and western blots

For western blots, protein lysates were thawed on ice, mixed with water and 5x loading dye to a final total protein amount between 50-100 µg. SDS-PAGE was performed using a 4.5 % stacking gel and a 10 % resolving gel for proteins of molecular sizes between 30-100 kDa, while 8 % resolving gels were used for proteins with a molecular weight between 100-

250 kDa. Gels were run at 180 V for 1 h at room temperature. After that, proteins were transferred to a nitrocellulose blotting membrane at 100 V for 1 h at 4 °C. Membranes were blocked with 5 % BSA in TBS-T solution for 30 min while shaking at room temperature. The membranes were incubated with the primary antibodies overnight at 4 °C on the shaker (dilutions are shown in Table 18). The membranes were washed three times for 5 min each with TBS-T at room temperature and incubated with the appropriate secondary antibody for 1 h at room temperature (Table 18). After three times 5 min washing with TBS-T, proteins on the membranes were visualized using ECL western blotting substrate.

Table 18. Antibodies used for western blot

Protein	Dilution of primary antibody	Dilution of secondary antibody
Calpastatin	1:300	1:10 000
$Ca_v\beta_2$ (Atlas)	1:1000	1:10 000
$Ca_v\beta_2$ (Novus)	1:2000	1:10 000
$Ca_v\beta_{2b}$	1:250	1:10 000
$Ca_v1.2$	1:500	1:10 000
GAPDH	1:5000	1:10 000
Na^+ K^+ ATPase	1:5000	1:10 000
Histon	1:2000	1:10 000
GFP (YFP)	1:2000	1:10 000

3.7.2.3. Stripping of membranes

After finishing the detection of the proteins with ECL, the membranes were washed four times for 5 min each with TBS-T. Subsequently, the membranes were incubated with stripping buffer (100 ml stripping buffer containing 700 µl of β-mercaptoethanol) for 10 min at 50 °C in a water bath while shaking. The membranes were washed again six times for 5 min each with TBS-T at room temperature. After washing, membranes were blocked with 5 % BSA for 30 min at room temperature and incubated overnight at 4 °C with another antibody.

3.7.3. Immunocytochemistry

Cells used for immunocytochemistry were plated into coverslips. They were first washed three times with PBS and then fixed for 8 min with 4 % PFA. After fixation, the coverslips were again washed three times with PBS to remove residual PFA and the cells were permeabilized with PBS containing 0.2 % Triton for 15 min. The coverslips were then washed

three times with PBS and the cells were blocked with 5 % NGS (normal goat serum) in PBS for 1 h at room temperature. Thereafter, cells were incubated overnight at 4 °C with the primary antibodies diluted in PBS containing 1.5 % NGS. The following table (Table 19) shows the dilution of the primary and secondary antibodies used for immunocytochemistry.

Table 19. Antibodies used for immunocytochemistry

Protein	Dilution of primary antibody	Dilution of secondary antibody
$Ca_v\beta_2$ (Atlas)	1:400	1:300
$Ca_v\beta_2$ (Novus)	1:400	1:300
$Ca_v\beta_{2b}$	1:100	1:300
$Ca_v1.2$	1:400	1:300
α-actinin	1:250	1:300
RYR2	1:400	1:300

On the next day, the coverslips were washed three times with PBS and incubated for 2 h in the dark at room temperature with the secondary antibodies labelled with a fluorescent tag and diluted in 1.5 % NGS in PBS. The cells were washed again three times with PBS, and after drying they were mounted on slides with one drop of DAPI mounting medium. The slides were left in the dark at room temperature until the next day and finally the edges of the coverslips were rounded with nail polish. All slides were then stored at 4 °C in the dark until use.

After staining of the cells, fluorescence microscopy was perfomed using a Leica inverted confocal microscope or an Olympus inverted fluorescence microscope with a 63 x oil immersion objective. The area of cardiomyocytes was measured using Image J software. Only cells fitting completely in the image field were analyzed. For each experiment, the sizes of 100-250 cells were evaluated. The average cell size from each experiment was calculated and used to determine the mean of three replicated experiments. Finally, the mean of each group of cells was normalized to the control. Quantification of nuclear localization of $Ca_v\beta_2$ in NRCs was perfomed by analysis of Manders colocalization coefficient via the plugin JACoP using Image J. JACoP measures the ratio of colocalized pixels between $Ca_v\beta_2$ staining and DAPI staining in the nucleus.

3.8. Ca^{2+} measurements

NRCs were cultured on coverslips (25 x 25) previously coated with laminin. The cells were either not treated or treated with 50 µM phenylephrine. On the day of measurement, the cells were washed twice with Ca^{2+}-free normal tyrode solution and then loaded for 20 min at room temperature with Fura-2 in normal Tyrode´s solution. After incubation with Fura-2, the cells were washed during an additional 5 min with normal Tyrode´s solution containing 1 mM $CaCl_2$.

To measure diastolic/systolic Ca^{2+} transients the "Myocyte and Contractility System" from Ionoptix was used. The cardiomyocytes were paced at 1 Hz and 12 V and perfused with normal Tyrode´s solution containing 1 mM $CaCl_2$. The calcium transients of every single cardiomyocyte were recorded for 60 s. The data were analysed using the IonWizard 6.3 software. The data were corrected for background 340/380 fluorescence (R =340/380) and Ca^{2+} transient amplitude, peak time, departure velocity and decay time constant were analyzed.

3.9. Mass spectrometry and relative protein quantification

Cell lysates from NRCs transduced with scrambled shRNA (shRNAsc, shRNA338 or shRNA892, and untreated cells from four replicated preparations were used for analysis by mass spectrometry (MS). MS was performed and evaluated by the working group of Prof. Dr. Katrin Marcus (Medizinisches Proteom-Center, Ruhr University Bochum). Total cell lysates (10 µg in each lane) were separated by short gel SDS-PAGE. Afterwards, the protein bands were excised, hashed and destained by three times alternating 10-minute treatments with buffer A (10 mM ammonium bicarbonate, pH 8.3) and buffer B (buffer A + 100 % acetonitrile in a ratio of 50:50 (v/v)). After the second incubation with Buffer A, samples were treated with 50 µl of 10 mM DTT for 1 hour at 56°C and with 50 µl of 50 mM iodoacetamide for 45 minutes at room temperature before continuing with the destaining protocol. Finally, gel pieces were dried in a vacuum. Digestion was initiated by adding 8 µl of trypsin solution (0.015 µg/µl) and was performed overnight. The digestion was stopped, and the peptides were eluted by incubating the gel pieces two times during 15 min with 30 µl of a 1:1 solution containing 100 % acetonitrile and 0.1 % (v/v) TFA in an ice-cooled ultrasonic bath. Samples were dried in a vacuum concentrator and resuspended in 20 µl of 0.1 % (v/v) trifluoroacetic

acid. Afterwards, the peptide concentration was determined by amino acid analysis (AAA) as described [179]. According to the AAA, 200 ng per sample were taken for MS analysis.

Nano-HPLC-MS/MS was performed as previously described [180] by means of LC-MS/MS on an UltiMate 3000 RSLCnano system coupled online to an LTQ Orbitrap Elite mass spectrometer. For protein identification via database searches, the raw files were analyzed with the Proteom Discoverer software (v. 1.4.1.14) using the Mascot search algorithm (version 2.5) searching against the UniProtKB/Swiss-Prot database using rat taxonomy (released 2017_1,556,196 sequences entries in the whole database). The database search was performed with the following parameters: mass tolerance 5 ppm for precursor and 0.4 Da for fragment ions; missed cleavages: 2; modifications: methionine oxidation as dynamic and cysteine carbamidomethylation as fixed; FDR threshold: < 1 %.

Label-free quantification was performed by using the Progenesis QI software. Raw files generated by the mass spectrometer were imported in the software and all runs were matched to the most suitable run among them (by automatic selection). Afterwards, the software generated a list of features including the m/z values of all measured peptides at a given retention time. The following filters were used at feature level: allowed charge state in the range 2+ and 5+, reject the features with two or less isotopes. The raw abundances of each feature were automatically normalized in order to correct experimental variations. Experimental setup was set to within subject comparison three groups. Quantified features were then matched to peptide and protein identification by importing the search results generated by proteome discoverer (see protein identification). Only unique peptides were used for quantification.

3.10. Calpain activity assay

The calpain activity assay was performed using the Calpain-Glo™ protease assay. The calpain activity of NRCs transduced with shRNA338, shRNA892 and shRNAsc, and stimulated with PE or vehicle were measured. After 72 h of adenoviral expression, the cells were incubated for 1 h with 40 µM Suc-LLVY-Glo™ substrate at 37 °C. The cells were then washed 1 x with PBS and lysed at room temperature for 5 min with Glo Lysis buffer containing 1 x Halt protease inhibitor cocktail and 25 µM calpeptin. Subsequently, the cells were scraped off the plates and lysed for another 5 min at room temperature. Each lysate was diluted 1/1 (v/v) with the

calpain-Glo™ buffer containing the luciferin detection reagent. The mixture was incubated for 5 min at room temperature and then the luciferase activity of each lysate was measured in the 96-well plate using a Victor2 microplate multilabel reader. Three replicates were done from each lysate.

3.11. Statistics

All the data were evaluated using Microsoft Excel or the Image J (NIH) software. The results are represented as mean ± SEM. Significance test between groups was performed by one-way ANOVA. A p-value of $p \leq 0.05$ was considered as significant and $p \leq 0.01$ as highly significant.

4. Results

4.1. $Ca_v\beta_{2b}$ is the predominant splice variant of $Ca_v\beta_2$ in mouse hearts

$Ca_v\beta_2$ has several splice variants differing only in their NT region ($Ca_v\beta_{2a\text{-}e}$). To examine the expression of the five N-terminal splice variants of $Ca_v\beta_2$ in WT mouse hearts, we performed PCR experiments with specific primers for each variant. The PCRs revealed that $Ca_v\beta_{2b}$ had a higher expression than the $Ca_v\beta_{2d}$ and $Ca_v\beta_{2e}$ splice variants, while $Ca_v\beta_{2a}$ and $Cav\beta_{2c}$ could not be detected (Fig. 8 A).

Next, we investigated the relative expression of the $Ca_v\beta_2$ splice variants by qRT-PCR using the short FAM-labeled hydrolysis probe UPL16 and unique primers for each isoform, except for $Ca_v\beta_{2c}$ and $Ca_v\beta_{2d}$, since the sequence differences between these two variants are too small. Therefore, $Ca_v\beta_{2c}$ and $Ca_v\beta_{2d}$ were detected with the same pair of primers and were summarized as $Ca_v\beta_{2c\text{-}d}$. In agreement with the results from RT-PCR, qRT-PCR experiments with cDNA obtained from four different mouse hearts demonstrated that $Ca_v\beta_{2b}$ was significantly higher expressed than the other splice variants (Fig. 8 B). $Ca_v\beta_{2b}$ expression levels were 80 %, 85 % and 98 % higher than $Ca_v\beta_{2c\text{-}d}$, $Ca_v\beta_{2e}$ and $Ca_v\beta_{2a}$ levels, respectively. Therefore, it can be concluded that $Ca_v\beta_{2b}$ is the predominant isoform in mouse hearts.

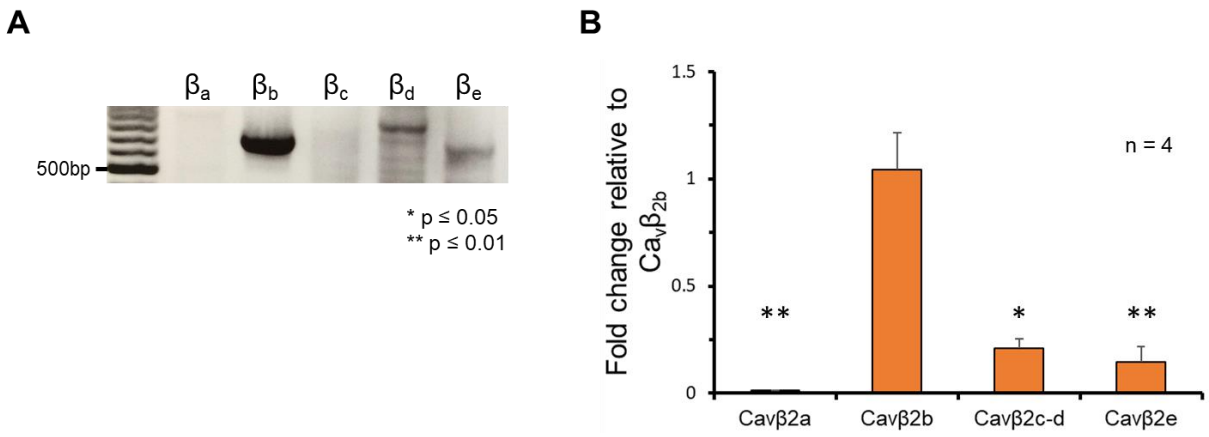

Figure 8. Expression of $Ca_v\beta_2$ N-terminal splice variants in mouse hearts by PCR and qRT-PCR
PCR and qRT-PCR were performed with primers specific for $Ca_v\beta_{2a\text{-}e}$ to check for expression differences in mouse hearts. (A) PCR showed a more abundant expression of $Ca_v\beta_{2b}$ compared to the other splice variants. (B) Expression of $Ca_v\beta_{2b}$ in mouse hearts was significantly higher than that of $Ca_v\beta_{2a}$, $Ca_v\beta_{2c\text{-}d}$ and $Ca_v\beta_{2e}$, as analyzed by qRT-PCR. qRT-PCR was performed with cDNA obtained from four different mouse hearts. Data were normalized to the expression of Rpl13. Fold change relative to $Ca_v\beta_{2b}$. *p ≤ 0.05; **p ≤ 0.01.

4.2. $Ca_v\beta_2$ also localizes in the nucleus of NRCs and AMCs

After addressing the expression levels of the different $Ca_v\beta_2$ splice variants, we examined the cellular localization of this protein. AMCs from WT mice were co-stained with antibodies against $Ca_v\beta_2$ and RyR2 and the two proteins were detected using fluorescent secondary antibodies and confocal microscopy. We observed that while most of $Ca_v\beta_2$ faced the RyR2 in the dyads, another pool of $Ca_v\beta_2$ was targeted to the nucleus (Fig. 9 A). To corroborate these results, we performed western blots from cellular fractionation lysates of WT mouse hearts and AMCs. In heart lysates, we could slightly detect $Ca_v\beta_2$ in the cytosolic fraction, whereas, as expected for an ion channel subunit, a huge amount of $Ca_v\beta_2$ was localized in the membrane fraction. Moreover, consistently with the AMC immunocytochemistry, the expression of $Ca_v\beta_2$ protein was also detected in the nuclear fraction, although to a lesser extent than in the membrane fraction. GAPDH, Na^+/K^+-ATPase and histone H3 were used as compartment-specific controls to check the purity of the different fractions (Fig. 9 B and C).

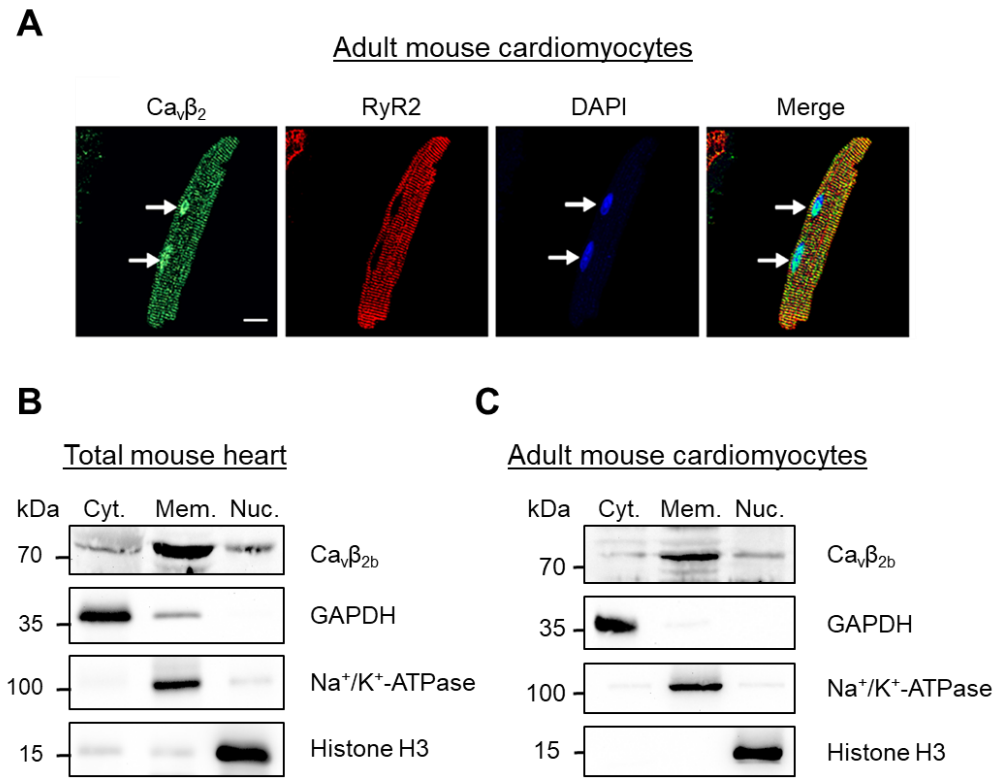

Figure 9. Cellular localization of $Ca_v\beta_2$ in mouse hearts and AMCs
(A) Immunocytochemical analyses of AMCs showed a fraction of $Ca_v\beta_2$ co-localizing with the RyR2, but also the targeting of $Ca_v\beta_2$ to the nucleus. Confocal fluorescence microscopy images of cells stained with antibodies against $Ca_v\beta_2$ (from the company Novus biologicals, green), RyR2 (red) or DAPI (blue). Western blots of cell fractionation products from (B) total mouse hearts or (C) AMCs showed the targeting of $Ca_v\beta_2$ to the cell membrane, with a fraction of the β subunit also translocated to the nucleus. Western blots against GAPDH (cytosol), Na^+/K^+-ATPase (membrane) and histone H3 (nucleus) were performed as compartment-specific controls. For $Ca_v\beta_2$ staining a $Ca_v\beta_{2b}$ antibody was used in western blots. Scale bar = 15 µm; Cyt. = cytosolic fraction; Mem. = membrane fraction; Nuc. = nuclear fraction.

We also performed immunostainings of NRCs. As in AMCs, in these cells a pool of $Ca_v\beta_2$ was also located in the nucleus where it co-localized with the DAPI staining (Fig. 10). These results from the experiments shown in Fig. 9 and 10 confirm that the localization of $Ca_v\beta_{2b}$ is not only restricted to the membrane compartment in AMCs and NRCs, but it is also present in the nucleus of these cells.

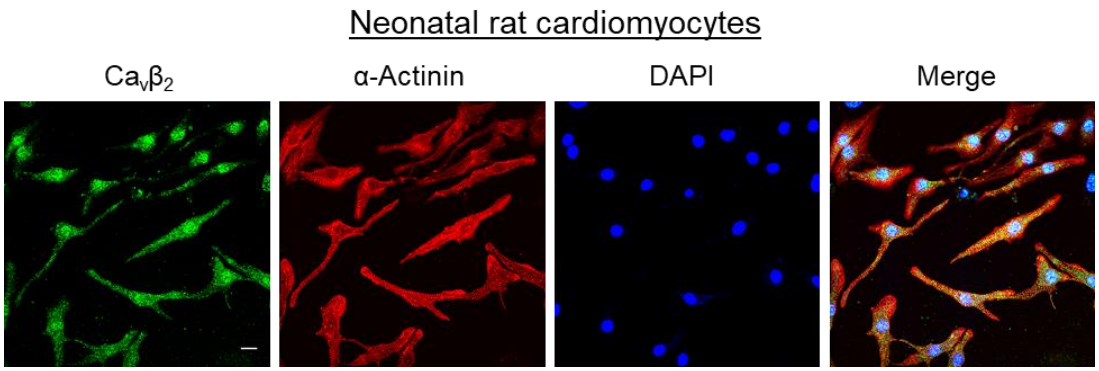

Figure 10. Cellular localization of $Ca_v\beta_2$ in NRCs
Immunocytochemistry of NRCs stained with anti-$Ca_v\beta_2$ (from the company Novus biologicals, green), anti-α-actinin (red) and DAPI (blue). Pictures were taken with a confocal fluorescence microscope. $Ca_v\beta_2$ was detected in the cytosol and also partially co-localized with DAPI in the nucleus. Scale bar = 15 µm.

4.3. Translocation of $Ca_v\beta_2$ to the nucleus is dependent on the SH3 domain

Since immunocytochemical and western blot experiments from AMCs and NRCs revealed the targeting of a fraction of $Ca_v\beta_2$ to the nucleus, the next question to address was how $Ca_v\beta_2$ translocates to the nucleus. To investigate if $Ca_v\beta_2$ contains some nuclear localization signals (NLS), we generated different $Ca_v\beta_{2b}$ constructs lacking one or more of its structural regions (Fig. 11). The construct $Ca_v\beta_{2b}\Delta$ NT and $Ca_v\beta_{2b}\Delta$ CT were missing the NT and CT domains, respectively. The constructs $Ca_v\beta_{2b}\Delta$ NT/CT and $Ca_v\beta_{2b}\Delta$ GK/CT lacked the NT and CT domains and the CT and GK domains, respectively. Furthermore, the NT and SH3 domains, were absent in the construct $Ca_v\beta_{2b}\Delta$ NT/SH3 and the NT, Hook and CT domains in the construct $Ca_v\beta_{2b}\Delta$ NT/Hook/CT. All truncated constructs, as well as the control plasmid containing the WT $Ca_v\beta_{2b}$, were tagged with YFP at the C-terminal region. These constructs were transfected into HEK293A cells and after 72 h of expression, cell fractionations were performed and the presence of the protein in the different cellular compartments was detected by western blot using an anti-YFP antibody.

The WT $Ca_v\beta_{2b}$ was detected in the cytosolic, membrane and nuclear fractions. Furthermore, the constrcuts $Ca_v\beta_{2b}\Delta$ NT, $Ca_v\beta_{2b}\Delta$ CT, $Ca_v\beta_{2b}\Delta$ NT/CT, $Ca_v\beta_{2b}\Delta$ GK/CT, and $Ca_v\beta_{2b}\Delta$ NT/Hook/CT were also detected in all the three compartments. However, the construct $Ca_v\beta_{2b}\Delta$ NT/SH3, which is the only lacking the SH3 domain, was not detected in the nuclear fraction, suggesting that the SH3 domain plays a role in the nuclear translocation of $Ca_v\beta_{2b}$.

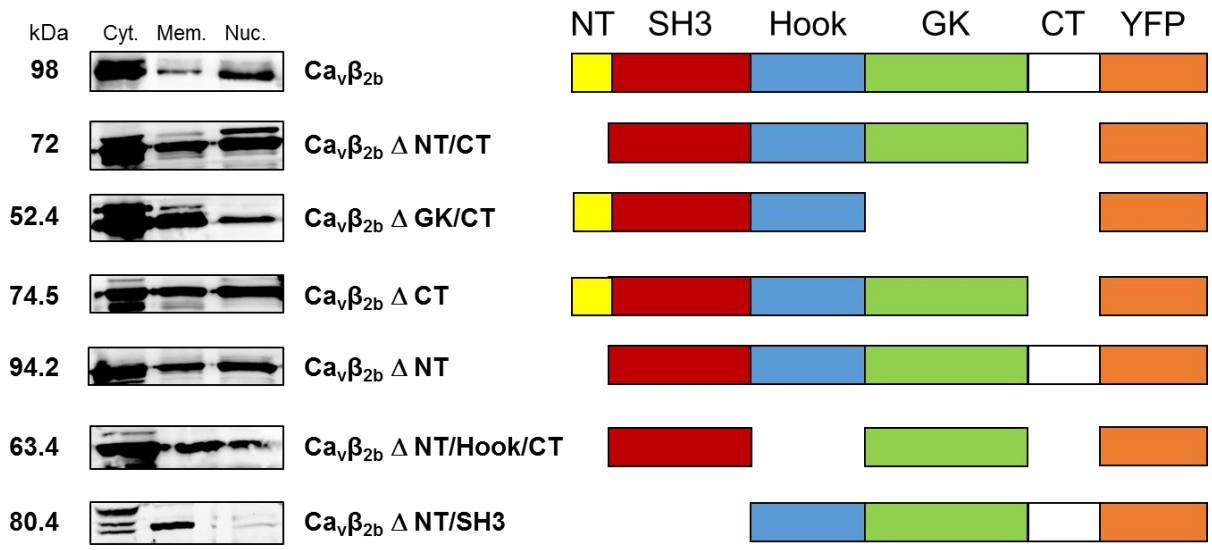

Figure 11. Nuclear translocation of constructs missing different regions of $Ca_v\beta_{2b}$
HEK293A cells were transfected with the WT $Ca_v\beta_{2b}$ or with either of six plasmids encoding $Ca_v\beta_{2b}$ lacking different structural parts. Each construct comprised an YFP tag fused to the C-terminus or most C-terminal structural region of the protein. Cell fractionations of the transfected HEK293A cells were done and western blots were performed with an antibody against YFP. Proteins from five of the truncated constructs of $Ca_v\beta_{2b}$ ($Ca_v\beta_{2b}\Delta$ NT/CT, $Ca_v\beta_{2b}\Delta$ GK/CT, $Ca_v\beta_{2b}\Delta$ CT, $Ca_v\beta_{2b}\Delta$ NT and $Ca_v\beta_{2b}\Delta$ NT/Hook/CT) and the wildtype $Ca_v\beta_{2b}$ were localized in the cytosolic, membrane and nuclear fractions. In contrast, no protein was detected in the nucleus of cells transfected with $Ca_v\beta_{2b}\Delta$ NT/SH3. The western blot is representative of three individual experiments. Cyt. = cytosolic fraction; Mem. = membrane fraction; Nuc. = nuclear fraction.

4.4. Decreased nuclear $Ca_v\beta_2$ after induction of hypertrophy *in vivo* and *in vitro*

Until now, the role of LTCCs and $Ca_v\beta_2$ during the development of cardiac hypertrophy remains controversial. To further enlighten the function of $Ca_v\beta_2$ in this pathology, we induced hypertrophy *in vitro* by treating NRCs with the α_1-adrenergic-receptor agonist PE. Cells treated with vehicle were used as control. PE-treated cardiomyocytes were 22 % larger as compared to the vehicle-treated cells, as shown in Fig. 12 A and B. Interestingly, a decrease in the ratio of nuclear versus total $Ca_v\beta_2$ was also observed in PE-treated NRCs as compared to vehicle-treated cells (Fig. 12 C).

With the aim to investigate *in vivo* if there is also a decrease in the expression of nuclear $Ca_v\beta_2$ during hypertrophy, TAC was performed in mice. Representative confocal microscopy

images of cardiomyocytes from sham- and TAC-operated mice, stained with anti-$Ca_v\beta_2$, anti α-actinin antibodies and DAPI are shown in Fig. 13 A. AMCs isolated from TAC-operated mice displayed a significant 20 % increase in cell area as compared to cells from sham-operated mice (Fig. 13 B).

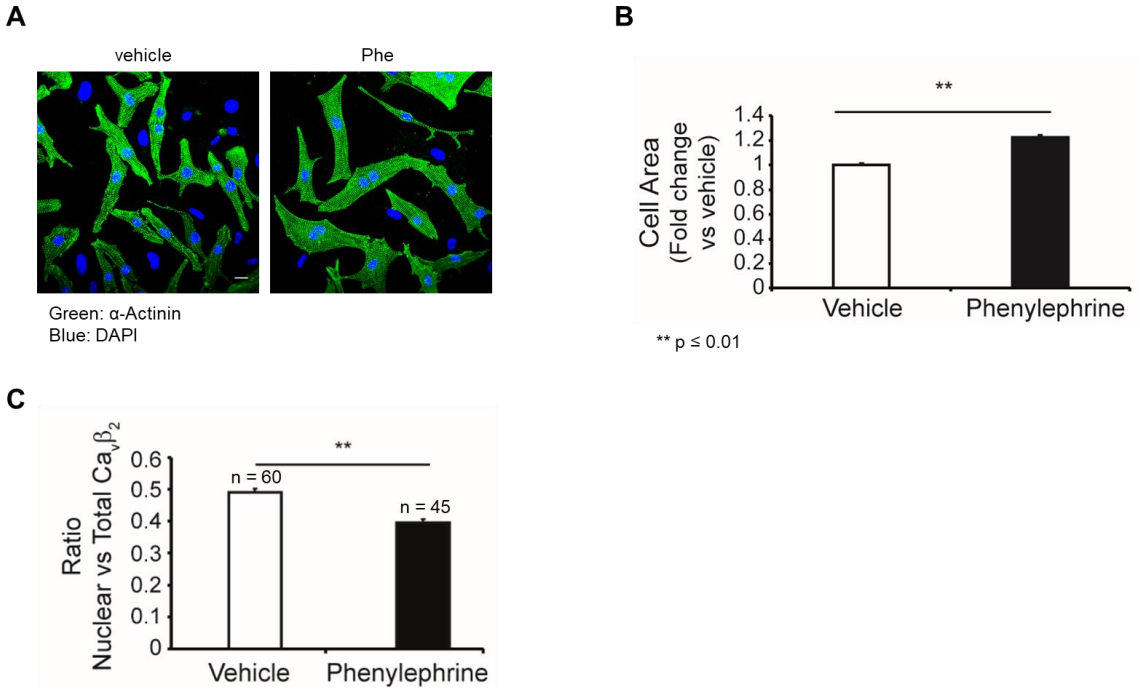

Figure 12. Cell area increases but nuclear $Ca_v\beta_2$ decreases after PE-induced hypertophy in NRCs
In vitro treatment of NRCs with PE stimulated the development of hypertrophy (A and B). (A) Confocal immunofluorescence microscopy images of PE- and vehicle-treated cells stained with α-actinin (green) and DAPI (blue). (B) Cell area of NRCs stimulated with PE or vehicle. PE treatment increased cardiomyocyte size by around 22 % compared to control cells. (C) Bar plot of Manders coefficient co-localization analyses between anti-$Ca_v\beta_2$ and DAPI nuclear staining in NRCs treated with PE or vehicle. Induction of hypertrophy led to a decrease in nuclear $Ca_v\beta_2$. For both experiments, cells from 10-20 randomly-chosen fields from three replicated experiments were evaluated; *p ≤ 0.05; **p ≤ 0.01; Scale bar = 15 µm.

TAC operation did not induce any change in the body weight of the animals (Fig. 13 C), however, the heart weight-to-body weight ratio (Fig. 13 D) and left ventricle (LV) weight-to-body weight ratio (Fig. 13 E) were significantly increased in TAC-operated mice as compared to sham-operated mice, confirming the development of LV hypertrophy in TAC-operated mice. Moreover, there were no differences in right ventricle (RV) weight-to-body weight ratio (Fig. 13 F).

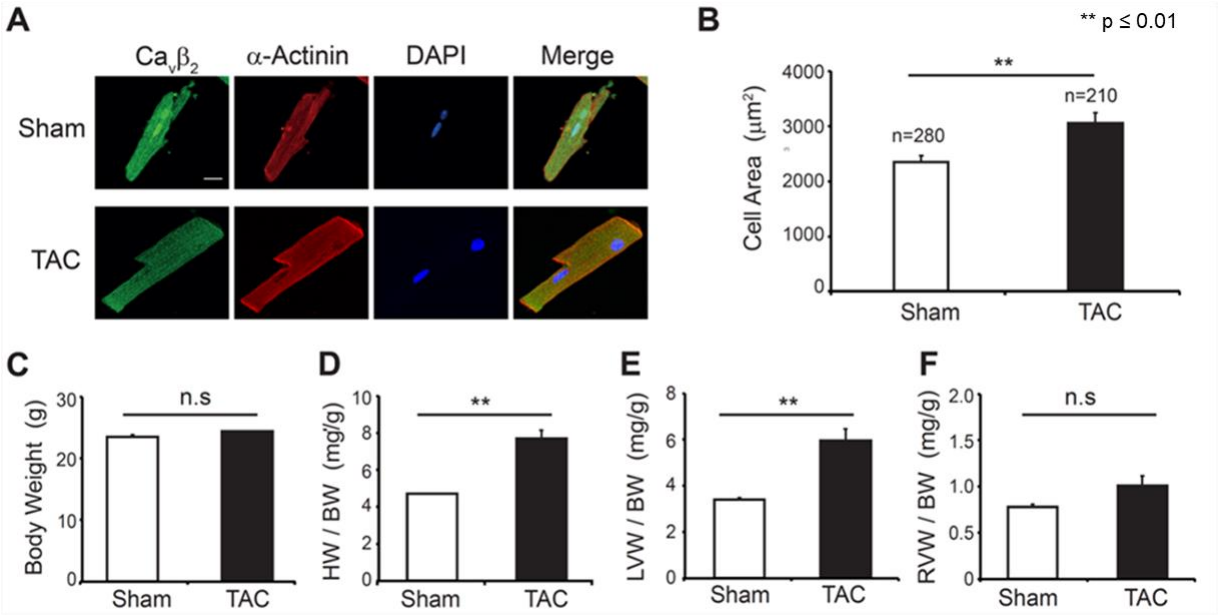

Figure 13. TAC-induced cardiac hypertrophy *in vivo*
(A) Confocal fluorescence microscopy images of cardiomyocytes from sham- and TAC-operated mice. Cells were stained with anti-Ca$_v$β$_2$ (Novus biologicals, green) and anti-α-actinin (red) antibodies and with DAPI (blue). (B) Measurement of cell area of cardiomyocytes from sham- or TAC-operated adult mice. Cardiomyocytes from three animals of each group were stained and analyzed. Cells from 10-20 randomly chosen fields were evaluated. (C) Comparison of body weight between sham- and TAC-operated mice. (D) Heart weight-to-body weight ratio between sham- and TAC-operated mice. (E) LV weight-to-body weight ratio. (F) RV weight-to-body weight ratio. (C-F) Each group consisted of three animals. **p ≤ 0.01; n.s = non-significant; Scale bar = 15 µm.

Western blots after cell fractionation of hearts from sham-operated and TAC-operated mice were performed to assess the expression of nuclear Cavβ$_2$. Induction of cardiac hypertrophy led to a significant decrease of nuclear Ca$_v$β$_2$ in the LV of TAC-operated mice as compared to sham-operated animals (Fig. 14 A). Contrastingly, there was no reduction of Ca$_v$β$_2$ in the membrane fractions of LV from TAC mice (Fig. 14 B). Additionally, western blots did not show any significant differences in Ca$_v$β$_2$ expression in the RV nuclear fractions from sham- and TAC-operated mice (Fig 14 C). The purity of the lysates was confirmed by western blot using compartment-specific controls.

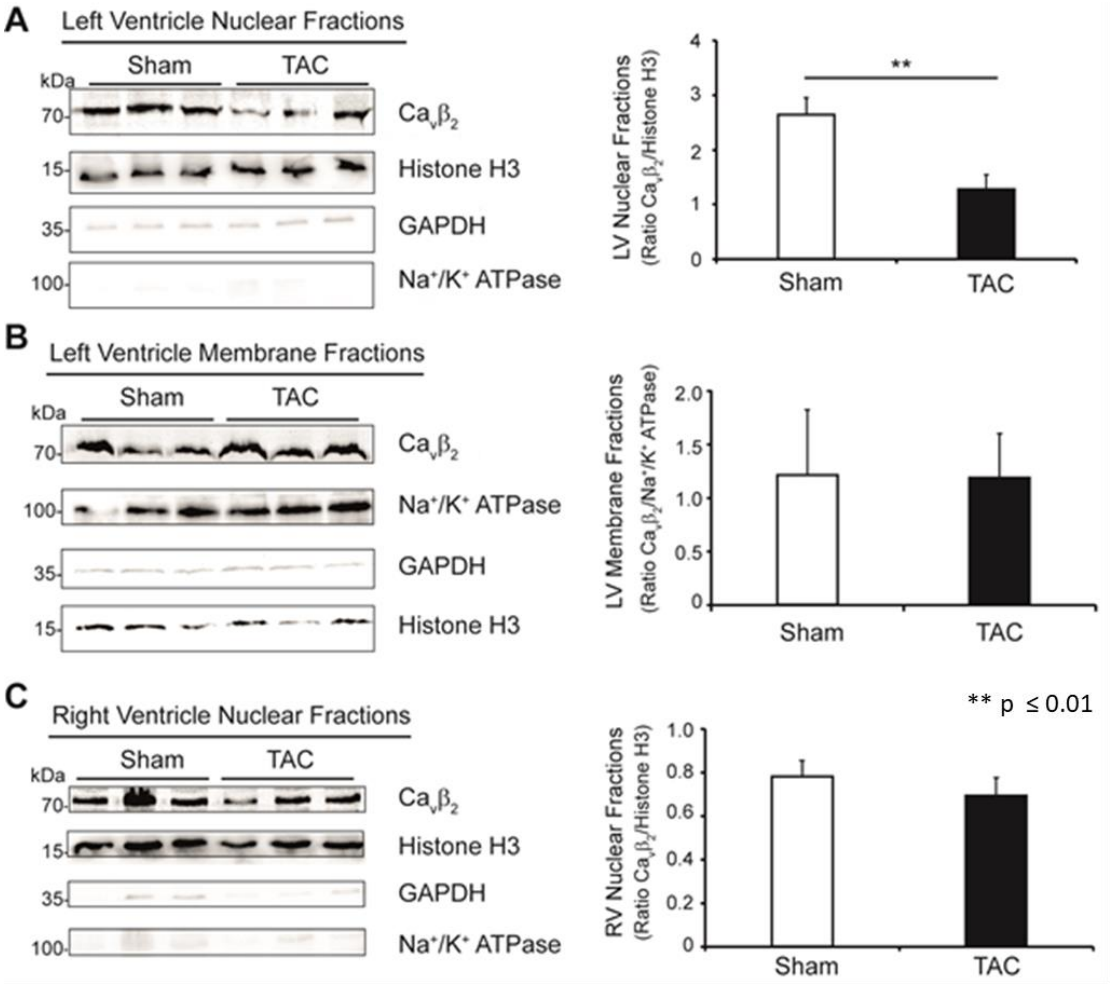

Figure 14. Induction of hypertrophy *in vivo* led to a decrease of nuclear $Ca_v\beta_2$
Western blots and densitometric analyses of cell fractionation products from (A) LV nuclear fractions, (B) LV membrane fractions and (C) RV nuclear fractions of sham-operated and TAC-operated mice. $Ca_v\beta_2$ was detected using a specific antibody (Novus biological). Additional immunoblots were performed to confirm the presence of the compartment-specific protein markers GAPDH (cytosol), Na+/K+ ATPase (membrane) and histone H3 (nucleus). In densitometric analyses (A) and (C), each lane was normalized to the corresponding histone H3 expression. (B) Lanes were normalized to the expression of Na^+/K^+ ATPase. Samples from three sham-operated and three TAC-operated mice were used for the western blots and densitometric analyses. **p ≤ 0.01; n.s = non-significant.

4.5. Downregulation of $Ca_v\beta_2$ enhances the hypertrophic response in NRCs

To investigate the role of $Ca_v\beta_2$ in the development of cardiac hypertrophy, we used shRNAs to downregulate $Ca_v\beta_2$ in NRCs. Four different shRNAs (shRNA18, shRNA338, shRNA508 and shRNA892) were designed, directed to different regions of $Ca_v\beta_2$. A scramble shRNA (shRNAsc) was used as negative control (Fig. 15 A). The shRNAs were delivered to the NRCs by adenoviral transduction and experiments were performed 72 h post viral infection. The efficacy of $Ca_v\beta_2$ downregulation was evaluated by western blots (Fig. 15 B), densitometric analyses (Fig. 15 C) and immunocytochemistry (Fig. 15 D) of NRCs infected with the shRNA adenoviruses.

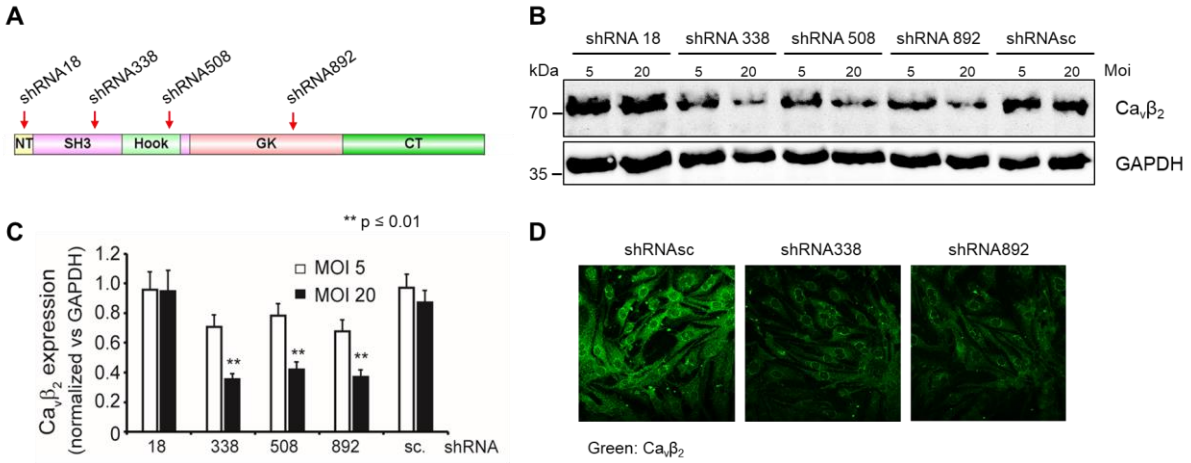

Figure 15. Downregulation of $Ca_v\beta_2$ by different shRNAs

(A) Linear structure of the different domains of $Ca_v\beta_2$. Arrows indicate the binding sites of the four used shRNAs: N-terminus (shRNA18), SH3 domain (shRNA338), Hook region (shRNA508) and GK domain (shRNA892). (B) Western blot of NRC lysates treated with the different shRNAs (Moi: 5 or 20) for the downregulation of $Ca_v\beta_2$. shRNAsc was used as a negative control. An anti-$Ca_v\beta_2$ antibody (Atlas) was used to observe the downregulation, while an anti-GAPDH antibody was used as a loading control. (C) Quantification of $Ca_v\beta_2$ intensity in three replicated western blots from shRNAsc-transduced or $Ca_v\beta_2$-deficient NRCs (shRNA18, 338, 508 and 892). For each shRNA, a Moi of 5 and 20 was used. **p ≤ 0.01 (D) Confocal immunofluorescence microscopy images of NRCs treated with vehicle, shRNAsc, shRNA338 or shRNA892. A Moi of 20 was used for transduction. Cells were stained with anti-$Ca_v\beta_2$ antibody (Atlas) to visualize downregulation. Scale bar = 15 µm.

Densitometric analyses of the western blots with NRC lysates from cells transduced with the shRNA338 or 892 at a Moi of 20 showed a 45 % decrease in $Ca_v\beta_2$ expression as compared to controls (Fig. 15 C). In contrast, shRNA18 and 508 induced less $Ca_v\beta_2$ downregulation. In the immunocytochemistry experiments (Fig. 15 D), downregulation of the $Ca_v\beta_2$ subunit by transduction of the cardiomyocytes with shRNA338 or 892 at a Moi of 20 induced a decrease in protein expression, as opposed to transduction with shRNAsc. ShRNA338 and 892 were used for further experiments because of their higher efficacy compared to the other shRNAs.

After $Ca_v\beta_2$ silencing in NRCs by transduction of shRNA338 or shRNA892, cardiomyocyte hypertrophy was induced by 24 h treatment with PE. Treatments with vehicle or PE and verapamil (PE + Vera.), a specific blocker of LTCCs, were used as controls. As negative controls for the viral infection, cells were also transduced with the shRNAsc. The cells were fixed, stained with an α-actinin antibody and DAPI mounting medium, and the area of cardiomyocytes treated with the different agents was measured. Fig. 16 shows the mean cell areas of NRCs treated with the different conditions (Fig. 16 A and B).

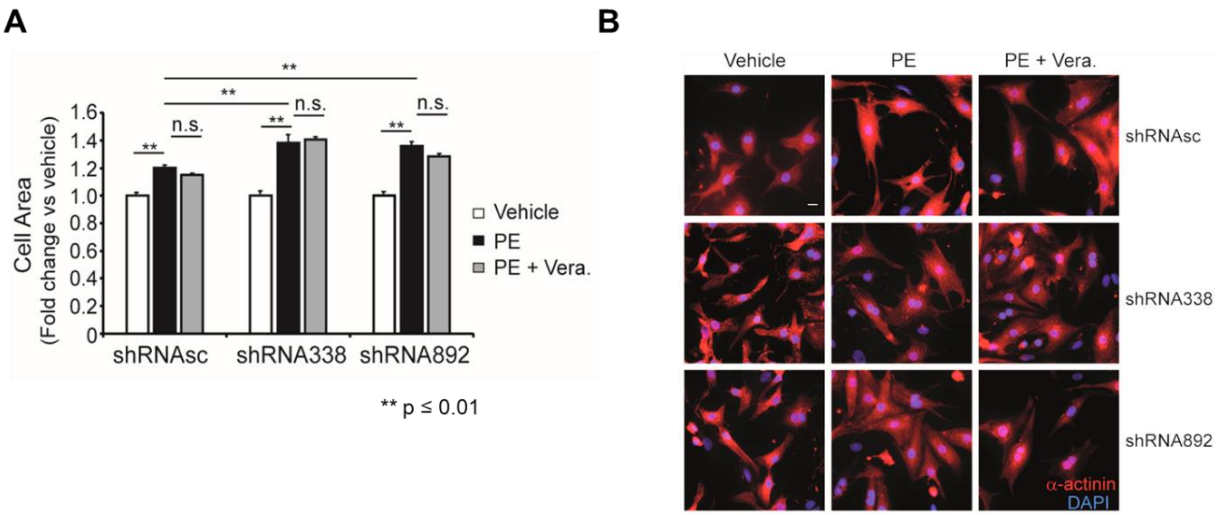

Figure 16. Downregulation of $Ca_v\beta_2$ increased cardiac hypertrophy
(A) Cell area measurement of NRCs transduced with shRNAsc (control), shRNA338 or shRNA892 ($Ca_v\beta_2$ downregulation). The cells were treated either with vehicle, PE or PE + Vera.. Mean values ± SEM were calculated from 150-250 cells of 10 images from three replicated experiments. Fold change relative to vehicle. (B) Fluorescence images of NRCs transduced with shRNAsc, shRNA338 or shRNA892. Cells were treated with vehicle, PE or PE + Vera.. Staining of the cells was done with α-actinin antibody and DAPI (nucleus). **p ≤ 0.01; n.s. = non-significant. Scale bar = 15 µm.

Stimulation of hypertrophy by PE induced a significant increase in the cell area of NRCs transduced with shRNAsc, shRNA338 or shRNA892 as compared to vehicle (Fig 16 A, white and black bars). However, while the size of shRNAsc-treated cells increases only 19 %, the area of $Ca_v\beta_2$-deficient NRCs augmented by 38 % and 41 % after transduction with shRNA338 and shRNA892, respectively. These results show that $Ca_v\beta_2$ downregulation enhances the effects of hypertrophic stimuli in cardiomyocytes.

Changes in the area of NRCs undergoing shRNA-mediated knockdown could also be attributed to a dysregulation of LTCC activity in the absence of $Ca_v\beta_2$. As mentioned previously, $Ca_v\beta_2$ can regulate the channel kinetics, the translocation of LTCCs to the membrane and the channel open probability. To address the question of whether changes in LTCC activity lead to enhanced hypertrophy in $Ca_v\beta_2$-deficient NRCs, we inhibited the LTCC activity by treating the cells with verapamil together with PE. Inhibition of LTCCs by verapamil did not change the magnitude of hypertrophy observed in shRNAsc-transduced NRCs when compared to cells treated only with PE (Fig. 16 A and B, black and grey bars). Furthermore, verapamil also did not alter the enhancement of hypertrophy in $Ca_v\beta_2$-deficient cells treated with PE (Fig. 16 A and B, black and grey bars). These findings show that the dysregulation of LTCC activity does not mediate the increase in NRC hypertrophy resulting from $Ca_v\beta_2$ downregulation. Therefore, these experiments reveal a non-LTCC-related regulatory role for $Ca_v\beta_2$ in PE-induced cardiac hypertrophy.

4.6. Hypertrophic changes in cells with shRNA-induced $Ca_v\beta_2$ knockdown are not mediated by the classical $Ca_v1.2$ channel functions

4.6.1. The enhanced hypertrophy in $Ca_v\beta_2$-deficient cells is not linked to changes in calcium homeostasis

To determine if the effects of $Ca_v\beta_2$ silencing on hypertrophy can be attributed to changes in Ca^{2+} homeostasis, we analyzed Ca^{2+} transients in NRCs transduced with shRNA-containing virus and stimulated with vehicle or PE. Fluorometric measurements of the calcium transients revealed an elevation of the amplitudes and rates of Ca^{2+} transients in PE-treated NRCs as compared to vehicle-treated cells (Fig. 17 A and B). The NRCs transduced with shRNA338 or 892, however, did not display any difference in Ca^{2+} transients as compared to shRNAsc-transduced cells.

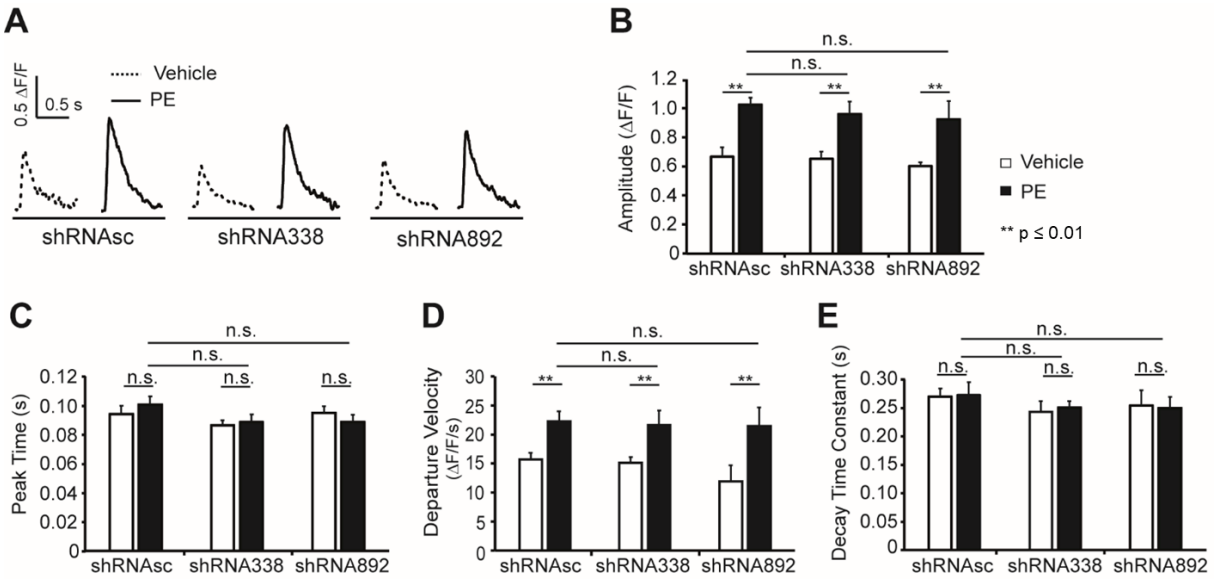

Figure 17. Calcium transients are not affected in $Ca_v\beta_2$-deficient NRCs.
(A) Representative graphs of calcium transients from NRCs transduced with control shRNAsc, shRNA338 or shRNA892. Cells were treated either with vehicle or PE and stimulated to beat at 1.0 Hz. Evaluations of the amplitude (B), peak time (C), the departure velocity (D) and the decay time constant (E) in control (shRNAsc) or $Ca_v\beta_2$-deficient cells treated with vehicle or PE were derived from calcium transients. For every condition, 11-14 cells from three different NRC preparations were examined. **p ≤ 0.01; n.s. = non-significant.

The cell response was further characterized by measuring the peak time, departure velocity and decay time constant (Fig. 17 C, D and E). Peak times and decay time constants did not differ significantly between control and $Ca_v\beta_2$-deficient cells, nor between vehicle-treated and PE-treated cells (Fig. 17 C and E). Departure velocity was also similar in control and $Ca_v\beta_2$-deficient cells, but it was significantly higher in PE-treated than in vehicle-treated cells.

Taken together, these results indicate that the effect of $Ca_v\beta_2$ on cardiac hypertrophy is not directly influenced by intracellular calcium homeostasis.

4.6.2. Overexpression of nuclear $Ca_v\beta_2$ abolishes the PE-induced hypertrophy in $Ca_v\beta_2$-knocked-down cells

The previous experiments showed that the role of $Ca_v\beta_2$ in the development of cardiac hypertrophy does not depend on the classical LTCC functions. To investigate the possible hyperthropic role of nuclear $Ca_v\beta_2$, we overexpressed a construct containing $Ca_v\beta_{2b}$-YFP with an NLS (NLS-$Ca_v\beta_{2b}$-YFP) from the SV40 T antigen fused at its N-terminus (Fig. 18 A), while a construct containing only YFP was used as negative control. Then, NRCs were transduced with either of the constructs by means of adenoviral vectors. Fig. 18 B shows the subcellular localization of the two constructs with vehicle or PE treatment. As expected, NLS-$Ca_v\beta_{2b}$-YFP was only detected in the nucleus. In contrast, YFP was able to diffuse passively through the nuclear pores due to its low molecular weight and therefore was equally distributed between the cytosol and the nucleus of the cardiomyocytes (Fig. 18 B).

To evaluate the role of nucleus-targeted $Ca_v\beta_{2b}$ in hypertrophy, NRCs transduced with NLS-$Ca_v\beta_{2b}$-YFP or YFP were stimulated with vehicle or PE (Fig. 18 B and C) and the cell areas were measured. Cells overexpressing YFP had a 20 % increase in cell area after PE stimulation as compared to the vehicle-treated NRCs. In contrast, the overexpression of NLS-$Ca_v\beta_{2b}$-YFP construct completely abolished PE-induced hypertrophy, suggesting that nuclear $Ca_v\beta_{2b}$ plays a regulatory role in cardiac hypertrophy.

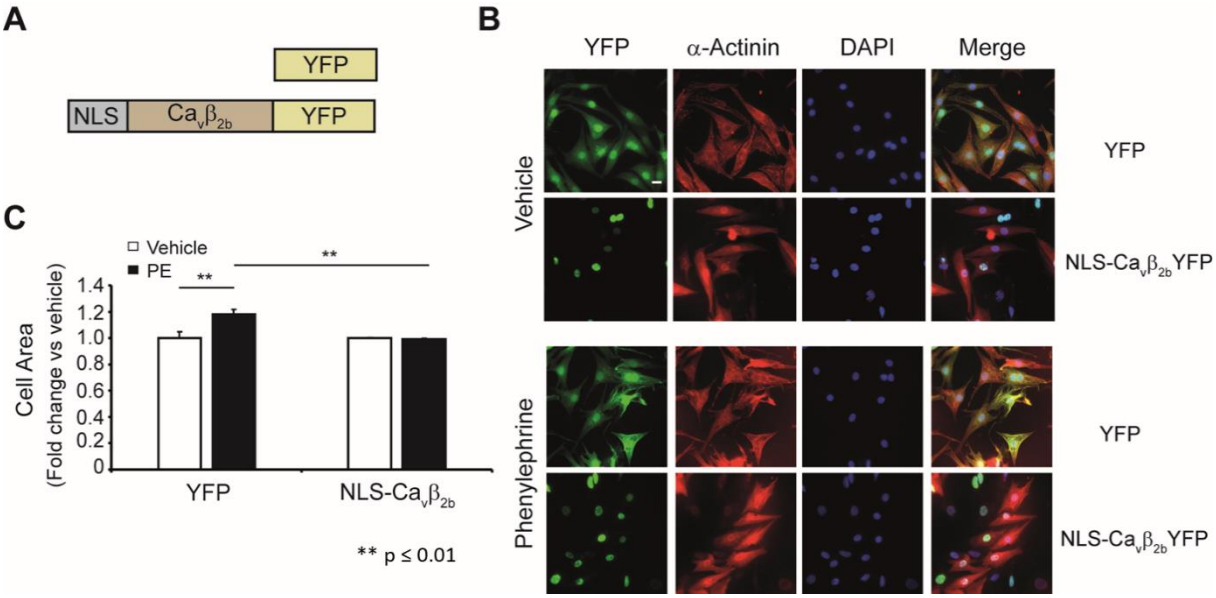

Figure 18. Overexpression of nuclear $Ca_v\beta_2$ completely abolishes PE-induced hypertrophy
(A) Two different constructs were produced, overexpressed in NRCs and evaluated. For nuclear targeting, an NLS from the SV40 large T-antigen (PPKKKRKV) was fused to the N-terminus of $Ca_v\beta_{2b}$-YFP (NLS-$Ca_v\beta_{2b}$-YFP). YFP was used as a control. (B) Representative fluorescence pictures of NRCs infected with the two different constructs. Cells were infected with adenovirus at a Moi of 50 and treated with vehicle or PE. NRCs were stained with α-actinin antibody (red) and DAPI (blue) and to that YFP fluorescence was monitored. (C) Cell area analyses of NRCs treated with vehicle (white) or PE (black) after infection with adenovirus containing NLS-$Ca_v\beta_{2b}$-YFP or YFP. Fold change is relative to vehicle treatment. The graph represents mean values for each treatment of three replicated experiments. In each experiment, 100-250 cells per group from 10 image fields were evaluated. **p ≤ 0.01; scale bar = 15 µm.

4.7. $Ca_v\beta_2$ regulates calpastatin expression and calpain activity in cardiomyocytes

4.7.1. Downregulation of $Ca_v\beta_2$ decreases calpastatin expression in cardiomyocytes

Our experiments demonstrated that the effects of $Ca_v\beta_2$ on cardiac hypertrophy are not mediated by changes in LTCC activity or in calcium homeostasis, but are instead related to the nuclear localization of $Ca_v\beta_2$. To investigate the relevance of $Ca_v\beta_2$ to protein expression in NRCs, we used lysates from cells transduced with shRNAsc, shRNA338 or shRNA892 and analyzed them by quantitative MS. The evaluation of the proteome of control and $Ca_v\beta_2$-deficient cells revealed several proteins that were up- (red, Fig. 19) or downregulated (green, fig. 19), after $Ca_v\beta_2$ silencing. In total, 17 proteins had increased expression and 35 proteins showed decreased expression levels (Supplements; Table 20 and 21). Proteins that were upregulated in $Ca_v\beta_2$-deficient NRCs included histone H2A.Z, neutropilin-1 and sarcoplasmic reticulum calcium ATPase 1 (Fig. 19). On the other hand, calpastatin, calponin-1, calumenin

and Ankyrin repeat domain-containing protein were among the downregulated proteins (Fig. 19).

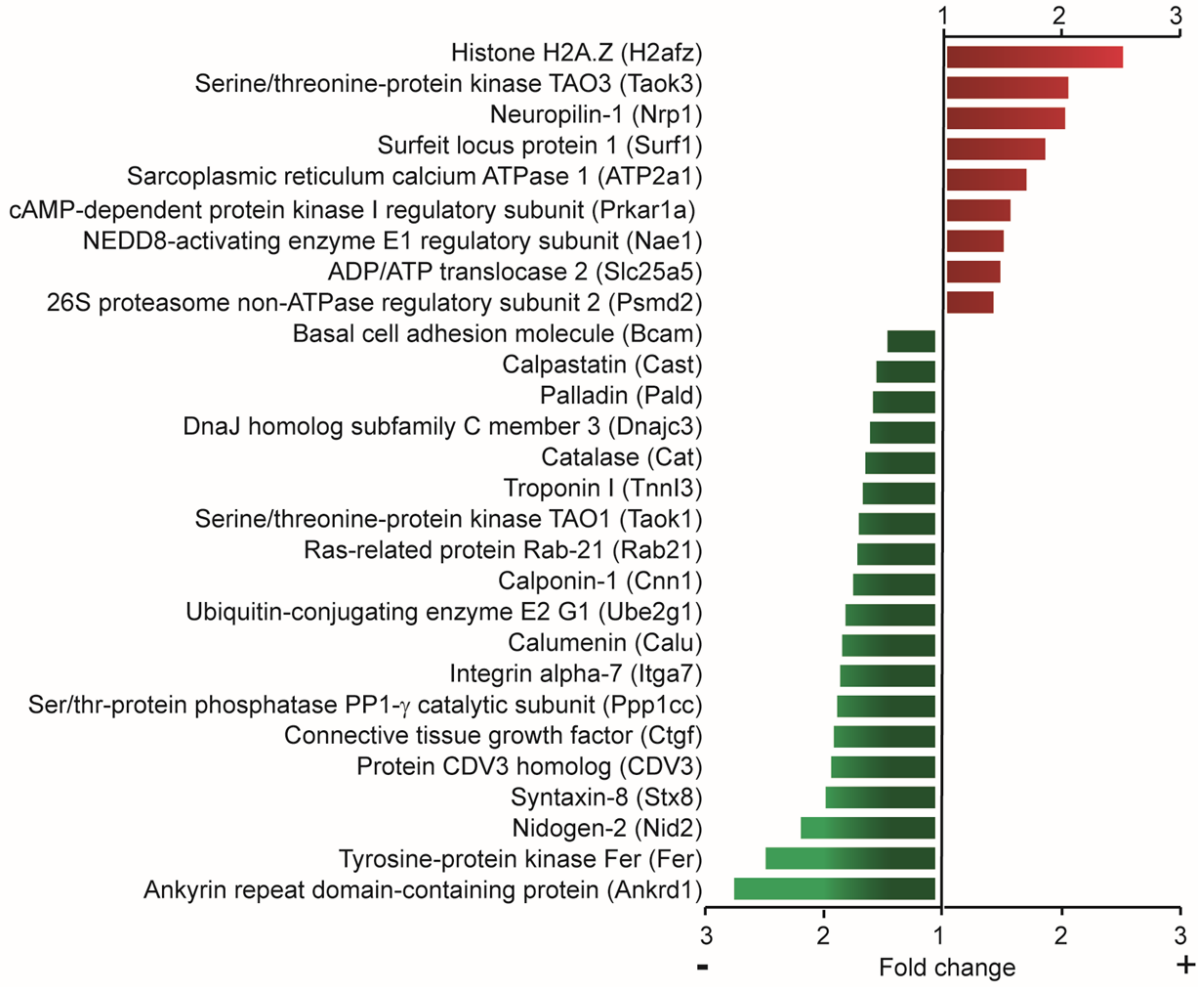

Figure 19. Analysis of protein expression in control and $Ca_v\beta_2$-deficient NRCs by mass spectrometry
Quantitative proteomic analysis of control and $Ca_v\beta_2$-deficient NRCs revealed various upregulated (red) and downregulated (green) proteins in $Ca_v\beta_2$-knocked-down cells. Cell lysates from four replicated experiments were analyzed. All of the mentioned proteins differ significantly (at least $p \leq 0.05$) from control cells in their expression.

The downregulation of calpastatin was of special interest for us, because it is an endogeneous specific inhibitor of calpain. Calpains are calcium-dependent non-lysosomal cysteine proteases and are known to participate in the development of hypertrophy [148], [172]. To verify the results from MS, we performed western blots and demonstrated that the expression of calpastatin was also decreased with the downregulation of $Ca_v\beta_2$ (shRNA338 and shRNA 892) (Fig. 20 A and B). Densitometric analyses revealed that calpastatin expression was reduced in $Ca_v\beta_2$-deficient NRCs by 25 % (shRNA338) and 30 % (shRNA892). Therefore, the western blot results corroborate the MS analyses and together suggest that downregulation of calpastatin could have an influence on the development of hypertrophy in cardiomyocytes.

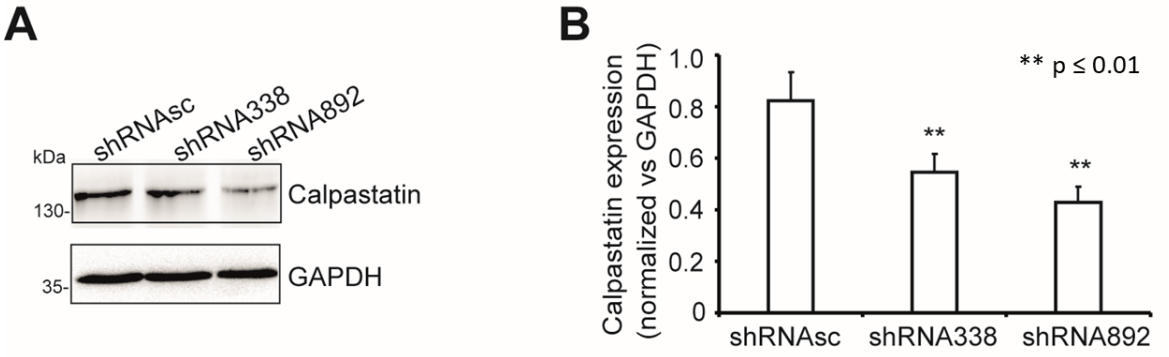

Figure 20. Downregulation of $Ca_v\beta_2$ reduces calpastatin expression in NRCs
(A) Detection of calpastatin expression in lysates from control (shRNAsc) and $Ca_v\beta_2$-deficient (shRNA338 and shRNA892) NRCs. An anti-GAPDH antibody was used as a loading control. Seventy-five micrograms of protein were loaded on a SDS gel. (B) Quantification of calpastatin intensity of three replicated western blots from control (shRNAsc) or $Ca_v\beta_2$-deficient (shRNA338 and 892) NRCs. A Moi of 20 was used for each shRNA. **p ≤ 0.01

4.7.2. $Ca_v\beta_2$ regulates calpain activity in cardiomyocytes

The results from mass spectrometry and western blots revealed less calpastatin expression in $Ca_v\beta_2$-deficient NRCs than in control cells. Since calpastatin is a specific inhibitor of calpain, we hypothesized that calpain activity is increased in $Ca_v\beta_2$-deficient NRCs. Moreover, we suggested that an elevated calpain activity promotes the PE-induced increase of hypertrophy in $Ca_v\beta_2$-downregulated cells. To examine this, we performed a calpain activity assay in lysates from shRNAsc-, shRNA338- and shRNA892-transduced cells (Fig. 21).

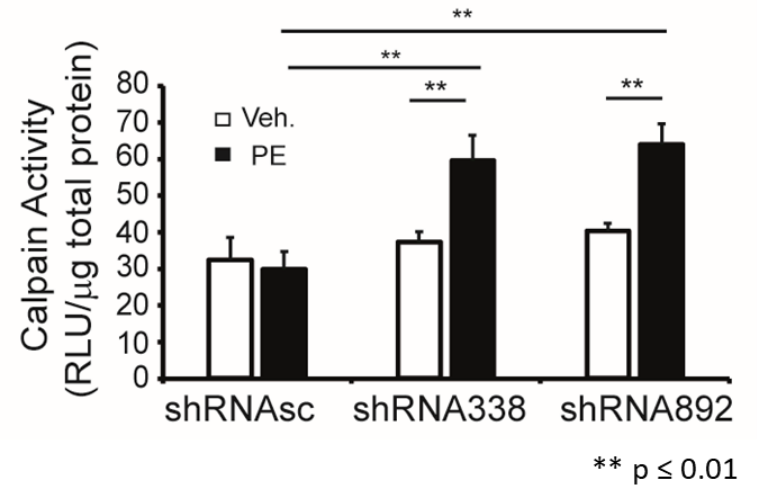

Figure 21. Increased calpain activity in $Ca_v\beta_2$-deficient NRCs
Calpain activity was analyzed in control cells (shRNAsc) and cells with $Ca_v\beta_2$ knockdown (shRNA338 or shRNA892), either untreated (vehicle; Veh.) or treated with PE. While the calpain activity in untreated NRCs (white) transduced with shRNA338, 892 or shRNAsc did not change, it was significantly higher in $Ca_v\beta_2$-deficient cells treated with PE (black). Results are presented as Mean ± SEM of three experiments. **p ≤ 0.01.

Treatment with vehicle did not affect the calpain activity in NRCs transduced with shRNAsc, shRNA338 or shRNA892 (Fig. 21). However, a 2-fold increase in the activity of the enzyme was detected in $Ca_v\beta_2$-deficient cells after treatment with PE (Fig. 21).

4.7.3. Calpain activity mediates the enhancement of hypertrophy in $Ca_v\beta_2$-deficient cardiomyocytes.

In order to elucidate if an increase in calpain activity in $Ca_v\beta_2$-deficent cardiomyocytes could explain the increased hypertrophy observed in these cells, we pre-treated control cells (shRNAsc) and $Ca_v\beta_2$-deficient cells (shRNA338 and shRNA892) with calpeptin, a specific inhibitor of calpain and then induced cardiac hypertrophy with PE. The area of cardiomyocytes transduced with shRNAsc was significantly higher after treatment with PE or PE + calpeptin than in cells treated with vehicle + calpeptin (Fig. 22). However, in $Ca_v\beta_2$-deficient NRCs, which have a chronically higher calpain activity, calpeptin prevented the enhanced cardiomyocyte hypertrophy induced by PE treatments (Fig. 16 and 22). These results indicate that in $Ca_v\beta_2$-deficient cells an increase in calpain activity plays an important role as a positive modulator of cardiac hypertrophy.

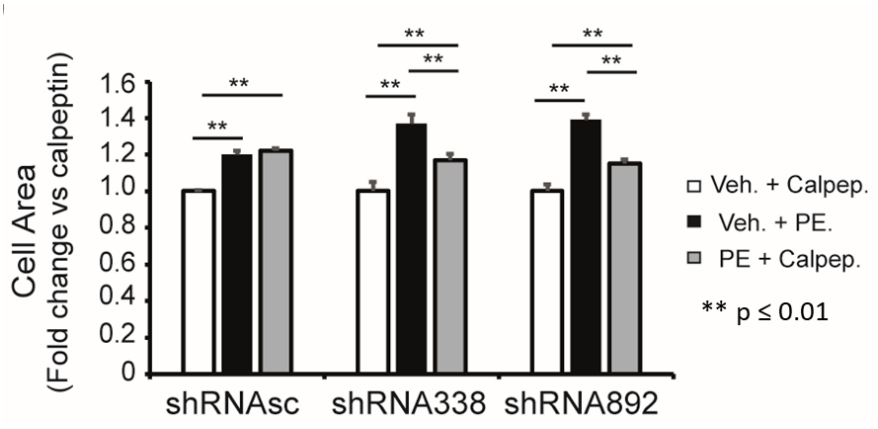

Figure 22. Inhibition of calpain activity by calpeptin reduces the hypertrophy induced by PE in $Ca_v\beta_2$-deficient cells
Area of NRCs transduced with shRNAsc, shRNA338 or shRNA892. Cells were treated with vehicle and calpeptin (Veh. + Calpep., white), vehicle + PE (Veh. + PE) or calpeptin + PE (PE + Calpep., black). Fold change is relative to Veh + Calpep.-treated cells. For each condition, 100-250 cells were measured from three replicated experiments. The results are presented as Mean ± SEM. **p ≤ 0.01.

5. Discussion

5.1. Expression and nuclear localization of $Ca_v\beta_2$

It is already known from previous studies that of the four nonallelic isoforms of $Ca_v\beta$ ($Ca_v\beta_{1-4}$), $Ca_v\beta_2$ is predominant in murine and human cardiomyocytes [52]. Accordingly, mutations in the CACNB2 gene are associated with cardiac arrhythmias and sudden death [20]. However, $Ca_v\beta_2$ has five different splice variants, $Ca_v\beta_{2a-e}$, which confer different electrophysiological properties to LTCCs when co-expressed with the channel in heterologous expression systems. Our PCR and qRT-PCR results (Fig. 8 A and B) showed that $Ca_v\beta_{2b}$ is the predominant splice variant in the mouse heart. These results suggest that the majority of $Ca_v\beta_2$ detected in the heart by commercially available antibodies correspond to $Ca_v\beta_{2b}$ and that most of the LTCC complexes in cardiomyocytes have the same electrophysiological properties.

Using immunocytochemistry, we corroborated that $Ca_v\beta_2$, which lies on the dyads as part of the LTCC complexes, is in close proximity to the RyR2 in the sarcoplasmic reticulum of AMCs. Apart from this pool of $Ca_v\beta_2$, we also detected a fraction of the subunit targeted to the nucleus of AMCs and NRCs. Moreover, western blots from cellular fractionation samples of mouse hearts and AMCs confirmed that most $Ca_v\beta_2$ is located on the membrane, and showed that an additional fraction also translocated to the nucleus. The nuclear localization of different $Ca_v\beta$ isoforms has been previously reported. For example, $Ca_v\beta_{4b}$ was detected in the nucleus of neurons and muscle cells [126], while nuclear $Ca_v\beta_2$ was found in cardiac muscle cells of the HL-1 cell line [130]. Another report confirmed the presence of $Ca_v\beta_{1a}$ in the nucleus of muscle progenitor cells [125]. The targeting of $Ca_v\beta_2$ to the nucleus suggests that this protein has a potential alternative role that is not linked to the regulation of LTCC activity and trafficking. LTCC-independent functions of $Ca_v\beta$ were already described for different $Ca_v\beta$ isoforms acting as transcriptional regulators in different cell types [123], [124], [181]. Therefore, $Ca_v\beta_2$ could also have LTCC-independent functions in cardiomyocytes.

To asses, which region of $Ca_v\beta_{2b}$ is needed for the translocation to the nucleus, HEK293A cells were transfected with different constructs lacking one or more structural domains. WT $Ca_v\beta_{2b}$ was used as control. Since the size limit for passive diffusion through the nuclear pores is around 40 kDa [182] and the smallest construct ($Ca_v\beta_{2b}\Delta$ GK/CT) had a molecular

weight of 52 kDa, the designed $Ca_v\beta_{2b}$ contructs could only cross the nuclear membrane by means of an active transporter.

Our nuclear translocation experiments in HEK293A cells (section 4.3) showed that all $Ca_v\beta_2$ constructs lacking the NT, Hook, GK, or CT regions ($Ca_v\beta_{2b}\Delta$ NT/CT, $Ca_v\beta_{2b}\Delta$ GK/CT, $Ca_v\beta_{2b}\Delta$ CT, $Ca_v\beta_{2b}\Delta$ NT and $Ca_v\beta_{2b}\Delta$ NT/Hook/CT) were detected at some extend in the nuclear fraction, just as the control full-length $Ca_v\beta_{2b}$. These results indicate that the NT, Hook, GK and CT domains probably do not contain any NLS or are not important for nuclear translocation. In contrast, the construct lacking the NT and SH3 regions ($Ca_v\beta_{2b}\Delta$ NT/SH3) was not detected in the nuclear fraction. Since the N-terminal region is absent also in other constructs that were detected in the nucleus, the exclusion of $Ca_v\beta_{2b}\Delta$ NT/SH3 from the nucleus can be attributed only to the SH3 domain.

Proteins that do not passively diffuse through the nuclear pore can use alternative ways to translocate to the nucleus. These alternatives include an NLS in their amino acid sequence and/or interacting with nucleus-targeted proteins. Our results suggest either or both of these mechanisms (i.e., the presence of an NLS in the amino acid sequence of the SH3 domain and/or the interaction of the SH3 domain with a nucleus-targeted protein) could mediate the nuclear translocation of $Ca_v\beta$. Different $Ca_v\beta$ isoforms have been reported to contain an NLS in their amino acid sequence [125], [126]. Accordingly, the presence of $Ca_v\beta_{4b}$ in the nucleus of neurons and skeletal cells is dependent on an Arg-Arg-Ser motif in the protein´s N-terminus [126]. Furthermore, another report showed that the nuclear translocation of $Ca_v\beta_{1a}$ in muscle progenitor cells depends on the SH3 domain or the middle region of $Ca_v\beta$´s amino acid sequence [125].

$Ca_v\beta_2$ could also translocate to the nucleus by interacting with nucleus-targeted proteins. SH3 domains are common interaction regions that can mediate protein-protein interactions by binding to a proline rich domain (PRD) motif in target proteins. It has been reported that, for example, $Ca_v\beta$ interacts with members of the RGK protein family (Ras-related small GTP-binding proteins) [117], [118], [183], and this interaction is sufficient to transfer $Ca_v\beta_2$ to the nucleus [130]. Moreover, other groups also identified various nucleus-targeted proteins as potential binding partners of $Ca_v\beta$. For example, in skeletal muscle cells the interaction of the $Ca_v\beta_{1a}$ NT domain with troponin T3 regulates the translocation of $Ca_v\beta_{1a}$ to the nucleus

[184]. Hibino *et al* demonstrated that the translocation of $Ca_v\beta_4$ to the nucleus required its interaction with a heterochromatin protein 1 [124] and that this interaction occurred through the SH3 domain or middle region of $Ca_v\beta_4$. Furthermore, the interaction of a Pax6 splicing form with $Ca_v\beta_3$ led to the translocation of the two proteins to the nucleus. Since the nuclear translocation of Pax6 also occurred with the other three isoforms of $Ca_v\beta$, it was suggested that the binding site for Pax6 is located in the conserved regions of $Ca_v\beta$, such as SH3 or GK [123]. These previous studies highlight the importance of the SH3 domain for the translocation of different $Ca_v\beta$ isoforms and are in agreement with our results indicating the involvement of this domain in the targeting of $Ca_v\beta_2$ to the nucleus. Presumably, $Ca_v\beta_2$ is conveyed to the nucleus by some of these already reported proteins, although it is still unknown which nucleus-targeted binding partners of the $Ca_v\beta_2$-SH3 domain could be involved. Further experiments, like the expression of plasmids only encoding the SH3 domain, need to be performed in order to elucidate the remaining questions concerning the translocation of $Ca_v\beta_2$ to the nucleus.

5.2. $Ca_v\beta_2$ in cardiomyocyte hypertrophy

Nuclear $Ca_v\beta_2$ expression is downregulated in cardiomyocytes from TAC-operated mice as compared to Sham-operated. Moreover, *in vitro* treatment of cardiomyocytes with the hypertrophy-inducing α_1-adrenergic agonists PE produced an increase in cell size together with a reduction in nuclear $Ca_v\beta_2$. The increase in cardiomyocyte size could be attributed to the activation of the calcineurin/NFAT and CaMKII signalling pathways by α_1-adrenergic agonists. Changes in nuclear $Ca_v\beta_2$ could also have influenced the expression of diverse proteins and the development of hypertrophy. Until now most of the studies addressing the function of $Ca_v\beta$ concentrated mainly on its impact on LTCC activity and regulation. However, it was recently reported that $Ca_v1.2$ had normal calcium currents in murine cardiomyocytes even if the $Ca_v\beta$ subunit was not bound to the channel [115]. Based on these results, it can be assumed that $Ca_v\beta_2$ could have other functions besides regulating LTCC activity in cardiomyocytes.

In our experiments, $Ca_v\beta_2$-deficient NRCs developed greater hypertrophy than the control cells after treatment with PE. This enhanced hypertrophic effect was also observed when the NRCs were treated with PE and the LTCC inhibitor verapamil, indicating that this effect was

mediated by an LTCC-independent mechanism, since differences in cell size were not the result of modified LTCC activity.

The above mentioned results contrast with two studies that evaluated the impact of $Ca_v\beta_2$ on hypertrophy *in vitro* and *in vivo*. Chen *et al* overexpressed $Ca_v\beta_{2a}$ in NRCs, adult feline cardiomyocytes and in a transgenic mouse model [163], and observed enhanced LTCC Ca^{2+} currents *in vitro* and *in vivo,* which were sufficient to induce hypertrophy. However, the splice variant ($Ca_v\beta_{2a}$) overexpressed in their experiments is barely expressed in cardiomyocytes. As our results from qRT-PCR experiments showed, $Ca_v\beta_{2b}$ is the predominant isoform in the heart. Moreover, $Ca_v\beta_{2a}$ is a palmitoylated variant that localizes in the plasma membrane and therefore can have distinct properties compared to $Ca_v\beta_{2b}$ [127], [185], [186]. The palmitoylation of $Ca_v\beta_{2a}$ at the plasma membrane could also have an influence on the translocation of this splice variant to the nucleus or other cellular compartments. Furthermore, also the interaction between this splice variant and other non-LTCC-related proteins, especially in distinct cellular compartments, could be altered. For that reason, it is difficult to compare the results from this study with our experiments. However, given its predominant expression in cardiomyocytes, we think that $Ca_v\beta_{2b}$ should be preferably used to determine the role of the $Ca_v\beta$ subunit in cardiac hypertrophy.

In another study, Cingolani *et al* [187] described that the downregulation of $Ca_v\beta_2$ using shRNAs *in vivo* and *in vitro* led to attenuated hypertrophy and reduced LTCC currents *in vivo*. These experiments were conducted in NRCs, adult rat cardiomyocytes and mouse models. However, the authors used HEK293 cells transfected with $Ca_v\beta_2$-GFP to examine the efficacy of the shRNAs in downregulating $Ca_v\beta_2$. No validation of the functionality of the shRNAs in NRCs was performed to confirm the downregulation of $Ca_v\beta_2$ observed in HEK293 cells.

We also checked the calcium transients in control (shRNAsc-transduced) and $Ca_v\beta_2$-deficient NRCs and observed no difference in calcium homeostasis between them. These results further support the assumption that the interaction between $Ca_v\beta_2$ and the $Ca_v\alpha_1$ subunit is not required for the membrane expression of the channel. Furthermore, $Ca_v\beta_2$ is also apparently not required for the regulation of the channels in NRCs, since $Ca_v\beta_2$-deficient cells still display normal calcium transients. Therefore, $Ca_v\beta_2$ is presumably not needed for the normal function of the channel and it has LTCC-independent functions. This is consistent with data from previous studies [114], [115] showing that cardiomyocytes isolated from

adult mice with a conditional specific deletion of $Ca_v\beta_2$ showed only mild decrease in LTCC currents and no cardiac hypertrophy under physiological conditions [114].

In our experiments, we could detect $Ca_v\beta_2$ in the nucleus, which further leads to the suggestion of an LTCC-independent function of this protein in cardiomyocytes. Furthermore, the expression of the nuclear-targeted $Ca_v\beta_2$ decreased when the cells were stimulated with PE. To validate our observations on the effect of nuclear $Ca_v\beta_2$ on the development of cardiac hypertrophy, we fused an NLS to the N-terminus of $Ca_v\beta_2$, to completely target the protein to the nucleus, and overexpressed it in NRCs. This nuclear overexpressed $Ca_v\beta_2$ completely inhibited the PE-induced hypertrophy. This result together with the observation that the expression of $Ca_v\beta_2$ in the nucleus decreases after the induction of hypertrophy, support the potential regulatory role of $Ca_v\beta_2$ in the nucleus of cardiomyocytes and its importance in the control of hypertrophy.

5.3. $Ca_v\beta_2$ regulates protein expression and participates in antihypertrophic pathways

To asses the role of nuclear $Ca_v\beta_2$ in cardiomyocytes and how changes in its expression levels can influence the expression of other proteins, we downregulated $Ca_v\beta_2$ in NRCs and analysed the cellular proteome by mass spectrometry. The silencing of $Ca_v\beta_2$ modified the expression of different proteins, suggesting a direct or indirect regulatory role in the transcription of diverses genes. Transcriptional regulation by $Ca_v\beta$ subunits in diverse cell types has been reported. For example, $Ca_v\beta_{1a}$ is known to regulate gene expression and to inhibit the expression of myogenin in muscle progenitor cells [125]. $Ca_v\beta_3$ and $Ca_v\beta_4$ have also been reported to act as transcription regulators [123], [124].

Of special interest in the list of upregulated or downregulated proteins is calpastatin, whose expression was 20 % lower in $Ca_v\beta_2$-deficient NRCs as compared to control cells. A decreased calpastatin expression might suggest that the activity of calpain could consequently increase. Calpain activity was not affected by $Ca_v\beta_2$ expression in NRCs under basal conditions, but significantly increased in $Ca_v\beta_2$-deficient NRCs after the induction of hypertrophy. Increasing calpain activity requires not only less calpastatin, but also more intracellular calcium. In $Ca_v\beta_2$-deficient NRCs, the reduced calpastatin expression does not result in increased calpain activity, since intracellular calcium levels are not high enough to activate the calcium-

dependent hypertrophy signaling pathways. On the other hand, PE treatment increases intracellular calcium levels, which combined with the lower calpastatin expression in $Ca_v\beta_2$-deficient NRCs leads to an increase in calapin activity in these cells. Several authors have reported that calpastatin or calpain expression levels influence the development of cardiovascular pathophysiological processes like cardiac hypertrophy [148], [170], [172]. In 2008, Letavernier *et al* reported that overexpression of calpastatin in transgenic mice treated with Ang II resulted in partial inhibition of calpain, prevented cardiovascular remodelling and attenuated hypertrophy [148]. Similarly, another group observed that transgenic mice overexpressing calpastatin had lower calpain expression and activity after myocardial infaction [170]. Moreover, cardiac hypertrophy and fibrosis were attenuated in these animals. These authors proposed that cardiac remodelling was associated with the upregulation of calpain or the downregulation of calpastatin. In a type 1 diabetes mouse model, targeted inhibition of calpain reduced hypertrophy and fibrosis [171]. All these studies concluded that the regulation of calpain activity could be an important target to inhibit cardiac hypertrophy.

Burkard *et al* proposed a calpain-mediated mechanism for the activation of cardiomyocyte hypertrophy through calcineurin/NFAT signaling. They described that Ang II treatment elevated calpain activity in cardiomyocytes and promoted the cleavage of the autoinhibitory domain of calcineurin by calpain [172], increasing its phosphatase activity. This enabled calcineurin to dephosphorylate NFAT and translocate together with NFAT to the nucleus, where they regulated hypertrophy-related gene transcription. The increased transcriptional activity of calcineurin persisted even after removal of the hypertrophy-inducing stimulus. Therefore, this permanent calpain-mediated mechanism is likely to induce a stronger hypertrophy-inducing effect than the ones triggered by calpain-independent mechanisms. Calpain also participates in the activation of NFκB [148], a transcription factor known to be involved in the induction of cardiac hypertrophy. Calpains are known to degrade the NFκB inhibitor IkBa and thereby enable NFκB to translocate to the nucleus. In addition, calpain presumably activates chromogranin B, a protein that regulates NFκB activity [139], [169], [188]. In our experiments, we showed that calpastatin expression was downregulated in $Ca_v\beta_2$-deficient NRCs, which in turn resulted in a higher calpain activity. This higher calpain activity could lead to an increased hypertrophy in $Ca_v\beta_2$-knocked-down NRCs as compared to control cells, probably through the activation of calpain-mediated mechanisms like the

calcineurin/NFAT or NFκB signaling cascades. Both of these mechanisms could contribute to pathological cardiac hypertrophy.

Finally, we performed pharmacological experiments with NRCs, using the calpain inhibitor calpeptin together with hypertrophy-inducing agent PE. In control cells, calpain inhibition did not modify the increase in cell area induced by PE, which indicates that hypertrophy is mainly triggered by calpain-independent signaling pathways. On the other hand, $Ca_v\beta_2$-deficient NRCs had a higher baseline calpain activity and developed greater hypertrophy when treated with PE as compared to the control cells. Inhibition of calpain prevented this increased hypertrophy in $Ca_v\beta_2$-deficient NRCs when treated with PE, suggesting that the activation of calpain probably switches on calpain-dependent hypertrophy signaling pathways.

5.4. Conclusion and prospect of the project

In summary, our results show that $Ca_v\beta_2$ downregulation can lead to an enhanced cardiomoycyte hypertrophy. Moreover, we demonstrated for the first time the presence of $Ca_v\beta_2$ in the nucleus of AMCs and NRCs and that $Ca_v\beta_2$ downregulation affects the expression of diverse proteins, inducing, for instance, a decrease in calpastatin levels. The reduction of calpastatin expression could enable the activation and upregulation of calpain-mediated hypertrophy signaling pathways. By regulating such calpain-mediated hypertrophy signaling, $Ca_v\beta_2$ seems to play an important protective role against the development of hypertrophy in cardiomyocytes.

To extend the knowledge resulting from this study, more experiments could be performed *in vivo* using mouse models with conditional cardiomyocyte-specific deletion of $Ca_v\beta_2$. This would complement the findings described in this work and reduce the limitations resulting from the differences between these models in terms of physiology of the cardiac muscle cells and/or the functionality of $Ca_v\beta_2$. Additionally, to elucidate whether $Ca_v\beta_2$ directly or only indirectly regulates transcriptional activity, a luciferase assay could be performed that predicts if $Ca_v\beta_2$ alone is sufficient to start transcription

We detected 17 upregulated and 35 downregulated proteins in $Ca_v\beta_2$-deficient NRCs. Therefore, the analysis of the role of other of these proteins, like ankyrin repeat domain-containing protein 1, in cardiomyocyte hypertrophy could contribute to a better

understanding of the role of $Ca_v\beta_2$ in the physiology of cardiomyocytes and in the development of cardiomyocyte hypertrophy.

Overall, this project provides new knowledge on the hypertrophy signaling mechanisms induced by G_q-protein-coupled receptor agonists and reveals a new regulatory role for the nucleus-targeted $Ca_v\beta_2$ in this pathology. Moreover, our results suggest that nuclear $Ca_v\beta_2$ is important for calpain-mediated signaling, which could be of high clinical relevance.

Literature

[1] P. Fatt and B. Katz, 'The electrical properties of crustacean muscle fibres', *J. Physiol.*, vol. 120, no. 1–2, pp. 171–204, Apr. 1953.

[2] M. Takahashi, M. J. Seagar, J. F. Jones, B. F. Reber, and W. A. Catterall, 'Subunit structure of dihydropyridine-sensitive calcium channels from skeletal muscle', *Proc. Natl. Acad. Sci. U. S. A.*, vol. 84, no. 15, pp. 5478–5482, Aug. 1987.

[3] B. M. Curtis and W. A. Catterall, 'Purification of the calcium antagonist receptor of the voltage-sensitive calcium channel from skeletal muscle transverse tubules', *Biochemistry*, vol. 23, no. 10, pp. 2113–2118, May 1984.

[4] T. Tanabe *et al.*, 'Primary structure of the receptor for calcium channel blockers from skeletal muscle', *Nature*, vol. 328, no. 6128, pp. 313–318, Jul. 1987.

[5] A. Gambardella and A. Labate, 'The role of calcium channel mutations in human epilepsy', *Prog. Brain Res.*, vol. 213, pp. 87–96, 2014.

[6] E. Carbone and H. D. Lux, 'A low voltage-activated, fully inactivating Ca channel in vertebrate sensory neurones', *Nature*, vol. 310, no. 5977, pp. 501–502, Aug. 1984.

[7] E. A. Ertel *et al.*, 'Nomenclature of Voltage-Gated Calcium Channels', *Neuron*, vol. 25, no. 3, pp. 533–535, Mar. 2000.

[8] D. Hillman, S. Chen, T. T. Aung, B. Cherksey, M. Sugimori, and R. R. Llinás, 'Localization of P-type calcium channels in the central nervous system.', *Proc. Natl. Acad. Sci.*, vol. 88, no. 16, pp. 7076–7080, Aug. 1991.

[9] M. C. Nowycky, A. P. Fox, and R. W. Tsien, 'Three types of neuronal calcium channel with different calcium agonist sensitivity', *Nature*, vol. 316, no. 6027, pp. 440–443, Aug. 1985.

[10] A. Randall and R. W. Tsien, 'Pharmacological dissection of multiple types of Ca2+ channel currents in rat cerebellar granule neurons', *J. Neurosci. Off. J. Soc. Neurosci.*, vol. 15, no. 4, pp. 2995–3012, Apr. 1995.

[11] E. Bourinet *et al.*, 'Splicing of α_{1A} subunit gene generates phenotypic variants of P- and Q-type calcium channels', *Nat. Neurosci.*, vol. 2, no. 5, pp. 407–415, May 1999.

[12] E. Perez-Reyes, 'Molecular Physiology of Low-Voltage-Activated T-type Calcium Channels', *Physiol. Rev.*, vol. 83, no. 1, pp. 117–161, Jan. 2003.

[13] W. A. Catterall, 'Voltage-Gated Calcium Channels', *Cold Spring Harb. Perspect. Biol.*, vol. 3, no. 8, p. a003947, Jan. 2011.

[14] P. Hess, J. B. Lansman, and R. W. Tsien, 'Different modes of Ca channel gating behaviour favoured by dihydropyridine Ca agonists and antagonists', *Nature*, vol. 311, no. 5986, pp. 538–544, Oct. 1984.

[15] E. W. McCleskey *et al.*, 'Omega-conotoxin: direct and persistent blockade of specific types of calcium channels in neurons but not muscle.', *Proc. Natl. Acad. Sci. U. S. A.*, vol. 84, no. 12, pp. 4327–4331, Jun. 1987.

[16] I. M. Mintz, V. J. Venema, K. M. Swiderek, T. D. Lee, B. P. Bean, and M. E. Adams, 'P-type calcium channels blocked by the spider toxin ω-Aga-IVA', *Nature*, vol. 355, no. 6363, pp. 827–829, Feb. 1992.

[17] R. Newcomb *et al.*, 'Selective Peptide Antagonist of the Class E Calcium Channel from the Venom of the Tarantula Hysterocrates gigas', *Biochemistry*, vol. 37, no. 44, pp. 15353–15362, Nov. 1998.

[18] V. N. Uebele *et al.*, 'Positive Allosteric Interaction of Structurally Diverse T-Type Calcium Channel Antagonists', *Cell Biochem. Biophys.*, vol. 55, no. 2, pp. 81–93, Nov. 2009.

[19] R. L. Kraus *et al.*, 'In Vitro Characterization of T-Type Calcium Channel Antagonist TTA-A2 and In Vivo Effects on Arousal in Mice', *J. Pharmacol. Exp. Ther.*, vol. 335, no. 2, pp. 409–417, Nov. 2010.

[20] G. W. Zamponi, J. Striessnig, A. Koschak, and A. C. Dolphin, 'The Physiology, Pathology, and Pharmacology of Voltage-Gated Calcium Channels and Their Future Therapeutic Potential', *Pharmacol. Rev.*, vol. 67, no. 4, pp. 821–870, Oct. 2015.

[21] I. Bodi, G. Mikala, S. E. Koch, S. A. Akhter, and A. Schwartz, 'The L-type calcium channel in the heart: the beat goes on', *J. Clin. Invest.*, vol. 115, no. 12, pp. 3306–3317, Dec. 2005.

[22] K. Takimoto, D. Li, J. M. Nerbonne, and E. S. Levitan, 'Distribution, Splicing and Glucocorticoid-Induced Expression of Cardiacα1Candα1DVoltage-gated Ca2+Channel mRNAs', *J. Mol. Cell. Cardiol.*, vol. 29, no. 11, pp. 3035–3042, Nov. 1997.

[23] J. Platzer *et al.*, 'Congenital Deafness and Sinoatrial Node Dysfunction in Mice Lacking Class D L-Type Ca2+ Channels', *Cell*, vol. 102, no. 1, pp. 89–97, Jul. 2000.

[24] M. E. Mangoni *et al.*, 'Functional role of L-type Cav1.3 Ca2+ channels in cardiac pacemaker activity', *Proc. Natl. Acad. Sci.*, vol. 100, no. 9, pp. 5543–5548, Apr. 2003.

[25] Zhang Zhao *et al.*, 'Functional Roles of Cav1.3 (α1D) Calcium Channel in Sinoatrial Nodes', *Circ. Res.*, vol. 90, no. 9, pp. 981–987, May 2002.

[26] A. Fabiato, 'Calcium-induced release of calcium from the cardiac sarcoplasmic reticulum', *Am. J. Physiol.-Cell Physiol.*, Jul. 1983.

[27] X. Zhen, C. Xie, A. Fitzmaurice, C. E. Schoonover, E. T. Orenstein, and J. Yang, 'Functional Architecture of the Inner Pore of a Voltage-gated Ca2+ Channel', *J. Gen. Physiol.*, vol. 126, no. 3, pp. 193–204, Sep. 2005.

[28] W. A. Catterall, 'Structure and Regulation of Voltage-Gated Ca2+ Channels', *Annu. Rev. Cell Dev. Biol.*, vol. 16, no. 1, pp. 521–555, 2000.

[29] M. Pragnell, M. De Waard, Y. Mori, T. Tanabe, T. P. Snutch, and K. P. Campbell, 'Calcium channel beta-subunit binds to a conserved motif in the I-II cytoplasmic linker of the alpha 1-subunit', *Nature*, vol. 368, no. 6466, pp. 67–70, Mar. 1994.

[30] Z. Buraei and J. Yang, 'Structure and function of the β subunit of voltage-gated Ca2+ channels', *Biochim. Biophys. Acta BBA - Biomembr.*, vol. 1828, no. 7, pp. 1530–1540, Jul. 2013.

[31] R. J. Diebold *et al.*, 'Mutually exclusive exon splicing of the cardiac calcium channel alpha 1 subunit gene generates developmentally regulated isoforms in the rat heart', *Proc. Natl. Acad. Sci.*, vol. 89, no. 4, pp. 1497–1501, Feb. 1992.

[32] W. J. Koch, P. T. Ellinor, and A. Schwartz, 'cDNA cloning of a dihydropyridine-sensitive calcium channel from rat aorta. Evidence for the existence of alternatively spliced forms.', *J. Biol. Chem.*, vol. 265, no. 29, pp. 17786–17791, Oct. 1990.

[33] T. P. Snutch, W. J. Tomlinson, J. P. Leonard, and M. M. Gilbert, 'Distinct calcium channels are generated by alternative splicing and are differentially expressed in the mammalian CNS', *Neuron*, vol. 7, no. 1, pp. 45–57, Jul. 1991.

[34] D. Lipscombe, J. Q. Pan, and A. C. Gray, 'Functional diversity in neuronal voltage-gated calcium channels by alternative splicing of Cavα1', *Mol. Neurobiol.*, vol. 26, no. 1, pp. 21–44, Aug. 2002.

[35] J. Arikkath and K. P. Campbell, 'Auxiliary subunits: essential components of the voltage-gated calcium channel complex', *Curr. Opin. Neurobiol.*, vol. 13, no. 3, pp. 298–307, Jun. 2003.

[36] K. S. D. Jongh, C. Warner, and W. A. Catterall, 'Subunits of purified calcium channels. Alpha 2 and delta are encoded by the same gene.', *J. Biol. Chem.*, vol. 265, no. 25, pp. 14738–14741, May 1990.

[37] S. B. Ellis *et al.*, 'Sequence and expression of mRNAs encoding the alpha 1 and alpha 2 subunits of a DHP-sensitive calcium channel', *Science*, vol. 241, no. 4873, pp. 1661–1664, Sep. 1988.

[38] A. Davies *et al.*, 'The α2δ subunits of voltage-gated calcium channels form GPI-anchored proteins, a posttranslational modification essential for function', *Proc. Natl. Acad. Sci.*, vol. 107, no. 4, pp. 1654–1659, Jan. 2010.

[39] S. D. Jay, A. H. Sharp, S. D. Kahl, T. S. Vedvick, M. M. Harpold, and K. P. Campbell, 'Structural characterization of the dihydropyridine-sensitive calcium channel alpha 2-subunit and the associated delta peptides.', *J. Biol. Chem.*, vol. 266, no. 5, pp. 3287–3293, Feb. 1991.

[40] R. Felix, C. A. Gurnett, M. D. Waard, and K. P. Campbell, 'Dissection of Functional Domains of the Voltage-Dependent Ca2+ Channel α2δ Subunit', *J. Neurosci.*, vol. 17, no. 18, pp. 6884–6891, Sep. 1997.

[41] K. Itagaki, W. J. Koch, I. Bodi, U. Klöckner, D. F. Slish, and A. Schwartz, 'Native-type DHP-sensitive calcium channel currents are produced by cloned rat aortic smooth muscle and cardiac α1 subunits expressed in Xenopus laevis ooeytes and are regulated by α2- and β-subunits', *FEBS Lett.*, vol. 297, no. 3, pp. 221–225, Feb. 1992.

[42] D. Singer, M. Biel, I. Lotan, V. Flockerzi, F. Hofmann, and N. Dascal, 'The roles of the subunits in the function of the calcium channel', *Science*, vol. 253, no. 5027, pp. 1553–1557, Sep. 1991.

[43] R. Bangalore, G. Mehrke, K. Gingrich, F. Hofmann, and R. S. Kass, 'Influence of L-type Ca channel alpha 2/delta-subunit on ionic and gating current in transiently transfected HEK 293 cells', *Am. J. Physiol.-Heart Circ. Physiol.*, vol. 270, no. 5, pp. H1521–H1528, May 1996.

[44] E. Shistik, T. Ivanina, T. Puri, M. Hosey, and N. Dascal, 'Ca2+ current enhancement by alpha 2/delta and beta subunits in Xenopus oocytes: contribution of changes in channel gating and alpha 1 protein level.', *J. Physiol.*, vol. 489, no. 1, pp. 55–62, Nov. 1995.

[45] N. Qin, S. Yagel, M.-L. Momplaisir, E. E. Codd, and M. R. D'Andrea, 'Molecular Cloning and Characterization of the Human Voltage-Gated Calcium Channel α2δ-4 Subunit', *Mol. Pharmacol.*, vol. 62, no. 3, pp. 485–496, Sep. 2002.

[46] N. Klugbauer, L. Lacinová, E. Marais, M. Hobom, and F. Hofmann, 'Molecular Diversity of the Calcium Channel α2δ Subunit', *J. Neurosci.*, vol. 19, no. 2, pp. 684–691, Jan. 1999.

[47] J. Barclay and M. Rees, 'Genomic organization of the mouse and human α2δ2 voltage-dependent calcium channel subunit genes', *Mamm. Genome*, vol. 11, no. 12, pp. 1142–1144, Dec. 2000.

[48] N. Klugbauer, E. Marais, and F. Hofmann, 'Calcium Channel α2δ Subunits: Differential Expression, Function, and Drug Binding', *J. Bioenerg. Biomembr.*, vol. 35, no. 6, pp. 639–647, Dec. 2003.

[49] D. R. Witcher, M. D. Waard, J. Sakamoto, C. Franzini-Armstrong, M. Pragnell, and K. P. Campbell, 'Subunit Identification and Reconstitution of the N-Type Ca2l Channel Complex Purified from Brain', vol. 261, p. 5, 1993.

[50] H. Tokumaru, K. Anzai, T. Abe, and Y. Kirino, 'Purification of the cardiac 1,4-dihydropyridine receptor using immunoaffinity chromatography with a monoclonal

antibody against the α2δ subunit of the skeletal muscle dihydropyridine receptor', *Eur. J. Pharmacol. Mol. Pharmacol.*, vol. 227, no. 4, pp. 363–370, Dec. 1992.

[51] C. L. Cooper, S. Vandaele, J. Barhanin, M. Fosset, M. Lazdunski, and M. M. Hosey, 'Purification and characterization of the dihydropyridine-sensitive voltage-dependent calcium channel from cardiac tissue.', *J. Biol. Chem.*, vol. 262, no. 2, pp. 509–512, Jan. 1987.

[52] Z. Buraei and J. Yang, 'The β Subunit of Voltage-Gated Ca2+ Channels', *Physiol. Rev.*, vol. 90, no. 4, pp. 1461–1506, Oct. 2010.

[53] G. A. Fuller-Bicer *et al.*, 'Targeted disruption of the voltage-dependent calcium channel α2/δ-1-subunit', *Am. J. Physiol.-Heart Circ. Physiol.*, vol. 297, no. 1, pp. H117–H124, Jul. 2009.

[54] C.-Y. Li *et al.*, 'Calcium channel alpha2delta1 subunit mediates spinal hyperexcitability in pain modulation', *Pain*, vol. 125, no. 1–2, pp. 20–34, Nov. 2006.

[55] C.-Y. Li, Y.-H. Song, E. S. Higuera, and Z. D. Luo, 'Spinal Dorsal Horn Calcium Channel α2δ-1 Subunit Upregulation Contributes to Peripheral Nerve Injury-Induced Tactile Allodynia', *J. Neurosci.*, vol. 24, no. 39, pp. 8494–8499, Sep. 2004.

[56] S. D. Jay *et al.*, 'Primary structure of the gamma subunit of the DHP-sensitive calcium channel from skeletal muscle', *Science*, vol. 248, no. 4954, pp. 490–492, Apr. 1990.

[57] N. Klugbauer *et al.*, 'A family of γ-like calcium channel subunits', *FEBS Lett.*, vol. 470, no. 2, pp. 189–197, Mar. 2000.

[58] R.-S. Chen, T.-C. Deng, T. Garcia, Z. M. Sellers, and P. M. Best, 'Calcium channel gamma subunits: a functionally diverse protein family', *Cell Biochem. Biophys.*, vol. 47, no. 2, pp. 178–186, 2007.

[59] D. L. Burgess, L. A. Gefrides, P. J. Foreman, and J. L. Noebels, 'A Cluster of Three Novel Ca2+ Channel γ Subunit Genes on Chromosome 19q13.4: Evolution and Expression Profile of the γ Subunit Gene Family', *Genomics*, vol. 71, no. 3, pp. 339–350, Feb. 2001.

[60] R. Eberst, S. Dai, N. Klugbauer, and F. Hofmann, 'Identification and functional characterization of a calcium channel γ subunit', *Pflüg. Arch.*, vol. 433, no. 5, pp. 633–637, Feb. 1997.

[61] D. Freise *et al.*, 'Absence of the γ Subunit of the Skeletal Muscle Dihydropyridine Receptor Increases L-type Ca2+ Currents and Alters Channel Inactivation Properties', *J. Biol. Chem.*, vol. 275, no. 19, pp. 14476–14481, Dec. 2000.

[62] M.-G. Kang *et al.*, 'Biochemical and Biophysical Evidence for γ2 Subunit Association with Neuronal Voltage-activated Ca2+Channels', *J. Biol. Chem.*, vol. 276, no. 35, pp. 32917–32924, Aug. 2001.

[63] M. Rousset *et al.*, 'Functional roles of γ2, γ3 and γ4, three new Ca2+ channel subunits, in P/Q-type Ca2+ channel expressed in Xenopus oocytes', *J. Physiol.*, vol. 532, no. 3, pp. 583–593, May 2001.

[64] C. A. Ahern *et al.*, 'Modulation of L-type Ca2+ current but not activation of Ca2+ release by the gamma1 subunit of the dihydropyridine receptor of skeletal muscle', *BMC Physiol.*, vol. 1, no. 1, p. 8, Jul. 2001.

[65] S. Tomita *et al.*, 'Functional studies and distribution define a family of transmembrane AMPA receptor regulatory proteins', *J. Cell Biol.*, vol. 161, no. 4, pp. 805–816, May 2003.

[66] A. S. Kato, E. R. Siuda, E. S. Nisenbaum, and D. S. Bredt, 'AMPA Receptor Subunit-Specific Regulation by a Distinct Family of Type II TARPs', *Neuron*, vol. 59, no. 6, pp. 986–996, Sep. 2008.

[67] P. Ruth *et al.*, 'Primary structure of the beta subunit of the DHP-sensitive calcium channel from skeletal muscle', *Science*, vol. 245, no. 4922, pp. 1115–1118, Sep. 1989.
[68] E. Perez-Reyes *et al.*, 'Cloning and expression of a cardiac/brain beta subunit of the L-type calcium channel', *J. Biol. Chem.*, vol. 267, no. 3, pp. 1792–1797, Jan. 1992.
[69] A. Castellano, X. Wei, L. Birnbaumer, and E. Perez-Reyes, 'Cloning and expression of a neuronal calcium channel beta subunit', *J. Biol. Chem.*, vol. 268, no. 17, pp. 12359–12366, Jun. 1993.
[70] A. Castellano, X. Wei, L. Birnbaumer, and E. Perez-Reyes, 'Cloning and expression of a third calcium channel beta subunit', *J. Biol. Chem.*, vol. 268, no. 5, pp. 3450–3455, Feb. 1993.
[71] M. De Waard, M. Pragnell, and K. P. Campbell, 'Ca2+ channel regulation by a conserved β subunit domain', *Neuron*, vol. 13, no. 2, pp. 495–503, Aug. 1994.
[72] M. R. Hanlon, N. S. Berrow, A. C. Dolphin, and B. A. Wallace, 'Modelling of a voltage-dependent Ca2+ channel β subunit as a basis for understanding its functional properties', *FEBS Lett.*, vol. 445, no. 2–3, pp. 366–370, Feb. 1999.
[73] Y. Chen *et al.*, 'Structural basis of the α_1–β subunit interaction of voltage-gated Ca^{2+} channels', *Nature*, vol. 429, no. 6992, pp. 675–680, Jun. 2004.
[74] A. C. Vendel, C. D. Rithner, B. A. Lyons, and W. A. Horne, 'Solution structure of the N-terminal A domain of the human voltage-gated Ca2+channel β4a subunit', *Protein Sci.*, vol. 15, no. 2, pp. 378–383, Feb. 2006.
[75] L. He, Y. Zhang, Y. Chen, Y. Yamada, and J. Yang, 'Functional Modularity of the β-Subunit of Voltage-Gated Ca2+ Channels', *Biophys. J.*, vol. 93, no. 3, pp. 834–845, Aug. 2007.
[76] A. W. McGee, D. A. Nunziato, J. M. Maltez, K. E. Prehoda, G. S. Pitt, and D. S. Bredt, 'Calcium Channel Function Regulated by the SH3-GK Module in β Subunits', *Neuron*, vol. 42, no. 1, pp. 89–99, Apr. 2004.
[77] S. M. Larson and A. R. Davidson, 'The identification of conserved interactions within the SH3 domain by alignment of sequences and structures', *Protein Sci. Publ. Protein Soc.*, vol. 9, no. 11, pp. 2170–2180, Nov. 2000.
[78] Y. Opatowsky, C.-C. Chen, K. P. Campbell, and J. A. Hirsch, 'Structural Analysis of the Voltage-Dependent Calcium Channel β Subunit Functional Core and Its Complex with the α1 Interaction Domain', *Neuron*, vol. 42, no. 3, pp. 387–399, May 2004.
[79] F. Van Petegem, K. A. Clark, F. C. Chatelain, and D. L. Minor Jr, 'Structure of a complex between a voltage-gated calcium channel β-subunit and an α-subunit domain', *Nature*, vol. 429, no. 6992, pp. 671–675, Jun. 2004.
[80] D. Grabs *et al.*, 'The SH3 Domain of Amphiphysin Binds the Proline-rich Domain of Dynamin at a Single Site That Defines a New SH3 Binding Consensus Sequence', *J. Biol. Chem.*, vol. 272, no. 20, pp. 13419–13425, May 1997.
[81] L. Luo *et al.*, 'The Binding of Syndapin SH3 Domain to Dynamin Proline-rich Domain Involves Short and Long Distance Elements', *J. Biol. Chem.*, vol. 291, no. 18, pp. 9411–9424, Apr. 2016.
[82] C. Baumann, C. K. Lindholm, D. Rimoldi, and F. Lévy, 'The E3 ubiquitin ligase Itch regulates sorting nexin 9 through an unconventional substrate recognition domain', *FEBS J.*, vol. 277, no. 13, pp. 2803–2814, 2010.
[83] G. Gonzalez-Gutierrez, E. Miranda-Laferte, A. Neely, and P. Hidalgo, 'The Src Homology 3 Domain of the β-Subunit of Voltage-gated Calcium Channels Promotes Endocytosis via Dynamin Interaction', *J. Biol. Chem.*, vol. 282, no. 4, pp. 2156–2162, Jan. 2007.

[84] Y. Li, O. Spangenberg, I. Paarmann, M. Konrad, and A. Lavie, 'Structural Basis for Nucleotide-dependent Regulation of Membrane-associated Guanylate Kinase-like Domains', *J. Biol. Chem.*, vol. 277, no. 6, pp. 4159–4165, Aug. 2002.

[85] S. X. Takahashi, J. Miriyala, L. H. Tay, D. T. Yue, and H. M. Colecraft, 'A CaVβ SH3/Guanylate Kinase Domain Interaction Regulates Multiple Properties of Voltage-gated Ca2+ Channels', *J. Gen. Physiol.*, vol. 126, no. 4, pp. 365–377, Oct. 2005.

[86] Y. Chen, L. He, D. R. Buchanan, Y. Zhang, A. Fitzmaurice, and J. Yang, 'Functional dissection of the intramolecular Src homology 3-guanylate kinase domain coupling in voltage-gated Ca2+ channel β-subunits', *FEBS Lett.*, vol. 583, no. 12, pp. 1969–1975, Jun. 2009.

[87] R. Hullin *et al.*, 'Cardiac L-type Calcium Channel β-Subunits Expressed in Human Heart Have Differential Effects on Single Channel Characteristics', *J. Biol. Chem.*, vol. 278, no. 24, pp. 21623–21630, Jun. 2003.

[88] M. Pragnell, J. Sakamoto, S. D. Jay, and K. P. Campbell, 'Cloning and tissue-specific expression of the brain calcium channel β-subunit', *FEBS Lett.*, vol. 291, no. 2, pp. 253–258, Oct. 1991.

[89] T. Collin, J. J. Wang, J. Nargeot, and A. Schwartz, 'Molecular cloning of three isoforms of the L-type voltage-dependent calcium channel beta subunit from normal human heart', *Circ. Res.*, vol. 72, no. 6, pp. 1337–1344, Jun. 1993.

[90] H. Hasse *et al.*, 'Expression of calcium channel subunits in the normal and diseased human myocardium', *J. Mol. Med.*, vol. 74, no. 2, pp. 99–104, Feb. 1996.

[91] M. Pichler *et al.*, 'β Subunit Heterogeneity in Neuronal L-type Ca2+Channels', *J. Biol. Chem.*, vol. 272, no. 21, pp. 13877–13882, May 1997.

[92] P.-J. Chu, J. K. Larsen, C.-C. Chen, and P. M. Best, 'Distribution and relative expression levels of calcium channel beta subunits within the chambers of the rat heart', *J. Mol. Cell. Cardiol.*, vol. 36, no. 3, pp. 423–434, Mar. 2004.

[93] M. W. McEnery, C. L. Vance, C. M. Begg, W.-L. Lee, Y. Choi, and S. J. Dubel, 'Differential Expression and Association of Calcium Channel Subunits in Development and Disease', *J. Bioenerg. Biomembr.*, vol. 30, no. 4, pp. 409–418, Aug. 1998.

[94] H. Haase, B. Pfitzmaier, M. W. McEnery, and I. Morano, 'Expression of Ca2+ channel subunits during cardiac ontogeny in mice and rats: Identification of fetal α1C and β subunit isoforms', *J. Cell. Biochem.*, vol. 76, no. 4, pp. 695–703, Mar. 2000.

[95] S. Link *et al.*, 'Diversity and Developmental Expression of L-type Calcium Channel β2 Proteins and Their Influence on Calcium Current in Murine Heart', *J. Biol. Chem.*, vol. 284, no. 44, pp. 30129–30137, Oct. 2009.

[96] H. Yamaguchi, M. Okuda, G. Mikala, K. Fukasawa, and G. Varadi, 'Cloning of the β2a Subunit of the Voltage-Dependent Calcium Channel from Human Heart: Cooperative Effect of α2/δ and β2a on the Membrane Expression of the α1C Subunit', *Biochem. Biophys. Res. Commun.*, vol. 267, no. 1, pp. 156–163, Jan. 2000.

[97] Y. Yamada *et al.*, 'Cloning of a Functional Splice Variant of L-type Calcium Channel β2 Subunit from Rat Heart', *J. Biol. Chem.*, vol. 276, no. 50, pp. 47163–47170, Dec. 2001.

[98] S. Dalton, S. X. Takahashi, J. Miriyala, and H. M. Colecraft, 'A single CaVβ can reconstitute both trafficking and macroscopic conductance of voltage-dependent calcium channels', *J. Physiol.*, vol. 567, no. Pt 3, pp. 757–769, Sep. 2005.

[99] I. R. Josephson and G. Varadi, 'The beta subunit increases Ca2+ currents and gating charge movements of human cardiac L-type Ca2+ channels.', *Biophys. J.*, vol. 70, no. 3, pp. 1285–1293, Mar. 1996.

[100] T. J. Kamp, M. T. Pérez-García, and E. Marban, 'Enhancement of ionic current and charge movement by coexpression of calcium channel β1A subunit with α1C subunit in a human embryonic kidney cell line', *J. Physiol.*, vol. 492, no. 1, pp. 89–96, Apr. 1996.
[101] D. Bichet *et al.*, 'The I-II Loop of the Ca2+ Channel α1 Subunit Contains an Endoplasmic Reticulum Retention Signal Antagonized by the β Subunit', *Neuron*, vol. 25, no. 1, pp. 177–190, Jan. 2000.
[102] K. Fang and H. M. Colecraft, 'Mechanism of auxiliary β-subunit-mediated membrane targeting of L-type (CaV1.2) channels', *J. Physiol.*, vol. 589, no. 18, pp. 4437–4455, Jul. 2011.
[103] C. Altier *et al.*, 'The Cavβ subunit prevents RFP2-mediated ubiquitination and proteasomal degradation of L-type channels', *Nat. Neurosci.*, vol. 14, no. 2, pp. 173–180, Feb. 2011.
[104] D. Waithe, L. Ferron, K. M. Page, K. Chaggar, and A. C. Dolphin, 'β-Subunits Promote the Expression of CaV2.2 Channels by Reducing Their Proteasomal Degradation', *J. Biol. Chem.*, vol. 286, no. 11, pp. 9598–9611, Mar. 2011.
[105] G. Varadi, P. Lory, D. Schultz, M. Varadi, and A. Schwartz, 'Acceleration of activation and inactivation by the β subunit of the skeletal muscle calcium channel', *Nature*, vol. 352, no. 6331, pp. 159–162, Jul. 1991.
[106] I. Dzhura and A. Neely, 'Differential Modulation of Cardiac Ca2+ Channel Gating by β-Subunits', *Biophys. J.*, vol. 85, no. 1, pp. 274–289, Jul. 2003.
[107] Y. Karunasekara, A. F. Dulhunty, and M. G. Casarotto, 'The voltage-gated calcium-channel β subunit: more than just an accessory', *Eur. Biophys. J.*, vol. 39, no. 1, pp. 75–81, Dec. 2009.
[108] R. Olcese *et al.*, 'The amino terminus of a calcium channel β subunitsets rates of channel inactivation independently of the subunit's effect on activation', *Neuron*, vol. 13, no. 6, pp. 1433–1438, Dec. 1994.
[109] A. J. Chien, T. Gao, E. Perez-Reyes, and M. M. Hosey, 'Membrane Targeting of L-type Calcium Channels ROLE OF PALMITOYLATION IN THE SUBCELLULAR LOCALIZATION OF THE β2a SUBUNIT', *J. Biol. Chem.*, vol. 273, no. 36, pp. 23590–23597, Apr. 1998.
[110] A. J. Chien, K. M. Carr, R. E. Shirokov, E. Rios, and M. M. Hosey, 'Identification of Palmitoylation Sites within the L-type Calcium Channel β2a Subunit and Effects on Channel Function', *J. Biol. Chem.*, vol. 271, no. 43, pp. 26465–26468, Oct. 1996.
[111] N. Qin, D. Platano, R. Olcese, J. L. Costantin, E. Stefani, and L. Birnbaumer, 'Unique regulatory properties of the type 2a Ca2+ channel β subunit caused by palmitoylation', *Proc. Natl. Acad. Sci.*, vol. 95, no. 8, pp. 4690–4695, Apr. 1998.
[112] E. Miranda-Laferte, D. Ewers, R. E. Guzman, N. Jordan, S. Schmidt, and P. Hidalgo, 'The N-terminal Domain Tethers the Voltage-gated Calcium Channel β2e-subunit to the Plasma Membrane via Electrostatic and Hydrophobic Interactions', *J. Biol. Chem.*, vol. 289, no. 15, pp. 10387–10398, Nov. 2014.
[113] P. Weissgerber *et al.*, 'Reduced Cardiac L-Type Ca2+ Current in Cavβ2−/− Embryos Impairs Cardiac Development and Contraction With Secondary Defects in Vascular Maturation', *Circ. Res.*, Sep. 2006.
[114] M. Meissner *et al.*, 'Moderate Calcium Channel Dysfunction in Adult Mice with Inducible Cardiomyocyte-specific Excision of the cacnb2 Gene', *J. Biol. Chem.*, vol. 286, no. 18, pp. 15875–15882, Jun. 2011.
[115] L. Yang *et al.*, 'Cardiac $Ca_V1.2$ channels require β subunits for β-adrenergic–mediated modulation but not trafficking', *J. Clin. Invest.*, Nov. 2018.

[116] S. Kiyonaka *et al.*, 'RIM1 confers sustained activity and neurotransmitter vesicle anchoring to presynaptic Ca^{2+} channels', *Nat. Neurosci.*, vol. 10, no. 6, pp. 691–701, Jun. 2007.
[117] T. Yang, A. Puckerin, and H. M. Colecraft, 'Distinct RGK GTPases Differentially Use α1- and Auxiliary β-Binding-Dependent Mechanisms to Inhibit CaV1.2/CaV2.2 Channels', *PLOS ONE*, vol. 7, no. 5, p. e37079, May 2012.
[118] T. Yang and H. M. Colecraft, 'Regulation of voltage-dependent calcium channels by RGK proteins', *Biochim. Biophys. Acta BBA - Biomembr.*, vol. 1828, no. 7, pp. 1644–1654, Jul. 2013.
[119] Y. Zhang *et al.*, 'Origin of the Voltage Dependence of G-Protein Regulation of P/Q-type Ca2+ Channels', *J. Neurosci.*, vol. 28, no. 52, pp. 14176–14188, Dec. 2008.
[120] A. Meir, D. C. Bell, G. J. Stephens, K. M. Page, and A. C. Dolphin, 'Calcium Channel β Subunit Promotes Voltage-Dependent Modulation of α1B by Gβγ', *Biophys. J.*, vol. 79, no. 2, pp. 731–746, Aug. 2000.
[121] H. Haase, 'Ahnak, a new player in β-adrenergic regulation of the cardiac L-type Ca2+ channel', *Cardiovasc. Res.*, vol. 73, no. 1, pp. 19–25, Jan. 2007.
[122] A. M. Ebert, C. A. McAnelly, A. Srinivasan, J. L. Linker, W. A. Horne, and D. M. Garrity, 'Ca2+ channel-independent requirement for MAGUK family CACNB4 genes in initiation of zebrafish epiboly', *Proc. Natl. Acad. Sci.*, vol. 105, no. 1, pp. 198–203, Jan. 2008.
[123] Y. Zhang, Y. Yamada, M. Fan, S. D. Bangaru, B. Lin, and J. Yang, 'The β Subunit of Voltage-gated Ca2+ Channels Interacts with and Regulates the Activity of a Novel Isoform of Pax6', *J. Biol. Chem.*, vol. 285, no. 4, pp. 2527–2536, Jan. 2010.
[124] H. Hibino *et al.*, 'Direct interaction with a nuclear protein and regulation of gene silencing by a variant of the Ca2+-channel β4 subunit', *Proc. Natl. Acad. Sci.*, vol. 100, no. 1, pp. 307–312, Jul. 2003.
[125] J. Taylor *et al.*, 'The Cavβ1a subunit regulates gene expression and suppresses myogenin in muscle progenitor cells', *J Cell Biol*, vol. 205, no. 6, pp. 829–846, Jun. 2014.
[126] P. Subramanyam *et al.*, 'Activity and calcium regulate nuclear targeting of the calcium channel β4b subunit in nerve and muscle cells', *Channels Austin Tex*, vol. 3, no. 5, pp. 343–355, 2009.
[127] H. M. Colecraft *et al.*, 'Novel functional properties of Ca2+ channel β subunits revealed by their expression in adult rat heart cells', *J. Physiol.*, vol. 541, no. Pt 2, pp. 435–452, Jun. 2002.
[128] P. Béguin *et al.*, 'Nuclear Sequestration of β-Subunits by Rad and Rem is Controlled by 14-3-3 and Calmodulin and Reveals a Novel Mechanism for Ca2+ Channel Regulation', *J. Mol. Biol.*, vol. 355, no. 1, pp. 34–46, Jan. 2006.
[129] J.-P. Leyris *et al.*, 'RGK GTPase-dependent CaV2.1 Ca2+ channel inhibition is independent of CaVβ-subunit-induced current potentiation', *FASEB J.*, vol. 23, no. 8, pp. 2627–2638, Jan. 2009.
[130] F. Rusconi *et al.*, 'Peptidomimetic Targeting of Cavβ2 Overcomes Dysregulation of the L-Type Calcium Channel Density and Recovers Cardiac FunctionClinical Perspective', *Circulation*, vol. 134, no. 7, pp. 534–546, Aug. 2016.
[131] I. Shimizu and T. Minamino, 'Physiological and pathological cardiac hypertrophy', *J. Mol. Cell. Cardiol.*, vol. 97, pp. 245–262, Aug. 2016.
[132] M. Maillet, J. H. van Berlo, and J. D. Molkentin, 'Molecular basis of physiological heart growth: fundamental concepts and new players', *Nat. Rev. Mol. Cell Biol.*, vol. 14, no. 1, pp. 38–48, Jan. 2013.

[133] J. A. Hill and E. N. Olson, 'Cardiac Plasticity', *N. Engl. J. Med.*, vol. 358, no. 13, pp. 1370–1380, Mar. 2008.
[134] E. Chung and L. A. Leinwand, 'Pregnancy as a cardiac stress model', *Cardiovasc. Res.*, vol. 101, no. 4, pp. 561–570, Mar. 2014.
[135] G. M. Ellison, C. D. Waring, C. Vicinanza, and D. Torella, 'Physiological cardiac remodelling in response to endurance exercise training: cellular and molecular mechanisms', *Heart*, vol. 98, no. 1, pp. 5–10, Jan. 2012.
[136] Pluim Babette M., Zwinderman Aeilko H., van der Laarse Arnoud, and van der Wall Ernst E., 'The Athlete's Heart', *Circulation*, vol. 101, no. 3, pp. 336–344, Jan. 2000.
[137] J. Kim *et al.*, 'Insulin-Like Growth Factor I Receptor Signaling Is Required for Exercise-Induced Cardiac Hypertrophy', *Mol. Endocrinol.*, vol. 22, no. 11, pp. 2531–2543, Nov. 2008.
[138] Lyon Robert C., Zanella Fabian, Omens Jeffrey H., and Sheikh Farah, 'Mechanotransduction in Cardiac Hypertrophy and Failure', *Circ. Res.*, vol. 116, no. 8, pp. 1462–1476, Apr. 2015.
[139] J. Heineke and J. D. Molkentin, 'Regulation of cardiac hypertrophy by intracellular signalling pathways', *Nat. Rev. Mol. Cell Biol.*, vol. 7, no. 8, p. 589, Aug. 2006.
[140] K. R. Chien *et al.*, 'Transcriptional Regulation During Cardiac Growth and Development', *Annu. Rev. Physiol.*, vol. 55, no. 1, pp. 77–95, 1993.
[141] M. Samak *et al.*, 'Cardiac Hypertrophy: An Introduction to Molecular and Cellular Basis', *Med. Sci. Monit. Basic Res.*, vol. 22, pp. 75–79, Jul. 2016.
[142] A. C. deAlmeida, R. J. van Oort, and X. H. T. Wehrens, 'Transverse Aortic Constriction in Mice', *JoVE J. Vis. Exp.*, no. 38, p. e1729, Apr. 2010.
[143] D. J. Cao *et al.*, 'Histone deacetylase (HDAC) inhibitors attenuate cardiac hypertrophy by suppressing autophagy', *Proc. Natl. Acad. Sci.*, vol. 108, no. 10, pp. 4123–4128, Mar. 2011.
[144] J. D. Molkentin *et al.*, 'A Calcineurin-Dependent Transcriptional Pathway for Cardiac Hypertrophy', *Cell*, vol. 93, no. 2, pp. 215–228, Apr. 1998.
[145] J. R. McMullen and G. L. Jennings, 'Differences Between Pathological and Physiological Cardiac Hypertrophy: Novel Therapeutic Strategies to Treat Heart Failure', *Clin. Exp. Pharmacol. Physiol.*, vol. 34, no. 4, pp. 255–262, Apr. 2007.
[146] R. Passier *et al.*, 'CaM kinase signaling induces cardiac hypertrophy and activates the MEF2 transcription factor in vivo', *J. Clin. Invest.*, vol. 105, no. 10, pp. 1395–1406, May 2000.
[147] N. H. Purcell, G. Tang, C. Yu, F. Mercurio, J. A. DiDonato, and A. Lin, 'Activation of NF-κB is required for hypertrophic growth of primary rat neonatal ventricular cardiomyocytes', *Proc. Natl. Acad. Sci.*, vol. 98, no. 12, pp. 6668–6673, Jun. 2001.
[148] Letavernier Emmanuel *et al.*, 'Targeting the Calpain/Calpastatin System as a New Strategy to Prevent Cardiovascular Remodeling in Angiotensin II–Induced Hypertension', *Circ. Res.*, vol. 102, no. 6, pp. 720–728, Mar. 2008.
[149] A. M. De Jong, A. H. Maass, S. U. Oberdorf-Maass, D. J. Van Veldhuisen, W. H. Van Gilst, and I. C. Van Gelder, 'Mechanisms of atrial structural changes caused by stretch occurring before and during early atrial fibrillation', *Cardiovasc. Res.*, vol. 89, no. 4, pp. 754–765, Mar. 2011.
[150] D. M. Bers, 'Cardiac excitation–contraction coupling', *Nature*, vol. 415, no. 6868, pp. 198–205, Jan. 2002.
[151] J. Shen, 'Isoprenaline enhances local Ca^{2+} release in cardiac myocytes', *Acta Pharmacol. Sin.*, vol. 27, no. 7, pp. 927–932, Jul. 2006.

[152] Song Long-Sheng *et al.*, 'Ca2+ Signaling in Cardiac Myocytes Overexpressing the α1 Subunit of L-Type Ca2+ Channel', *Circ. Res.*, vol. 90, no. 2, pp. 174–181, Feb. 2002.
[153] S. A. Goonasekera *et al.*, 'Decreased cardiac L-type Ca2+ channel activity induces hypertrophy and heart failure in mice', *J. Clin. Invest.*, vol. 122, no. 1, pp. 280–290, Jan. 2012.
[154] S. Richard, F. Leclercq, S. Lemaire, C. Piot, and J. Nargeot, 'Ca2+ currents in compensated hypertrophy and heart failure', *Cardiovasc. Res.*, vol. 37, no. 2, pp. 300–311, Feb. 1998.
[155] E. C. Keung, 'Calcium current is increased in isolated adult myocytes from hypertrophied rat myocardium', *Circ. Res.*, vol. 64, no. 4, pp. 753–763, Apr. 1989.
[156] A. Yatani, R. Honda, K. M. Tymitz, J. M. Lalli, and J. D. Molkentin, 'Enhanced Ca2+Channel Currents in Cardiac Hypertrophy Induced by Activation of Calcineurin-dependent Pathway', *J. Mol. Cell. Cardiol.*, vol. 33, no. 2, pp. 249–259, Feb. 2001.
[157] Wang Zhengyi, Kutschke William, Richardson Kenneth E., Karimi Mohsen, and Hill Joseph A., 'Electrical Remodeling in Pressure-Overload Cardiac Hypertrophy', *Circulation*, vol. 104, no. 14, pp. 1657–1663, Oct. 2001.
[158] H. Haase *et al.*, 'Expression of calcium channel subunits in the normal and diseased human myocardium', *J. Mol. Med. Berl. Ger.*, vol. 74, no. 2, pp. 99–104, Feb. 1996.
[159] I. Bodi *et al.*, 'Electrical remodeling in hearts from a calcium-dependent mouse model of hypertrophy and failure: Complex nature of k+current changes and action potential duration', *J. Am. Coll. Cardiol.*, vol. 41, no. 9, pp. 1611–1622, May 2003.
[160] I. Mahé, O. Chassany, A.-S. Grenard, C. Caulin, and J.-F. Bergmann, 'Defining the Role of Calcium Channel Antagonists in Heart Failure Due to Systolic Dysfunction', *Am. J. Cardiovasc. Drugs*, vol. 3, no. 1, pp. 33–41, Jan. 2003.
[161] H. M. Viola, W. A. Macdonald, H. Tang, and L. C. Hool, 'The L-type Ca(2+) channel as a therapeutic target in heart disease', *Curr. Med. Chem.*, vol. 16, no. 26, pp. 3341–3358, 2009.
[162] R. J. M. de Vries, D. J. van Veldhuisen, and P. H. J. M. Dunselman, 'Efficacy and safety of calcium channel blockers in heart failure: Focus on recent trials with second-generation dihydropyridines', *Am. Heart J.*, vol. 139, no. 2, Part 1, pp. 185–194, Feb. 2000.
[163] X. Chen *et al.*, 'Calcium influx through Cav1.2 is a proximal signal for pathological cardiomyocyte hypertrophy', *J. Mol. Cell. Cardiol.*, vol. 50, no. 3, pp. 460–470, Mar. 2011.
[164] W. R. Dayton, W. J. Reville, D. E. Goll, and M. H. Stromer, 'A calcium(2+) ion-activated protease possibly involved in myofibrillar protein turnover. Partial characterization of the purified enzyme', *Biochemistry*, vol. 15, no. 10, pp. 2159–2167, May 1976.
[165] J. Cong, D. E. Goll, A. M. Peterson, and H. P. Kapprell, 'The role of autolysis in activity of the Ca2+-dependent proteinases (mu-calpain and m-calpain).', *J. Biol. Chem.*, vol. 264, no. 17, pp. 10096–10103, Jun. 1989.
[166] W. R. Dayton and J. V. Schollmeyer, 'Immunocytochemical localization of a calcium-activated protease in skeletal muscle cells', *Exp. Cell Res.*, vol. 136, no. 2, pp. 423–433, Dec. 1981.
[167] D. A. Mohrhauser, K. R. Underwood, and A. D. Weaver, 'In vitro degradation of bovine myofibrils is caused by μ-calpain, not caspase-3', *J. Anim. Sci.*, vol. 89, no. 3, pp. 798–808, Mar. 2011.

[168] Gao Wei Dong, Atar Dan, Liu Yongge, Perez Nestor Gustavo, Murphy Anne M., and Marban Eduardo, 'Role of Troponin I Proteolysis in the Pathogenesis of Stunned Myocardium', *Circ. Res.*, vol. 80, no. 3, pp. 393–399, Mar. 1997.
[169] E. Letavernier, L. Zafrani, J. Perez, B. Letavernier, J.-P. Haymann, and L. Baud, 'The role of calpains in myocardial remodelling and heart failure', *Cardiovasc. Res.*, vol. 96, no. 1, pp. 38–45, Oct. 2012.
[170] T. Ye *et al.*, 'Over-Expression of Calpastatin Inhibits Calpain Activation and Attenuates Post-Infarction Myocardial Remodeling', *PLOS ONE*, vol. 10, no. 3, p. e0120178, Mar. 2015.
[171] Y. Li *et al.*, 'Targeted Inhibition of Calpain Reduces Myocardial Hypertrophy and Fibrosis in Mouse Models of Type 1 Diabetes', *Diabetes*, vol. 60, no. 11, pp. 2985–2994, Nov. 2011.
[172] Burkard Natalie, Becher Jan, Heindl Cornelia, Neyses Ludwig, Schuh Kai, and Ritter Oliver, 'Targeted Proteolysis Sustains Calcineurin Activation', *Circulation*, vol. 111, no. 8, pp. 1045–1053, Mar. 2005.
[173] Heidrich Felix M., Zhang Kun, Estrada Manuel, Huang Yan, Giordano Frank J., and Ehrlich Barbara E., 'Chromogranin B Regulates Calcium Signaling, Nuclear Factor κB Activity, and Brain Natriuretic Peptide Production in Cardiomyocytes', *Circ. Res.*, vol. 102, no. 10, pp. 1230–1238, May 2008.
[174] F. M. Heidrich and B. E. Ehrlich, 'Calcium, Calpains and Cardiac Hypertrophy – A New Link', *Circ. Res.*, vol. 104, no. 2, p. e19, Jan. 2009.
[175] C. Patterson, A. Portbury, J. C. Schisler, and M. S. Willis, 'Tear me down: Role of calpain in the development of cardiac ventricular hypertrophy', *Circ. Res.*, vol. 109, no. 4, pp. 453–462, Aug. 2011.
[176] G. Stölting *et al.*, 'Direct Interaction of CaVβ with Actin Up-regulates L-type Calcium Currents in HL-1 Cardiomyocytes', *J. Biol. Chem.*, vol. 290, no. 8, pp. 4561–4572, Feb. 2015.
[177] A. Baer and K. Kehn-Hall, 'Viral Concentration Determination Through Plaque Assays: Using Traditional and Novel Overlay Systems', *J. Vis. Exp. JoVE*, no. 93, Nov. 2014.
[178] M. Klaiber *et al.*, 'A cardiac pathway of cyclic GMP-independent signaling of guanylyl cyclase A, the receptor for atrial natriuretic peptide', *Proc. Natl. Acad. Sci.*, vol. 108, no. 45, pp. 18500–18505, Nov. 2011.
[179] S. Plum *et al.*, 'Combined enrichment of neuromelanin granules and synaptosomes from human substantia nigra pars compacta tissue for proteomic analysis', *J. Proteomics*, vol. 94, pp. 202–206, Dec. 2013.
[180] A. Maerkens *et al.*, 'New insights into the protein aggregation pathology in myotilinopathy by combined proteomic and immunolocalization analyses', *Acta Neuropathol. Commun.*, vol. 4, no. 1, p. 8, Feb. 2016.
[181] J. Taylor *et al.*, 'The Cavβ1a subunit regulates gene expression and suppresses myogenin in muscle progenitor cells', *J Cell Biol*, vol. 205, no. 6, pp. 829–846, Jun. 2014.
[182] B. L. Timney *et al.*, 'Simple rules for passive diffusion through the nuclear pore complex', *J Cell Biol*, vol. 215, no. 1, pp. 57–76, Oct. 2016.
[183] A. A. Puckerin, D. D. Chang, Z. Shuja, P. Choudhury, J. Scholz, and H. M. Colecraft, 'Engineering selectivity into RGK GTPase inhibition of voltage-dependent calcium channels', *Proc. Natl. Acad. Sci.*, vol. 115, no. 47, pp. 12051–12056, Nov. 2018.

[184] T. Zhang *et al.*, 'Troponin T3 regulates nuclear localization of the calcium channel Cavβ1a subunit in skeletal muscle', *Exp. Cell Res.*, vol. 336, no. 2, pp. 276–286, Aug. 2015.
[185] S. X. Takahashi, S. Mittman, and H. M. Colecraft, 'Distinctive Modulatory Effects of Five Human Auxiliary β2 Subunit Splice Variants on L-Type Calcium Channel Gating', *Biophys. J.*, vol. 84, no. 5, pp. 3007–3021, May 2003.
[186] E. Miranda-Laferte, S. Schmidt, A. C. Jara, A. Neely, and P. Hidalgo, 'A Short Polybasic Segment between the Two Conserved Domains of the β2a-Subunit Modulates the Rate of Inactivation of R-type Calcium Channel', *J. Biol. Chem.*, vol. 287, no. 39, pp. 32588–32597, Sep. 2012.
[187] Cingolani Eugenio, Ramirez Correa Genaro A., Kizana Eddy, Murata Mitsushige, Cho Hee Cheol, and Marbán Eduardo, 'Gene Therapy to Inhibit the Calcium Channel β Subunit', *Circ. Res.*, vol. 101, no. 2, pp. 166–175, Jul. 2007.
[188] Freund Christian *et al.*, 'Requirement of Nuclear Factor-κB in Angiotensin II– and Isoproterenol-Induced Cardiac Hypertrophy In Vivo', *Circulation*, vol. 111, no. 18, pp. 2319–2325, May 2005.

Index of figures

List of tables

Supplements

Table 20: List of upregulated proteins in $Ca_v\beta_2$-deficient NRCs identified by mass spectrometry

Description	Acc Num	Fold Change	*p* ANOVA
26S proteasome non-ATPase regulatory subunit 2 OS=Rattus norvegicus GN=Psmd2 PE=2 SV=1 - [PSMD2_RAT]	Q4FZT9	1.16787035	0.041207212
ADP/ATP translocase 2 OS=Rattus norvegicus GN=Slc25a5 PE=1 SV=3 - [ADT2_RAT]	Q09073	1.282262893	0.040263263
ATP-binding cassette sub-family B member 8, mitochondrial OS=Rattus norvegicus GN=Abcb8 PE=2 SV=1 - [ABCB8_RAT]	Q5RKI8	1.287409996	0.02740555
cAMP-dependent protein kinase type I-alpha regulatory subunit OS=Rattus norvegicus GN=Prkar1a PE=2 SV=2 - [KAP0_RAT]	P09456	1.317530583	0.00757153
DNA (cytosine-5)-methyltransferase 1 OS=Rattus norvegicus GN=Dnmt1 PE=1 SV=2 - [DNMT1_RAT]	Q9Z330	1.705558423	0.005625256
Glycylpeptide N-tetradecanoyltransferase 1 OS=Rattus norvegicus GN=Nmt1 PE=2 SV=1 - [NMT1_RAT]	Q8K1Q0	1.588480891	0.029316599
Histone H2A.Z OS=Rattus norvegicus GN=H2afz PE=1 SV=2 - [H2AZ_RAT]	P0C0S7	2.362713834	0.039372043
Mitochondrial-processing peptidase subunit beta OS=Rattus norvegicus GN=Pmpcb PE=1 SV=3 - [MPPB_RAT]	Q03346	1.114916456	0.034956911
NEDD8-activating enzyme E1 regulatory subunit OS=Rattus norvegicus GN=Nae1 PE=1 SV=1 - [ULA1_RAT]	Q9Z1A5	1.31008218	0.023091031
Neuropilin-1 OS=Rattus norvegicus GN=Nrp1 PE=1 SV=1 - [NRP1_RAT]	Q9QWJ9	1.814401405	0.02493678
Nuclear cap-binding protein subunit 1 OS=Rattus norvegicus GN=Ncbp1 PE=2 SV=1 - [NCBP1_RAT]	Q56A27	1.536517371	0.041306083
Phosphate carrier protein, mitochondrial OS=Rattus norvegicus GN=Slc25a3 PE=1 SV=1 - [MPCP_RAT]	P16036	1.227281768	0.043005195
Propionyl-CoA carboxylase alpha chain, mitochondrial OS=Rattus norvegicus GN=Pcca PE=1 SV=3 - [PCCA_RAT]	P14882	1.116104934	0.013713685
Protein argonaute-2 OS=Rattus norvegicus GN=Ago2 PE=2 SV=2 - [AGO2_RAT]	Q9QZ81	1.390514045	0.031003481
Sarcoplasmic/endoplasmic reticulum calcium ATPase 1 OS=Rattus norvegicus GN=Atp2a1 PE=2 SV=1 - [AT2A1_RAT]	Q64578	1.398165111	0.024670604
Serine/threonine-protein kinase TAO3 OS=Rattus norvegicus GN=Taok3 PE=2 SV=1 - [TAOK3_RAT]	Q53UA7	1.930310483	0.04780082
Surfeit locus protein 1 OS=Rattus norvegicus GN=Surf1 PE=2 SV=1 - [SURF1_RAT]	Q9QXU2	1.595919047	0.048687146

Table 21: List of downregulated proteins in $Ca_v\beta_2$-deficient NRCs identified by mass spectrometry

Description	Acc Num	Fold Change	*p* ANOVA
40S ribosomal protein S7 OS=Rattus norvegicus GN=Rps7 PE=1 SV=1 - [RS7_RAT]	P62083	1.189360333	0.022555218
60S ribosomal protein L18 OS=Rattus norvegicus GN=Rpl18 PE=2 SV=2 - [RL18_RAT]	P12001	1.202077736	0.026149829
60S ribosomal protein L22 OS=Rattus norvegicus GN=Rpl22 PE=2 SV=2 - [RL22_RAT]	P47198	1.333355966	0.023824229
60S ribosomal protein L28 OS=Rattus norvegicus GN=Rpl28 PE=1 SV=4 - [RL28_RAT]	P17702	1.310574819	0.041889247
Ankyrin repeat domain-containing protein 1 OS=Rattus norvegicus GN=Ankrd1 PE=1 SV=1 - [ANKR1_RAT]	Q8R560	2.988021471	0.000257829
Armadillo repeat-containing protein 5 OS=Rattus norvegicus GN=Armc5 PE=2 SV=1 - [ARMC5_RAT]	Q5PQP9	1.410901415	0.042908629
Basal cell adhesion molecule OS=Rattus norvegicus GN=Bcam PE=2 SV=1 - [BCAM_RAT]	Q9ESS6	1.147835917	0.024993901
Calpastatin OS=Rattus norvegicus GN=Cast PE=1 SV=3 - [ICAL_RAT]	P27321	1.17938942	0.046985205
Calponin-1 OS=Rattus norvegicus GN=Cnn1 PE=2 SV=1 - [CNN1_RAT]	Q08290	1.561433542	0.014915913
Calumenin OS=Rattus norvegicus GN=Calu PE=1 SV=1 - [CALU_RAT]	O35783	1.737452489	0.039540922
Catalase OS=Rattus norvegicus GN=Cat PE=1 SV=3 - [CATA_RAT]	P04762	1.436930442	0.039325514
Connective tissue growth factor OS=Rattus norvegicus GN=Ctgf PE=2 SV=1 - [CTGF_RAT]	Q9R1E9	1.816111274	0.023842941
Cysteine and glycine-rich protein 2 OS=Rattus norvegicus GN=Csrp2 PE=2 SV=3 - [CSRP2_RAT]	Q62908	1.408892407	0.022649482
DnaJ homolog subfamily C member 3 OS=Rattus norvegicus GN=Dnajc3 PE=2 SV=3 - [DNJC3_RAT]	Q9R0T3	1.285446971	0.036499629
Glycine amidinotransferase, mitochondrial OS=Rattus norvegicus GN=Gatm PE=1 SV=1 - [GATM_RAT]	P50442	1.791441966	0.00243023
Integrin alpha-7 OS=Rattus norvegicus GN=Itga7 PE=1 SV=2 - [ITA7_RAT]	Q63258	1.763462273	0.014316108
Isopentenyl-diphosphate Delta-isomerase 1 OS=Rattus norvegicus GN=Idi1 PE=2 SV=2 - [IDI1_RAT]	O35760	1.606276667	0.016544816
Laminin subunit beta-2 OS=Rattus norvegicus GN=Lamb2 PE=2 SV=1 - [LAMB2_RAT]	P15800	1.412266662	0.007081955
Multifunctional protein ADE2 OS=Rattus norvegicus GN=Paics PE=2 SV=3 - [PUR6_RAT]	P51583	1.227316417	0.004012698
Nidogen-2 OS=Rattus norvegicus GN=Nid2 PE=2 SV=1 - [NID2_RAT]	B5DFC9	2.26619518	0.002838909
Palladin (Fragment) OS=Rattus norvegicus GN=Palld PE=2 SV=1 - [PALLD_RAT]	P0C5E3	1.205339763	0.025472415
Procollagen-lysine,2-oxoglutarate 5-dioxygenase 3 OS=Rattus norvegicus GN=Plod3 PE=2 SV=1 - [PLOD3_RAT]	Q5U367	1.281681868	0.012258552
Protein CDV3 homolog OS=Rattus norvegicus GN=Cdv3 PE=2 SV=1 - [CDV3_RAT]	Q5XIM5	1.815679679	0.026063311
Protein Niban OS=Rattus norvegicus GN=Fam129a PE=1 SV=2 - [NIBAN_RAT]	Q9ESN0	1.379251553	0.044199852
Ras-related protein Rab-21 OS=Rattus norvegicus GN=Rab21 PE=2 SV=1 - [RAB21_RAT]	Q6AXT5	1.550670615	0.043884988

Redox-regulatory protein FAM213A OS=Rattus norvegicus GN=Fam213a PE=1 SV=1 - [F213A_RAT]	Q6AXX6	1.340088245	0.028553209
Serine/threonine-protein kinase TAO1 OS=Rattus norvegicus GN=Taok1 PE=1 SV=1 - [TAOK1_RAT]	O88664	1.520944241	0.050000631

Downregulated Proteins continuation

Description	Acc Num	Fold Change	p ANOVA
Serine/threonine-protein phosphatase PP1-gamma catalytic subunit OS=Rattus norvegicus GN=Ppp1cc PE=1 SV=1 - [PP1G_RAT]	P63088	1.792637295	0.021953385
Succinyl-CoA:3-ketoacid coenzyme A transferase 1, mitochondrial OS=Rattus norvegicus GN=Oxct1 PE=1 SV=1 - [SCOT1_RAT]	B2GV06	1.329569046	0.022029275
Syntaxin-8 OS=Rattus norvegicus GN=Stx8 PE=1 SV=1 - [STX8_RAT]	Q9Z2Q7	2.044382523	0.008415107
Transmembrane glycoprotein NMB OS=Rattus norvegicus GN=Gpnmb PE=2 SV=1 - [GPNMB_RAT]	Q6P7C7	1.533535639	0.037450852
Troponin I, cardiac muscle OS=Rattus norvegicus GN=Tnni3 PE=1 SV=2 - [TNNI3_RAT]	P23693	1.463064075	0.042372802
Tyrosine-protein kinase Fer OS=Rattus norvegicus GN=Fer PE=1 SV=2 - [FER_RAT]	P09760	2.620935533	0.031466003
Ubiquitin-conjugating enzyme E2 G1 OS=Rattus norvegicus GN=Ube2g1 PE=2 SV=3 - [UB2G1_RAT]	P62255	1.631654072	0.048342182
Vascular cell adhesion protein 1 OS=Rattus norvegicus GN=Vcam1 PE=2 SV=1 - [VCAM1_RAT]	P29534	1.725659217	0.048178355
Ubiquitin-conjugating enzyme E2 G1 OS=Rattus norvegicus GN=Ube2g1 PE=2 SV=3 - [UB2G1_RAT]	P62255	1.631654072	0.048342182
Vascular cell adhesion protein 1 OS=Rattus norvegicus GN=Vcam1 PE=2 SV=1 - [VCAM1_RAT]	P29534	1.725659217	0.048178355

Acknowledgments

Zuallererst bedanke ich mich sehr bei meinem Betreuer Dr. Erick Miranda-Laferte. Er hat mir die Möglichkeit gegeben an diesem interessanten Thema zu arbeiten und stand mir immer mit Rat und Tat zur Seite. Danke, für die schöne Zeit in den letzten 3 Jahren und für die vielen fachlichen und privaten Diskussionen.

Als nächstes möchte ich einen großen Dank an Prof. Dr. Michaela Kuhn aussprechen. Es war schön ein Teil ihrer Arbeitsgruppe zu sein. Auch die fachliche Unterstützung und die regen Diskussionen über mein Projekt haben zum Vorankommen und Gelingen dieser Arbeit maßgeblich beigetragen.

Weiterhin möchte ich mich auch bei Priv.- Doz. Dr. Sören Doose für das Mitwirken in meinem Promotionskomitee und die Erstellung des Zweitgutachtens bedanken. Er hat durch das Einbringen von Ideen und kritische Fragestellungen meine Arbeit verbessert.

Ein besonderer Dank geht auch an Priv.- Doz. Dr. Petra Eder-Negrin. Sie hat mich herzlich in ihrer Arbeitsgruppe aufgenommen, weshalb sich die Gruppe auch schnell zu meiner „2. Heimat“ entwickelt hat. Außerdem hatte sie immer ein offenes Ohr für Fragen oder Probleme und beeinflusste durch Einwände und Vorschläge zusammen mit Erick mein Projekt maßgeblich.

Darüber hinaus möchte ich mich von ganzem Herzen bei meinen beiden Kolleginnen Yiliam Cruz Garcia und Cornelia Heindl bedanken. Wir hatten viel Spaß in den letzten 3 Jahren und ich bin froh Teil unserer kleinen Arbeitsgruppe gewesen zu sein. Ich konnte mich immer auf euch verlassen und keine Hindernisse waren für euch zu groß um mir zu helfen.

Des Weiteren bedanke ich mich besonders bei Sandra Bandleon, Alice Schaaf und Antonella Cellini. Danke für eure Unterstützung! Ich konnte mich wirklich bei allem auf euch verlassen. Es war immer toll zu euch zum Arbeiten zu kommen und ich war euch stets dankbar, dass ihr mich auch mit Süßigkeiten versorgt habt. Es war eine schöne Zeit zusammen!

Als nächstes geht ein großer Dank auch an Frau Prof. Dr. Katrin Marcus und ihre Arbeitsgruppe. Vielen Dank für das Durchführen und das Auswerten der Massenspektrometrie-Experimente.

Außerdem danke ich der gesamten AG Kuhn für die letzten 3 Jahre. Wir hatten viel Spaß und ich hab mich sehr willkommen gefühlt. Ihr seid mir sehr ans Herz gewachsen. Besonders hervorheben möchte ich Marco Abeßer und Katharina Völker, die für mich die TAC-Operationen bzw. die Kardiomyozytenpräparation durchgeführt haben.

Auch AG Friebe und AG Schuh möchte ich für die tolle Arbeitsatmosphäre danken.

Zu guter Letzt bedanke ich mich noch bei meiner Familie, meinen Freunden und insbesondere bei Martin für die Unterstützung in den letzten Jahren. Bei Rückschlägen oder schlechteren Tagen haben sie es immer geschafft mich abzulenken, zu motivieren und wieder aufzubauen. Außerdem haben sie mir die Zeit versüßt. Danke, dass ihr für mich da ward!

Danke für alles! Thank you very much! Gracias!

Eidesstattliche Erklärungen nach §7 Abs. 2 Satz 3, 4, 5 der Promotionsordnung der Fakultät für Biologie

Eidesstattliche Erklärung

Hiermit erkläre ich an Eides statt, die Dissertation: „Die Rolle der β-Untereinheit von L-Typ Kalziumkänalen in der kardialen Hypertrophie“, eigenständig, d. h. insbesondere selbständig und ohne Hilfe eines kommerziellen Promotionsberaters, angefertigt und keine anderen, als die von mir angegebenen Quellen und Hilfsmittel verwendet zu haben.

Ich erkläre außerdem, dass die Dissertation weder in gleicher noch in ähnlicher Form bereits in einem anderen Prüfungsverfahren vorgelegen hat.

Weiterhin erkläre ich, dass bei allen Abbildungen und Texten bei denen die Verwertungsrechte (Copyright) nicht bei mir liegen, diese von den Rechtsinhabern eingeholt wurden und die Textstellen bzw. Abbildungen entsprechend den rechtlichen Vorgaben gekennzeichnet sind sowie bei Abbbildungen, die dem Internet entnommen wurden, der entsprechende Hypertextlink angegeben wurde.

Affidavit

I hereby declare that my thesis entitled: „Role of the β subunit of L-type calcium channels in cardiac hypertrophy” is the result of my own work. I did not receive any help or support from commercial consultants. All sources and / or materials applied are listed and specified in the thesis.

Furthermore I verify that the thesis has not been submitted as part of another examination process neither in identical nor in similar form.

Besides I declare that if I do not hold the copyright for figures and paragraphs, I obtained it from the rights holder and that paragraphs and figures have been marked according to law or for figures taken from the internet the hyperlink has been added accordingly.

Würzburg, den 12.08.2019

_____

Signature PhD-student